12 Appendices

University of Gloucestershire

Geochronology Laboratories

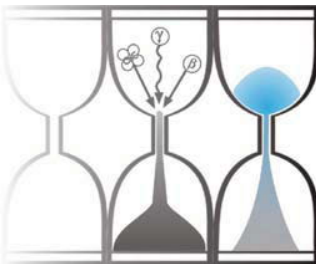

Optical dating report for the ALSF project 'Predictive Modelling of Multi-Period Geoarchaeological resources at a River confluence'

to

Prof. A.G. Brown, University of Exeter

Prepared by Dr P.S. Toms, 19th February 2007

English Heritage Centre for Archaeology Optical dating report for the ALSF project 'Predictive Modelling of Multi-Period Geoarchaeological resources at a River confluence'

Dr P.S. Toms[1], Prof. A.G. Brown[2], Dr C.J. Carey[2], Dr A.J. Howard[3] and Dr K. Challis[3]

Summary

This study contributes to Phase 2 of the 'Predictive Modelling of Multi-Period Geoarchaeological resources at a River confluence' ALSF project. The aim of this dating study is to generate chronological controls based on Optical dating to assist in the construction of a secure, high resolution stratigraphic framework to refine landscape evolution models of the Rivers Trent & Soar study area developed during Phase 1. Given the bulk of sediments of interest were likely deposited in the Holocene by fluvial processes, partial resetting of the time dependent signal prior to burial may force a significant age overestimation if adopting conventional multi-grain single aliquot methods of Optical dating. In an attempt to circumvent this issue, aliquots composed of single grains of quartz sand have been dated in order to gain a measure of inter-grain age variability and to isolate that minimum age region representing those grains whose time dependent signal was near or fully reset prior to burial. Age estimates span from as little as 0.38 ka to as much as 8.16 ka and, exceptionally, 25.3 ka. Five samples have proven analytically acceptable. Limits upon the mass of datable material create some minor uncertainty in the reliability of age estimates from four samples, whilst intrinsic tests and measures of U disequilibrium highlight some minor uncertainties in the remaining data set. However, only one sample is rejected outright.

Keywords

Optical dating, Single Grains, Holocene, Fluvial

Authors' addresses

[1]Geochronology Laboratories, Department of Natural and Social Sciences, University of Gloucestershire, Swindon Road, Cheltenham. GL50 4AZ. Tel: 01242 544091. Email: ptoms@glos.ac.uk

[2]Department of Geography, University of Exeter, Amory Building, Rennes Drive, Exeter. EX4 4RJ.

[3]Institute for Archaeology and Antiquity, University of Birmingham, Edgbaston, Birmingham. B15 2TT.

1.0 Introduction

This study contributes to Phase 2 of the 'Predictive Modelling of Multi-Period Geoarchaeological resources at a River confluence' project, funded through the Aggregates Levy sustainability Fund administered by English Heritage (EH project number: 3357MAIN). The aim of this ALSF project is to predictively model the landscape of a major river confluence over a time-scale of millennia and at a spatial scale appropriate for archaeological management. The study area is 2 by 4 km in extent located across the confluence of the Rivers Trent and Soar. The aim of this dating study is to generate chronological controls based on Optical dating to assist in the construction of a secure, high resolution stratigraphic framework, thereby refining the detailed surface and subsurface landscape evolution models of the study area developed during Phase 1. The rationale for this is to show how much archaeological data can be generated for alluviated aggregate sites prior to excavation.

2.0 Optical dating: Mechanisms and principles

Upon exposure to ionising radiation, electrons within the crystal lattice of insulating minerals are displaced from their atomic orbits. Whilst this dislocation is momentary for most electrons, a portion of charge is redistributed to meta-stable sites (traps) within the crystal lattice. In the absence of significant optical and thermal stimuli, this charge can be stored for extensive periods. The quantity of charge relocation and storage relates to the magnitude and period of irradiation. When the lattice is optically or thermally stimulated, charge is evicted from traps and may return to a vacant orbit position (hole). Upon recombination with a hole, an electron's energy can be dissipated in the form of light generating crystal luminescence providing a measure of dose absorption.

Herein, quartz is segregated for dating. The utility of this minerogenic dosimeter lies in the stability of its datable signal over the mid to late Quaternary period, predicted through isothermal decay studies (e.g. Smith *et al*., 1990; retention lifetime 630 Ma at 20°C) and evidenced by optical age estimates concordant with independent chronological controls (e.g. Murray and Olley, 2002) This stability is in contrast to the anomalous fading of comparable signals commonly observed for other ubiquitous sedimentary minerals such as feldspar and zircon (Wintle, 1973; Templer, 1985; Spooner, 1993).

Optical age estimates of sedimentation (Huntley *et al*., 1985) are premised upon reduction of the minerogenic time dependent signal (Optically Stimulated Luminescence, OSL) to zero through exposure to sunlight and, once buried, signal reformulation by absorption of litho- and cosmogenic radiation. The signal accumulated post burial acts as a dosimeter recording total dose absorption, converting to a chronometer by estimating the rate of dose absorption quantified through the assay of radioactivity in the surrounding lithology and streaming from the cosmos.

$$\text{Age} = \frac{\text{Mean Equivalent Dose } (D_e, \text{Gy})}{\text{Mean Dose Rate } (D_r, \text{Gy.ka}^{-1})}$$

Aitken (1998) and Bøtter-Jensen *et al*. (2003) offer a detailed review of optical dating.

3.0 Sample Collection and Preparation

Twenty one conventional sediment samples – those located within matrix-supported units composed predominantly of sand and silt - were collected within opaque plastic tubing from either sections by means of tubing (150x45 mm) forced into each face (samples GL06005 to GL06009) or from boreholes excavated by a Geoprobe (in tubing 1000x45 mm). Each sample location marked the deepest points of palaeochannels within the study area. Each tube was wrapped in cellophane and parcel tape in order to preserve moisture content and integrity until ready for laboratory preparation. To

preclude optical erosion of the datable signal prior to measurement, all samples were prepared under controlled laboratory illumination provided by Encapsulite RB-10 (red) filters. To isolate that material potentially exposed to daylight during sampling or that which had been relocated by the process of coring, sediment located within the outer 5 mm of each sample was removed.

The remaining sample was dried and then sieved. Quartz within the fine sand (125-180 μm or 180-250 μm) fraction was then segregated (Table 1). Samples were subjected to acid and alkali digestion (10% HCl, 15% H_2O_2) to attain removal of carbonate and organic components respectively.

A further acid digestion in HF (40%, 60 mins) was used to etch the outer 10-15 μm layer affected by α radiation and degrade each samples' feldspar content. During HF treatment, continuous magnetic stirring was used to effect isotropic etching of grains. 10% HCl was then added to remove acid soluble fluorides. Each sample was dried, resieved and quartz isolated from the remaining heavy mineral fraction using a sodium polytungstate density separation at 2.68g.cm^{-3}. Where sufficient datable mass existed, 24 multi-grain aliquots (*c.* 3-6 mg) of quartz from each sample were then mounted on aluminium discs to establish optimum, average measurement conditions for single grain aliquots. Around 2400 sand grains from each sample were located individually in 200 mm (diameter and depth) holes drilled as a 10x10 grid into anodised aluminium discs (Duller *et al*., 1999) to gain a measure of inter-grain D_e distribution.

All drying was conducted at 40°C to prevent thermal erosion of the signal. All acids and alkalis were Analar grade. All dilutions (removing toxic-corrosive and non-minerogenic, luminescence-bearing substances) were conducted with distilled water to prevent signal contamination by extraneous particles.

4.0 Acquisition and accuracy of D_e value

All minerals naturally exhibit marked inter-sample variability in luminescence per unit dose (sensitivity). Therefore, the estimation of D_e acquired since burial requires calibration of the natural signal using known amounts of laboratory dose. D_e values were quantified using a single-aliquot regenerative-dose (SAR) protocol (Murray and Wintle 2000; 2003) facilitated by a Risø TL-DA-15 irradiation-stimulation-detection system (Markey *et al*., 1997; Bøtter-Jensen *et al*., 1999; Duller *et al*., 1999). Within this apparatus, optical signal stimulation of multi-grain aliquots was provided by an assembly of blue diodes (5 packs of 6 Nichia NSPB500S), filtered to 470±80 nm conveying 15 mW.cm^{-2} using a 3 mm Schott GG420 positioned in front of each diode pack. Optical stimulation of single grain aliquots emanated from a focussed solid state 532 nm (green), 10 mW stabilised laser (Laser 2000 LCL-LCM-T-11ccs) scanned across grains by means of mirrors mounted on and moved by motorised linear stages. Infrared (IR) stimulation, provided by 6 IR diodes (Telefunken TSHA 6203) stimulating at 875±80nm delivering ~5 mW.cm^{-2}, was used to indicate the presence of contaminant feldspars (Duller, 2003). Stimulated photon emissions from quartz aliquots are in the ultraviolet (UV) range and were filtered from stimulating photons by 7.5 mm HOYA U-340 glass and detected by an EMI 9235QA photomultiplier fitted with a blue-green sensitive bialkali photocathode. Aliquot irradiation was conducted using a 1.48 GBq ^{90}Sr/^{90}Y β source calibrated for single and multi-grain aliquots of each isolated quartz fraction against the 'Hotspot 800' ^{60}Co γ source located at the National Physical Laboratory (NPL), UK. In calibrating single sand grain aliquots, no significant spatial variation in dose rate from the β source was found.

SAR by definition evaluates D_e through measuring the natural signal (Fig. 1) of a single aliquot and then regenerating that aliquot's signal by using known laboratory doses to enable calibration. For each aliquot, at least 4 different regenerative-doses were administered so as to image dose response. D_e values for each aliquot were then interpolated, and associated counting and fitting errors calculated, by way of exponential or exponential plus linear regression (Fig. 1). The accuracy with which D_e equates to total absorbed dose and that dose absorbed since burial is assessed. The former

can be considered a function of laboratory factors, the latter, one of environmental issues. Diagnostics were deployed to estimate the influence of these factors and criteria instituted to optimise the accuracy of D_e values.

4.1 Laboratory Factors

4.1.1 Feldspar contamination

The propensity of feldspar signals to fade and underestimate age, coupled with their higher sensitivity relative to quartz makes it imperative to quantify feldspar contamination. At room temperature, feldspars generate a signal (IRSL) upon exposure to IR whereas quartz does not. The signal from feldspars contributing to OSL can be depleted by prior exposure to IR. For all aliquots the contribution of any remaining feldspars was estimated from the OSL IR depletion ratio (Duller, 2003). If the addition to OSL by feldspars is insignificant, then the repeat dose ratio of OSL to post-IR OSL should be statistically consistent with unity. Any aliquots that did not fulfil this criterion were rejected.

4.1.2 Preheating

Preheating aliquots between irradiation and optical stimulation is necessary to ensure comparability between natural and laboratory-induced signals. However, the multiple irradiation and preheating steps that are required to define single-aliquot regenerative-dose response leads to signal sensitisation, rendering calibration of the natural signal inaccurate. The SAR protocol (Murray and Wintle, 2000; 2003) enables this sensitisation to be monitored and corrected using a test dose, here set at *c* 5 Gy preheated to 220°C for 10s, to track signal sensitivity between irradiation-preheat steps. However, the accuracy of sensitisation correction for both natural and laboratory signals can be preheat dependent. Three diagnostics were used to assess the optimal preheat temperature for accurate correction and calibration.

Irradiation-preheat cycling (Fig. 2) quantifies the preheat dependence of sensitisation correction for laboratory-induced signals. If sensitisation is accurately corrected, then the same regenerative-dose should yield an equivalent sensitivity corrected value irrespective of the number of times it is applied and its associated signal measured. The ratio of subsequent to initial corrected regenerative-dose signals should be statistically concordant with unity. Alternatively, this ratio may differ from unity yet attain consistency after one or more cycles evidencing accurate sensitivity correction exists if the sample is primed by irradiation-preheat cycles. For this diagnostic, and where sufficient material was available, 18 multi-grain aliquots were divided into sets of 3 and assigned a 10 s preheat between 180°C and 280°C.

D_e preheat dependence (Fig. 3) quantifies the combined effects of thermal transfer and sensitisation on the natural signal. Insignificant adjustment in D_e values in response to differing preheats may reflect limited influence of these effects. Samples generating D_e values <10Gy and exhibiting a systematic, statistically significant adjustment in D_e value with increasing preheat temperature may indicate the presence of significant thermal transfer; in such instances low temperature (<220°C) preheats may provide the apposite measure of D_e. For this diagnostic, the D_e value of each of the same 18 multi-grain aliquots and their assigned preheat was assessed.

Dose Recovery (Fig. 4) attempts to replicate the above diagnostic, yet provide improved resolution of thermal effects through removal of variability induced by heterogeneous dose absorption in the environment, using a precise laboratory dose to simulate natural dose. The ratio between the applied dose and recovered D_e value should be statistically concordant with unity. For this diagnostic, a further 6 multi-grain aliquots were each assigned a 10 s preheat between 180°C and 280°C.

That preheat treatment fulfilling the criterion of accuracy for all three diagnostics was selected to refine the final D_e value for 2400 single grain aliquots. Further thermal treatments, prescribed by Murray and Wintle (2000; 2003), were applied to optimise accuracy and precision. Optical stimulation occurred at 125ºC in order to minimise effects associated with

photo-transferred thermoluminescence and maximise signal to noise ratios. Inter-cycle optical stimulation was conducted at 280°C to minimise recuperation.

4.1.3 Irradiation

Laboratory irradiation effects may evolve from the contrasting rates of natural dose exposure and the calibrating laboratory dose, the latter delivered to each aliquot at 9 orders of magnitude faster than the former. Bailey (2004) has suggested that for doses in excess of ~40 Gy an overestimation of age may arise due to competing mechanisms of signal accumulation within the crystal lattice of quartz. Only one sample (GL06009) generated single grain D_e values >40 Gy. These accounted for the minority of D_e values obtained for GL06009 and therefore laboratory irradiation effects were not considered significant in this study.

4.1.4 Internal consistency

Radial plots (Fig. 5; *cf* Galbraith, 1990) are used to illustrate inter-aliquot D_e variability for natural and regenerated signals. D_e values are standardised relative to the central D_e value (Galbraith *et al*., 1999) for natural signals and applied dose for regenerated signals. D_e values are described as overdispersed when >5% lie beyond $\pm 2\sigma$ of the standardising value; resulting from a heterogeneous absorption of burial dose and/or response to the SAR protocol. Overdispersion for natural signals does not necessarily imply inaccuracy. However where overdispersion is observed for regenerated signals, the age estimate from that sample should be accepted tentatively.

4.2 Environmental factors

4.2.1 Incomplete zeroing

Post-burial OSL signals residual of pre-burial dose absorption can result where pre-burial sunlight exposure is limited in spectrum, intensity and/or period, leading to age overestimation. This effect is particularly acute for material eroded and redeposited sub-aqueously (Olley *et al*., 1998, 1999; Wallinga, 2002) and exposed to a burial dose of <20 Gy (e.g. Olley *et al*., 2004). It can have some influence in sub-aerial contexts but is rarely of consequence where aerial transport has occurred. Optical dating of dominantly Holocene fluvial sands within this study warrants that this environmental effect be addressed.

Within single-aliquot regenerative-dose optical dating there are two diagnostics of partial resetting (or bleaching); signal analysis (Agersnap-Larsen *et al*., 2000; Bailey *et al*., 2003) and inter-aliquot D_e distribution studies (Murray *et al*., 1995).

Within this study the latter has been used, taking aliquots of single sand grains to quantify inter-grain D_e distribution. At present, it is contended that asymmetric inter-grain D_e distributions are symptomatic of partial bleaching and/or pedoturbation (Murray *et al*., 1995; Olley *et al*., 1999; Olley *et al*., 2004; Bateman *et al*., 2003). For partial bleaching at least, it is further contended that the D_e acquired during burial is located in the minimum region of such ranges. The Minimum Age Model (Galbraith and Laslett, 1993) is the most regularly applied statistical approach in quantifying the breadth of minimum dose regions. Olley et al. (2004) recommend this model for Holocene fluvial samples based upon its agreement with independent age controls for a number of samples. Yet such models have been found to underestimate post-burial D_e values owing to post depositional turbation (Roberts et al., 1998) or as a product of a minority of outlying low D_e values (Rodnight, 2006). The Finite Mixture Model (Galbraith and Green, 1990) offers an alternative statistical method by which to compute the minimum dose region reflecting post-burial D_e. It identifies the number of dose components within an inter-grain D_e distribution along with the mean D_e and proportion of grains in each component. In the Finite Mixture Model each component is assumed to have an equivalent level of overdispersion (σ, herein set at 0.10; Jacobs *et al*., 2006; Rodnight *et al*., 2006). Rodnight *et al*. (2006) advocate use of the youngest component unless it comprises less than 10% of aliquots, whereupon the next youngest component is taken to reflect post-burial D_e. However, the mean and breadth of this minimum region in all models is the subject of current debate, as it is additionally

influenced by heterogeneity in microdosimetry, variable inter-grain response to SAR and residual to post-burial signal ratios. The Central Age Model (Galbraith et al., 1999) assumes all inter-grain D_e variation is forced by spatial variations in dose rate and natural irradiation effects that can be accurately replicated by laboratory irradiation, and thus the mean D_e value coupled with the mean D_r value will generate an accurate age estimate of burial. At present, it is clear that age defined by the D_e interval delimited by the Minimum and Central Age Models will be accurate but have limited precision (Table 1). In this study, the Finite Mixture Model has been adopted to produce a more refined estimate of age (Table 1) based on the success of its implementation by Rodnight *et al*. (2006) in sediments equivalent in age and genus to those in this study.

4.2.2 Turbation

The accuracy of sedimentation ages can further be controlled by post-burial trans-strata grain movements forced by pedo- or cryoturbation. Berger (2003) contends pedogenesis prompts a reduction in the apparent sedimentation age of parent material through bioturbation and illuviation of younger material from above and/or by biological recycling and resetting of the datable signal of surface material. Berger (2003) proposes that the chronological products of this remobilisation are A-horizon age estimates reflecting the cessation of pedogenic activity, Bc/C-horizon ages delimiting the maximum age for the initiation of pedogenesis with estimates obtained from Bt-horizons providing an intermediate age 'close to the age of cessation of soil development'. Singhvi *et al*. (2001), in contrast, suggest that B and C-horizons closely approximate the age of the parent material, the A-horizon, that of the 'soil forming episode'. At present there is no post-sampling mechanism for the direct detection of and correction for post-burial sediment remobilisation. However, intervals of palaeosol evolution can be delimited by a maximum age derived from parent material and a minimum age obtained from a unit overlying the palaeosol. Pedogenic effects are not considered significant within this study owing to the lack of visible soil development. Inaccuracy forced by cryoturbation may be bidirectional, heaving older material upwards or drawing younger material downwards into the level to be dated. However, only one sample (GL06009) was retrieved from a section of sediments likely dating to the last Glacial stage; no evidence was observed of cryogenic deformation.

5.0 Acquisition and accuracy of D_r value

Lithogenic D_r values were defined through measurement of U, Th and K radionuclide concentration and conversion of these quantities into β and γ D_r values (Table 1). β contributions were estimated from sub-samples by Neutron Activation Analysis (NAA) delivered by Becquerel Canada. γ dose rates were estimated for samples GL06005 to GL06009 from *in situ* NaI γ spectrometry. Where direct measurements of γ dose rate were not possible, laboratory-based Ge γ spectrometry was conducted on sub-samples composed of material at intervals within 300 mm above and below the centre of each sample within each core (weighted by relative γ contributions; Aitken, 1985) . *In situ* measurements were conducted using an EG&G μNomad portable NaI γ spectrometer (calibrated using the block standards at RLAHA, University of Oxford); these reduce uncertainty relating to potential heterogeneity in the γ dose field surrounding each sample. Laboratory-based γ spectrometry was conducted using an Ortec GEM-S high purity Ge coaxial detector system, calibrated using certified reference materials supplied by CANMET. Estimates of radionuclide concentration were converted into D_r values (Adamiec and Aitken, 1998), accounting for D_r modulation forced by grain size (Mejdahl, 1979) and present moisture content (Zimmerman, 1971). Cosmogenic D_r values are calculated on the basis of sample depth, geographical position and matrix density (Prescott and Hutton, 1994).

The spatiotemporal validity of D_r values can be considered as a function of five variables. Firstly, age estimates devoid of *in situ* γ spectrometry data should be accepted tentatively if the sampled unit is heterogeneous in texture or if the sample is located within 300 mm of strata consisting of differing texture and/or mineralogy. However, where samples are obtained throughout a vertical profile, consistent values of γ D_r based solely on, for example, NAA may evidence the

homogeneity of the γ field and hence accuracy of γ D_r values. Secondly, disequilibrium can force temporal instability in U and Th emissions. In this study, the potential for long-term instability in D_r values forced by U disequilibrium has been considered. The impact of this infrequent phenomenon (Olley *et al*., 1996) upon age estimates is usually insignificant given their associated margins of error, however this effect is pronounced for at least two samples in this study (>50% disequilibrium between ^{238}U and ^{226}Ra, samples GL06014 & GL06025; Fig. 6). Thirdly, pedogenically-induced variations in matrix composition of B and C-horizons, such as radionuclide and/or mineral remobilisation, may alter the rate of energy emission and/or absorption. If D_r is invariant through a dated profile and samples encompass primary parent material, then element mobility is likely limited in effect. In this study, there is limited evidence of pedogenesis in any unit sampled. Fourthly, spatiotemporal deviations from present moisture content are difficult to assess directly, requiring knowledge of the magnitude and timing of differing contents. However, the maximum influence of moisture content variations can be delimited by recalculating D_r for minimum (zero) and maximum (saturation) content. Finally, temporal alteration in the thickness of overburden alters cosmic D_r values. Cosmic D_r often forms a negligible portion of total D_r. It is possible to quantify the maximum influence of overburden flux by recalculating D_r for minimum (zero) and maximum (surface sample) cosmic D_r.

6.0 Estimation of Age

Age estimates reported in Table 1 provide an estimate of sediment burial period based on mean D_r values and D_e values derived from Minimum, Finite Mixture and Central Age Models, along with associated analytical uncertainties. Uncertainty in Finite Mixture age estimates is reported as a product of systematic and experimental errors, with the magnitude of experimental errors alone shown in parenthesis (Table 1). Probability distributions indicate the inter-aliquot variability in age (Fig. 7). The maximum influence of temporal variations in D_r forced by minima-maxima variation in moisture content and overburden thickness, coupled with Finite Mixture D_e values, is illustrated in Fig. 7. Where uncertainty in these parameters exists this age range may prove instructive, however the combined extremes represented should not be construed as preferred age estimates.

7.0 Analytical uncertainty

All errors are based upon analytical uncertainty and quoted at 1σ confidence. Error calculations account for the propagation of systematic and/or experimental (random) errors associated with D_e and D_r values.

For D_e values, systematic errors are confined to laboratory β source calibration. Uncertainty in this respect is that combined from the delivery of the calibrating γ dose (1.2%; NPL, pers. comm.), the conversion of this dose for SiO_2 using the respective mass energy-absorption coefficient (2%; Hubbell, 1982), reproducibility in laser positioning (3.5%; Truscott *et al*., 2000) and experimental error, totalling 4.3%. Mass attenuation and bremsstrahlung losses during γ dose delivery are considered negligible. Experimental errors relate to D_e interpolation using sensitisation corrected dose responses. Natural and regenerated sensitisation corrected dose points (S_i) are quantified by,

$$S_i = (D_i - x.L_i) / (d_i - x.L_i) \qquad \textbf{Eq.1}$$

where D_i = Natural or regenerated OSL, initial 0.2 s
L_i = Background natural or regenerated OSL, final 5 s
d_i = Test dose OSL, initial 0.2 s
x = Scaling factor, 0.08

The error on each signal parameter is based on counting statistics, reflected by the square-root of measured values. The propagation of these errors within Eq. 1 generating σS_i follows the general formula given in Eq. 2. σS_i are then used to define fitting and interpolation errors within linear or exponential regressions (Green and Margerison, 1978; Ixaru *et al*., 2004).

For D_r values, systematic errors accommodate uncertainty in radionuclide conversion factors (5%), β attenuation coefficients (5%), matrix density (0.20 $g.cm^{-3}$), vertical thickness of sampled section (specific to sample collection device), saturation moisture content (3%), moisture content attenuation (2%), burial moisture content (25% relative, unless direct evidence exists of the magnitude and period of differing content), NaI gamma spectrometer calibration (3%) and/or NAA (2%). Experimental errors are associated with radionuclide quantification for each sample by γ spectrometry and/or NAA.

The propagation of these errors through to age calculation is quantified using the expression,

$$\sigma y\ (\delta y/\delta x) = (\Sigma\ ((\delta y/\delta x_n).\sigma x_n)^2)^{1/2} \qquad \textbf{Eq. 2}$$

where y is a value equivalent to that function comprising terms x_n and where σy and σx_n are associated uncertainties.

Errors on age estimates based on the Finite Mixture Model are presented as combined systematic and experimental errors and experimental errors alone. The former (combined) error should be considered when comparing luminescence ages herein with independent chronometric controls. The latter assumes systematic errors are common to luminescence age estimates generated by means equal to those detailed herein and enable direct comparison with those estimates.

8.0 Intrinsic Assessment of Reliability

In this study, intrinsic assessment of reliability is restricted to analytical acceptability. Table 2 details the analytical acceptability of age estimates evolved in this study, drawn principally from diagnostics illustrated in Figs. 1 to 6 and detailed in sections 4.0 to 5.0. Other indexes of reliability in Optical dating can be drawn by inference. Intra-site stratigraphic consistency of ages, quantified by Bayesian modelling, and the convergence of age estimates from stratigraphically equivalent units of divergent dosimetry are key intrinsic measures of reliability (Toms *et al*., 2005). However, the low sampling density per dated level and ambiguity in inter-core relative stratigraphic position of samples precluded the use of these inferential methods.

9.0 Summary

This study has generated optical age estimates which commonly span from as little as 0.38 ka to as much as 8.16 ka, with one sample potentially as old as 25.3 ka. Five samples (GL06 006, 008, 020, 024, 026) have proven analytically acceptable. The quality of the data from four samples (GL06 016, 018, 022, 028) is potentially limited by a dearth of datable material whilst overdispersion in regenerative-dose data and minor U disequilibrium may have some bearing on the accuracy of the remaining age estimates. However, the age estimate from only one sample (GL06017) is rejected.

Field Code	Lab Code	Location	Overburden (m)	Grain size (μm)	Moisture content	Ge γ-spectrometry (lab based) († or NaI γ-spectrometry (in situ))			γ D_r ($Gy.ka^{-1}$)	Neutron Activation Analysis			β D_r ($Gy.ka^{-1}$)	Cosmic D_r ($Gy.ka^{-1}$)	Total D_r ($Gy.ka^{-1}$)	Preheat (°C for 10s)	MAM D_e (Gy)	CAM D_e (Gy)	FMM D_e (Gy)	FMMAge (ka)	MAM to CAM Age (ka)
						K (%)	Th (ppm)	U (ppm)		K (%)	Th (ppm)	U (ppm)									
SOAR01†	GL06005	53°N, 1°W, 20 m	0.9	125-180	0.21 ± 0.05	0.38 ± 0.01	1.53 ± 0.11	0.86 ± 0.11	0.26 ± 0.01	2.06 ± 0.09	7.60 ± 0.32	1.76 ± 0.09	1.45 ± 0.16	0.18 ± 0.02	1.89 ± 0.16	260	1.6 ± 0.1	2.4 ± 0.3	1.8 ± 0.1	0.94 ± 0.09 (0.08)	0.83 – 1.43
SOAR02†	GL06006	53°N, 1°W, 20 m	2.0	125-180	0.22 ± 0.06	0.62 ± 0.02	3.26 ± 0.16	2.57 ± 0.12	0.60 ± 0.02	1.43 ± 0.07	6.86 ± 0.31	2.55 ± 0.13	1.14 ± 0.13	0.15 ± 0.01	1.88 ± 0.13	260	3.2 ± 0.7	5.6 ± 0.5	4.9 ± 0.3	2.62 ± 0.24 (0.22)	1.53 – 3.30
SOAR03†	GL06007	53°N, 1°W, 20 m	1.5	125-180	0.12 ± 0.03	0.54 ± 0.02	2.48 ± 0.15	1.73 ± 0.11	0.45 ± 0.02	0.62 ± 0.03	2.87 ± 0.14	1.33 ± 0.07	0.59 ± 0.05	0.16 ± 0.02	1.20 ± 0.05	280	2.2 ± 0.4	3.7 ± 0.4	4.2 ± 0.3	3.49 ± 0.31 (0.30)	1.51 – 3.43
SOAR04†	GL06008	53°N, 1°W, 20 m	1.6	125-180	0.14 ± 0.04	0.60 ± 0.02	3.42 ± 0.17	2.56 ± 0.13	0.60 ± 0.02	0.96 ± 0.05	4.41 ± 0.20	1.87 ± 0.09	0.87 ± 0.07	0.16 ± 0.02	1.63 ± 0.08	240	3.9 ± 0.4	4.3 ± 0.5	4.1 ± 0.3	2.52 ± 0.22 (0.21)	2.02 – 2.98
SOAR05	GL06009	53°N, 1°W, 20 m	3.7	125-180	0.15 ± 0.04	0.85 ± 0.04	4.05 ± 0.35	0.87 ± 0.07	0.41 ± 0.05	1.47 ± 0.06	2.54 ± 0.12	0.81 ± 0.05	1.02 ± 0.10	0.11 ± 0.01	1.55 ± 0.11	220	24.0 ± 8.0	34.1 ± 4.3	34.1 ± 4.3	22.1 ± 3.2 (3.0)	11.6 – 25.3
GEO 2	GL06014	53°N, 1°W, 20 m	1.3	125-180	0.17 ± 0.04	0.84 ± 0.05	4.32 ± 0.47	1.71 ± 0.11	0.49 ± 0.06	1.04 ± 0.05	5.57 ± 0.26	2.22 ± 0.12	0.93 ± 0.09	0.17 ± 0.02	1.59 ± 0.11	240	2.1 ± 0.5	3.4 ± 0.5	2.2 ± 0.4	1.38 ± 0.25 (0.24)	0.96 – 2.49
GEO 3	GL06015	53°N, 1°W, 20 m	1.4	125-180	0.15 ± 0.04	0.77 ± 0.04	4.35 ± 0.37	1.49 ± 0.09	0.47 ± 0.05	0.73 ± 0.03	3.55 ± 0.15	1.81 ± 0.08	0.68 ± 0.06	0.17 ± 0.02	1.31 ± 0.08	260	1.7 ± 0.1	2.2 ± 0.4	2.0 ± 0.1	1.50 ± 0.14 (0.12)	1.24 – 2.00
GEO 4	GL06016	53°N, 1°W, 20 m	1.0	125-180	0.13 ± 0.03	0.79 ± 0.05	4.62 ± 0.51	1.55 ± 0.11	0.50 ± 0.06	0.80 ± 0.03	3.93 ± 0.16	1.94 ± 0.08	0.78 ± 0.06	0.18 ± 0.02	1.46 ± 0.09	260	3.7 ± 0.8	4.5 ± 0.5	4.1 ± 0.3	2.80 ± 0.27 (0.23)	1.69 – 3.43
GEO 5	GL06017	53°N, 1°W, 20 m	0.7	125-180	0.07 ± 0.02	0.81 ± 0.04	4.88 ± 0.39	1.35 ± 0.08	0.54 ± 0.05	0.79 ± 0.03	4.20 ± 0.17	1.65 ± 0.07	0.82 ± 0.05	0.18 ± 0.02	1.55 ± 0.08	240	2.1± 0.9	2.1 ± 0.7	-	1.36 ± 0.46 (0.44)	0.75 – 3.43
GEO 7	GL06018	53°N, 1°W, 20 m	2.1	125-180	0.21 ± 0.05	0.91 ± 0.05	5.73 ± 0.43	1.74 ± 0.10	0.53 ± 0.06	1.14 ± 0.05	5.76 ± 0.23	2.27 ± 0.09	0.95 ± 0.10	0.15 ± 0.01	1.62 ± 0.12	260	1.6 ± 0.5	2.0 ± 0.2	2.0 ± 0.2	1.21 ± 0.16 (0.15)	0.76 – 1.37
GEO 11	GL06019	53°N, 1°W, 20 m	1.0	125-180	0.17 ± 0.04	0.80 ± 0.05	4.20 ± 1.51	1.51 ± 0.10	0.46 ± 0.06	1.01 ± 0.04	3.66 ± 0.15	1.55 ± 0.06	0.81 ± 0.08	0.18 ± 0.02	1.45 ± 0.10	260	0.7 ± 0.2	1.2 ± 0.2	0.7 ± 0.2	0.51 ± 0.11 (0.11)	0.38 – 1.01
GEO 12	GL06020	53°N, 1°W, 20 m	1.2	125-180	0.20 ± 0.05	1.00 ± 0.06	5.21 ± 0.47	1.63 ± 0.11	0.53 ± 0.07	1.26 ± 0.06	5.70 ± 0.26	2.10 ± 0.11	1.02 ± 0.11	0.17 ± 0.02	1.72 ± 0.13	260	1.8 ± 0.1	2.0 ± 0.3	1.8 ± 0.1	1.06 ± 0.11 (0.10)	0.96 – 1.36
GEO 14	GL06021	53°N, 1°W, 20 m	1.5	125-180	0.16 ± 0.04	0.90 ± 0.05	6.33 ± 0.46	1.85 ± 0.10	0.60 ± 0.07	1.22 ± 0.05	6.27 ± 0.26	2.47 ± 0.10	1.10 ± 0.10	0.16 ± 0.02	1.86 ± 0.12	260	4.1 ± 0.7	5.8 ± 0.5	5.8 ± 0.5	3.12 ± 0.34 (0.31)	1.90 – 3.46
GEO 17	GL06022	53°N, 1°W, 20 m	1.5	125-180	0.16 ± 0.04	0.71 ± 0.05	2.77 ± 0.41	0.87 ± 0.09	0.33 ± 0.05	0.83 ± 0.03	3.08 ± 0.13	1.63 ± 0.07	0.72 ± 0.06	0.16 ± 0.02	1.21 ± 0.09	260	2.6 ± 0.7	3.5 ± 0.4	3.5 ± 0.4	2.86 ± 0.38 (0.35)	1.66 – 3.24
GEO 18	GL06023	53°N, 1°W, 20 m	1.2	125-180	0.19 ± 0.05	1.04 ± 0.07	7.41 ± 0.73	2.32 ± 0.16	0.68 ± 0.09	1.17 ± 0.05	5.42 ± 0.22	2.50 ± 0.10	1.01 ± 0.10	0.17 ± 0.02	1.86 ± 0.14	260	3.0 ± 0.6	6.2 ± 0.8	4.8 ± 0.8	2.59 ± 0.47 (0.45)	1.28 – 3.86
GEO 22	GL06024	53°N, 1°W, 20 m	0.7	125-180	0.19 ± 0.05	1.54 ± 0.07	6.95 ± 0.46	1.37 ± 0.09	0.68 ± 0.008	2.23 ± 0.09	7.26 ± 0.29	1.73 ± 0.07	1.58 ± 0.16	0.19 ± 0.02	2.45 ± 0.18	240	2.1 ± 0.3	15.1 ± 2.9	2.1 ± 0.3	0.87 ± 0.14 (0.13)	0.68 – 7.41
GEO 24	GL06025	53°N, 1°W, 20 m	1.4	125-180	0.21 ± 0.05	0.92 ± 0.06	7.00 ± 0.56	2.25 ± 0.13	0.62 ± 0.08	1.17 ± 0.05	7.27 ± 0.29	2.81 ± 0.12	1.04 ± 0.11	0.17 ± 0.02	1.83 ± 0.14	280	1.2 ± 0.3	3.3 ± 0.6	1.3 ± 0.3	0.73 ± 0.17 (0.17)	0.54 – 2.14
GEO 25	GL06026	53°N, 1°W, 20 m	2.3	180-250	0.14 ± 0.04	0.70 ± 0.05	3.39 ± 0.53	1.04 ± 0.09	0.38 ± 0.06	0.84 ± 0.04	2.34 ± 0.10	0.86 ± 0.04	0.63 ± 0.06	0.14 ± 0.01	1.15 ± 0.08	260	5.6 ± 1.2	8.2 ± 1.1	6.4 ± 0.8	5.52 ± 0.78 (0.72)	3.68 – 8.16
GEO 27	GL06028	53°N, 1°W, 20 m	0.7	125-180	0.19 ± 0.05	1.04 ± 0.06	6.70 ± 0.56	2.03 ± 0.13	0.63 ± 0.08	1.24 ± 0.05	6.23 ± 0.26	2.47 ± 0.10	1.06 ± 0.11	0.18 ± 0.02	1.88 ± 0.13	260	2.3 ± 0.2	3.1 ± 0.4	2.4 ± 0.2	1.25 ± 0.13 (0.12)	1.08 – 1.86
GEO 29	GL06030	53°N, 1°W, 20 m	1.1	125-180	0.19 ± 0.05	0.78 ± 0.05	5.56 ± 0.55	1.91 ± 0.13	0.53 ± 0.07	0.91 ± 0.05	4.94 ± 0.23	2.06 ± 0.11	0.82 ± 0.08	0.18 ± 0.02	1.52 ± 0.11	280	3.3 ± 0.6	4.9 ± 0.7	3.4 ± 0.5	2.23 ± 0.35 (0.33)	1.67 – 3.70
GEO 30	GL06031	53°N, 1°W, 20 m	2.5	125-180	0.23 ± 0.06	1.15 ± 0.06	4.71 ± 0.40	1.09 ± 0.08	0.46 ± 0.06	1.44 ± 0.06	4.72 ± 0.19	1.89 ± 0.08	1.02 ± 0.12	0.14 ± 0.01	1.63 ± 0.14	240	5.4 ± 0.8	6.6 ± 0.4	5.3 ± 1.7	3.24 ± 1.09 (1.08)	2.87 – 4.47

Table 1 D_r, D_e and Age data of submitted samples. Uncertainties in age are quoted at 1σ confidence, are based on analytical errors and reflect combined systematic and experimental variability and (in parenthesis) experimental variability alone (see 6.0). Blue indicates samples with accepted age estimates, red, age estimates with caveats (see Table 2). MAM, Minimum Age Model; FMM, Finite Mixture Model; CAM, Central Age Model (see 4.2.1)

Generic considerations	Field Code	Lab Code	Sample specific considerations
None	SOAR01	GL06005	Overdispersion of regenerative-dose data (see 4.1.4). Minor disequilibrium (see 5.0). Accept tentatively
	SOAR02	GL06006	Accept
	SOAR03	GL06007	Overdispersion of regenerative-dose data (see 4.1.4). Accept tentatively
	SOAR04	GL06008	Accept
	SOAR05	GL06009	Minor disequilibrium (see 5.0). Accept tentatively
	GEO 2	GL06014	Major disequilibrium (see 5.0). Accept tentatively
	GEO 3	GL06015	Minor disequilibrium (see 5.0). Accept tentatively
	GEO 4	GL06016	Insufficient mass to verify optimum D_e measurement conditions (see 4.1.2). Accept tentatively
	GEO 5	GL06017	Insufficient mass to verify optimum D_e measurement conditions (see 4.1.2). Insufficient number of aliquots to accurately quantify D_e value. Reject
	GEO 7	GL06018	Insufficient mass to verify optimum D_e measurement conditions (see 4.1.2). Accept tentatively
	GEO 11	GL06019	Insufficient mass to verify optimum D_e measurement conditions (see 4.1.2). Accept tentatively Minor disequilibrium (see 5.0). Accept tentatively
	GEO 12	GL06020	Accept
	GEO 14	GL06021	Overdispersion of regenerative-dose data (see 4.1.4). Minor disequilibrium (see 5.0). Accept tentatively
	GEO 17	GL06022	Insufficient mass to verify optimum D_e measurement conditions (see 4.1.2). Accept tentatively
	GEO 18	GL06023	Minor disequilibrium (see 5.0). Accept tentatively
	GEO 22	GL06024	Accept
	GEO 24	GL06025	Insufficient mass to verify optimum D_e measurement conditions (see 4.1.2). Major disequilibrium (see 5.0). Accept tentatively
	GEO 25	GL06026	Accept
	GEO 27	GL06028	Insufficient mass to verify optimum D_e measurement conditions (see 4.1.2). Accept tentatively
	GEO 29	GL06030	Overdispersion of regenerative-dose data (see 4.1.4). Accept tentatively
	GEO 30	GL06031	Overdispersion of regenerative-dose data (see 4.1.4). Accept tentatively

Table 2 Analytical acceptability of sample suite age estimates and caveats for consideration

Fig. 1 Signal Calibration

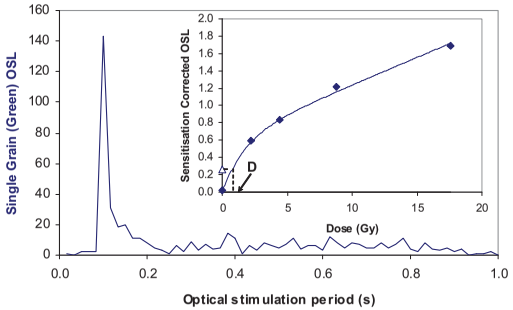

Fig. 1 Signal Calibration Single quartz sand grain natural (green) OSL signal. Inset, the natural green OSL signal (open triangle) of each aliquot is calibrated against known laboratory doses to yield equivalent dose (D_e) values.

Fig. 2 Irradiation-Preheat Cycling The acquisition of D_e values is necessarily predicated upon thermal treatment of aliquots succeeding environmental and laboratory irradiation. Repeated irradiation and thermal treatment results in aliquot sensitisation, rendering calibration of the natural signal inaccurate. This sensitisation can be monitored and corrected for. The accuracy of correction can be preheat dependent; irradiation-preheat cycling quantifies this dependence for laboratory-induced signals, examining the reproducibility of corrected OSL resultant of repeat laboratory doses. This element was based on multi-grain aliquots.

Fig. 3 D_e Preheat Dependence Quantifies the combined effects of thermal transfer and sensitisation on the natural signal. Insignificant adjustment in D_e may reflect limited influence of these effects. This element was based on multi-grain aliquots.

Fig. 4 Dose Recovery Attempts to replicate the above diagnostic, yet provide improved resolution of thermal effects through removal of variability induced by heterogeneous dose absorption in the environment and using a precise lab dose to simulate natural dose. This element was performed on multi-grain aliquots. Based on this and preceding data an appropriate thermal treatment is selected to refine the final D_e value.

Fig. 5 Inter-grain D_e distribution Provides a measure of inter-grain dispersion in D_e values derived from **natural** and **laboratory** irradiation. Discordant data (those points lying beyond **±2 standardised ln D_e**) reflects heterogeneous dose absorption and/or inaccuracies in calibration. Three estimates of post-burial D_e values are illustrated based on the Minimum, Finite Mixture and Central Age Models. n is the number of grains fulfilling acceptability citeria; σ_N is the fractional overdispersion of D_e values about the Central De value; σ_R is the fractional overdispersion of D_e values about a known regenerative-dose value; k indicates the component number and P the proportion of grains within that component generated by the Finite Mixture Model.

Fig. 7 U Activity Statistical concordance (equilibrium) in the activities of the daughter radioisotope ^{226}Ra with its parent ^{238}U may signify the temporal stability of D_r emissions from these chains. Significant differences (disequilibrium; >50%) in activity indicate addition or removal of isotopes creating a time-dependent shift in D_r values and increased uncertainty in the accuracy of age estimates. 20% disequilibrium marker also shown.

Fig. 8 Age Range An estimate of sediment burial period based on mean D_r values and D_e values derived from Minimum, Finite Mixture and Central Age Models, along with associated analytical uncertainties. The probability distribution indicates the inter-grain variability in age. The maximum influence of temporal variations in D_r forced by minima-maxima variation in moisture content and overburden thickness, here coupled with Finite Mixture D_e values, may prove instructive where there is uncertainty in these parameters, however the combined extremes represented should not be construed as preferred age estimates.

Fig. 2 Irradiation-Preheat Cycling

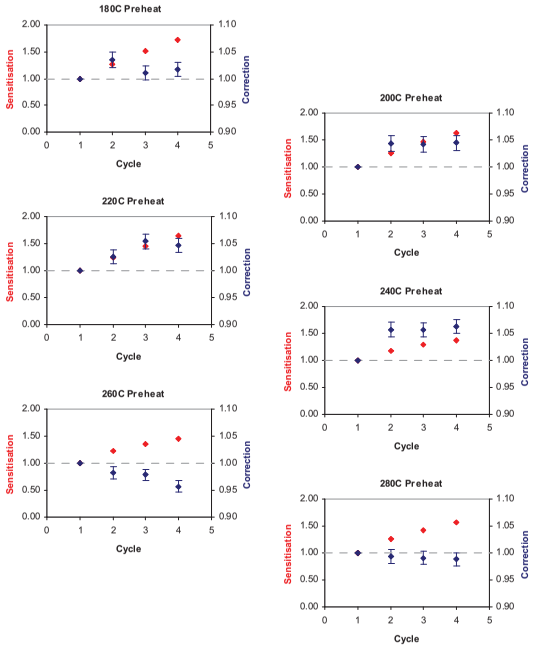

Fig. 3 D_e Preheat Dependence

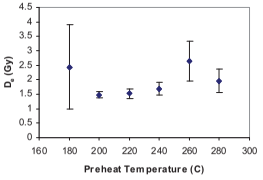

Fig. 4 Dose Recovery

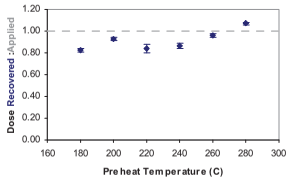

Fig. 5 Inter-grain D_e distribution

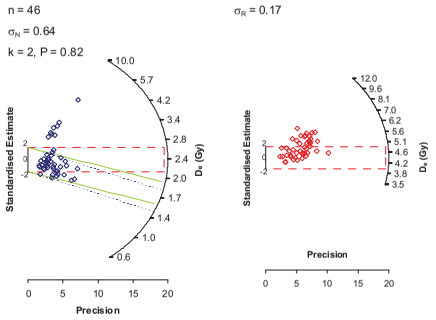

Fig. 6 U Activity

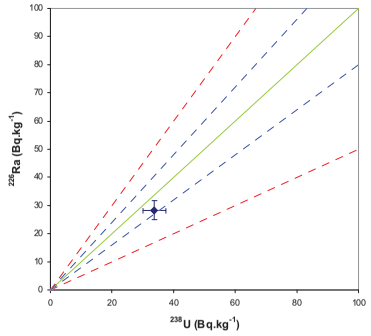

Fig. 7 Age Range

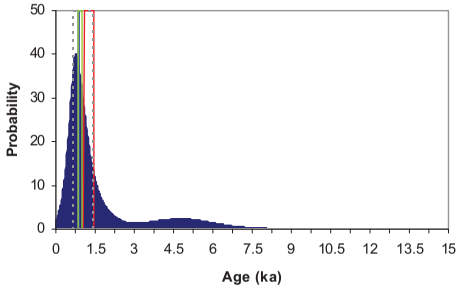

Sample: GL06005

Fig. 1 Signal Calibration

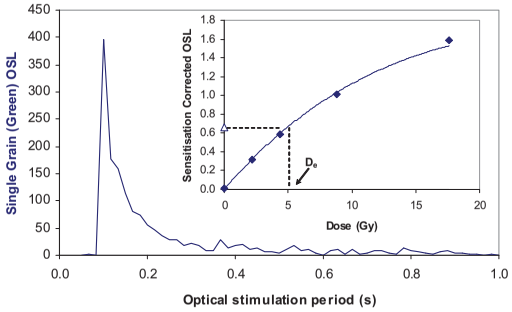

Fig. 1 Signal Calibration Single quartz sand grain natural (green) OSL signal. Inset, the natural green OSL signal (open triangle) of each aliquot is calibrated against known laboratory doses to yield equivalent dose (D_e) values.

Fig. 2 Irradiation-Preheat Cycling The acquisition of D_e values is necessarily predicated upon thermal treatment of aliquots succeeding environmental and laboratory irradiation. Repeated irradiation and thermal treatment results in aliquot sensitisation, rendering calibration of the natural signal inaccurate. This sensitisation can be monitored and corrected for. The accuracy of correction can be preheat dependent; irradiation-preheat cycling quantifies this dependence for laboratory-induced signals, examining the reproducibility of corrected OSL resultant of repeat laboratory doses. This element was based on multi-grain aliquots.

Fig. 3 D_e Preheat Dependence Quantifies the combined effects of thermal transfer and sensitisation on the natural signal. Insignificant adjustment in D_e may reflect limited influence of these effects. This element was based on multi-grain aliquots.

Fig. 4 Dose Recovery Attempts to replicate the above diagnostic, yet provide improved resolution of thermal effects through removal of variability induced by heterogeneous dose absorption in the environment and using a precise lab dose to simulate natural dose. This element was performed on multi-grain aliquots. Based on this and preceding data an appropriate thermal treatment is selected to refine the final D_e value.

Fig. 5 Inter-grain D_e distribution Provides a measure of inter-grain dispersion in D_e values derived from **natural** and **laboratory** irradiation. Discordant data (those points lying beyond **±2 standardised ln D_e**) reflects heterogeneous dose absorption and/or inaccuracies in calibration. Three estimates of post-burial D_e values are illustrated based on the Minimum, Finite Mixture and Central Age Models. n is the number of grains fulfilling acceptability citeria; σ_N is the fractional overdispersion of D_e values about the Central De value; σ_R is the fractional overdispersion of D_e values about a known regenerative-dose value; k indicates the component number and P the proportion of grains within that component generated by the Finite Mixture Model.

Fig. 7 U Activity Statistical concordance (equilibrium) in the activities of the daughter radioisotope ^{226}Ra with its parent ^{238}U may signify the temporal stability of D_e emissions from these chains. Significant differences (disequilibrium; >50%) in activity indicate addition or removal of isotopes creating a time-dependent shift in D_e values and increased uncertainty in the accuracy of age estimates. 20% disequilibrium marker also shown.

Fig. 8 Age Range An estimate of sediment burial period based on mean D_e values and D_e values derived from Minimum, Finite Mixture and Central Age Models, along with associated analytical uncertainties. The probability distribution indicates the inter-grain variability in age. The maximum influence of temporal variations in D_e forced by minima-maxima variation in moisture content and overburden thickness, here coupled with Finite Mixture D_e values, may prove instructive where there is uncertainty in these parameters, however the combined extremes represented should not be construed as preferred age estimates.

Fig. 2 Irradiation-Preheat Cycling

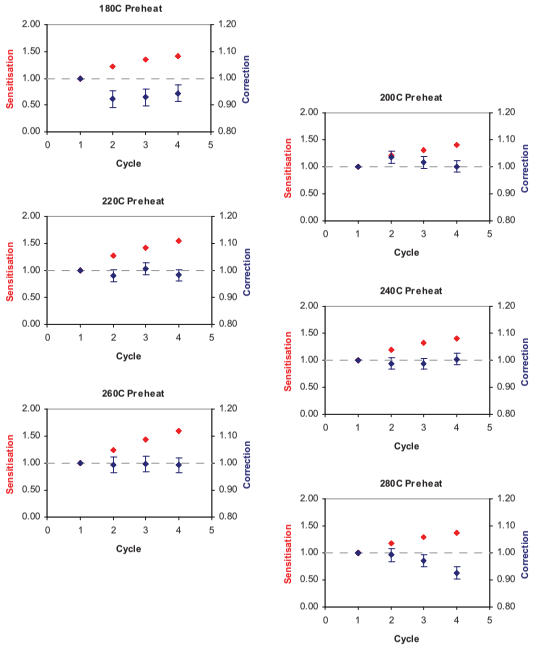

Fig. 3 D_e Preheat Dependence

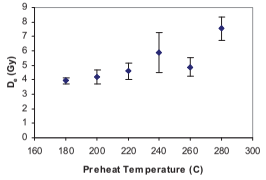

Fig. 4 Dose Recovery

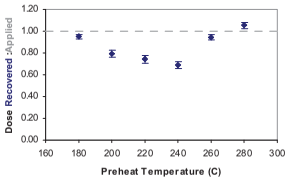

Sample: GL06006

Fig. 5 Inter-grain D_e distribution

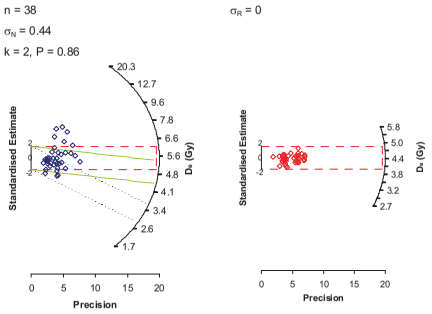

Fig. 6 U Activity

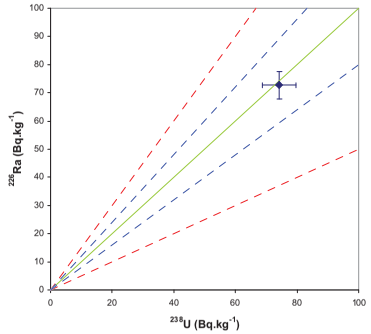

Fig. 7 Age Range

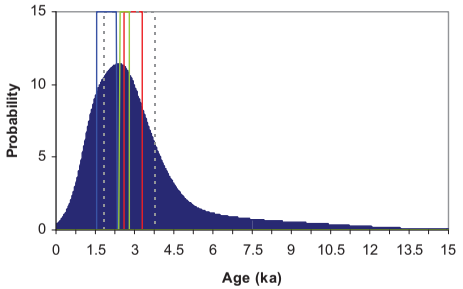

Fig. 1 Signal Calibration

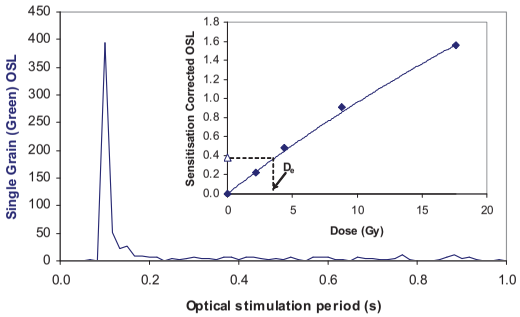

Fig. 1 Signal Calibration Single quartz sand grain natural (green) OSL signal. Inset, the natural green OSL signal (open triangle) of each aliquot is calibrated against known laboratory doses to yield equivalent dose (D_e) values.

Fig. 2 Irradiation-Preheat Cycling The acquisition of D_e values is necessarily predicated upon thermal treatment of aliquots succeeding environmental and laboratory irradiation. Repeated irradiation and thermal treatment results in aliquot sensitisation, rendering calibration of the natural signal inaccurate. This sensitisation can be monitored and corrected for. The accuracy of correction can be preheat dependent; irradiation-preheat cycling quantifies this dependence for laboratory-induced signals, examining the reproducibility of corrected OSL resultant of repeat laboratory doses. This element was based on multi-grain aliquots.

Fig. 3 D_e Preheat Dependence Quantifies the combined effects of thermal transfer and sensitisation on the natural signal. Insignificant adjustment in D_e may reflect limited influence of these effects. This element was based on multi-grain aliquots.

Fig. 4 Dose Recovery Attempts to replicate the above diagnostic, yet provide improved resolution of thermal effects through removal of variability induced by heterogeneous dose absorption in the environment and using a precise lab dose to simulate natural dose. This element was performed on multi-grain aliquots. Based on this and preceding data an appropriate thermal treatment is selected to refine the final D_e value.

Fig. 5 Inter-grain D_e distribution Provides a measure of inter-grain dispersion in D_e values derived from **natural** and **laboratory** irradiation. Discordant data (those points lying beyond **±2 standardised ln D_e**) reflects heterogeneous dose absorption and/or inaccuracies in calibration. Three estimates of post-burial D_e values are illustrated based on the Minimum, Finite Mixture and Central Age Models. n is the number of grains fulfilling acceptability citeria; σ_N is the fractional overdispersion of D_e values about the Central De value; σ_R is the fractional overdispersion of D_e values about a known regenerative-dose value; k indicates the component number and P the proportion of grains within that component generated by the Finite Mixture Model.

Fig. 7 U Activity Statistical concordance (equilibrium) in the activities of the daughter radioisotope ^{226}Ra with its parent ^{238}U may signify the temporal stability of D_r emissions from these chains. Significant differences (disequilibrium; >50%) in activity indicate addition or removal of isotopes creating a time-dependent shift in D_r values and increased uncertainty in the accuracy of age estimates. 20% disequilibrium marker also shown.

Fig. 8 Age Range An estimate of sediment burial period based on mean D_r values and D_e values derived from Minimum, Finite Mixture and Central Age Models, along with associated analytical uncertainties. The probability distribution indicates the inter-grain variability in age. The maximum influence of temporal variations in D_r forced by minima-maxima variation in moisture content and overburden thickness, here coupled with Finite Mixture D_e values, may prove instructive where there is uncertainty in these parameters, however the combined extremes represented should not be construed as preferred age estimates.

Fig. 2 Irradiation-Preheat Cycling

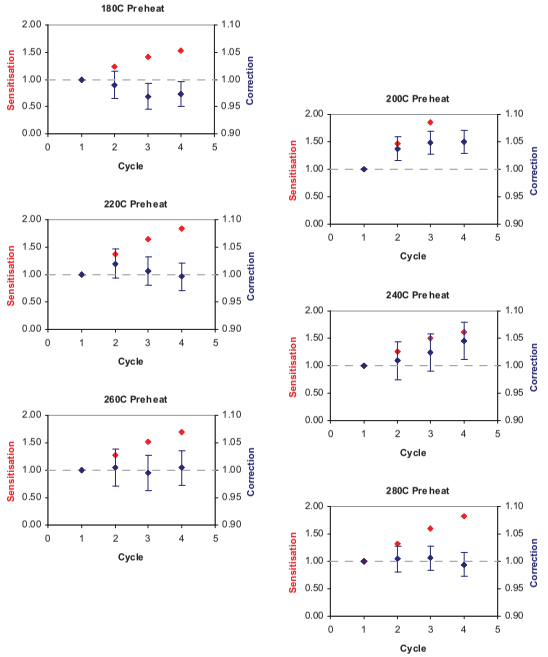

Fig. 3 D_e Preheat Dependence

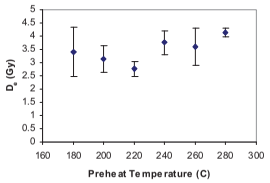

Fig. 4 Dose Recovery

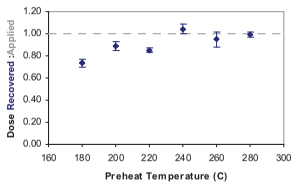

Sample: GL06007

Fig. 5 Inter-grain D_e distribution

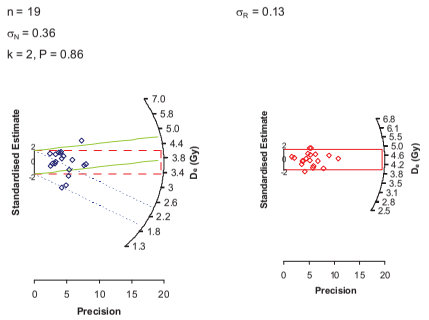

Fig. 6 U Activity

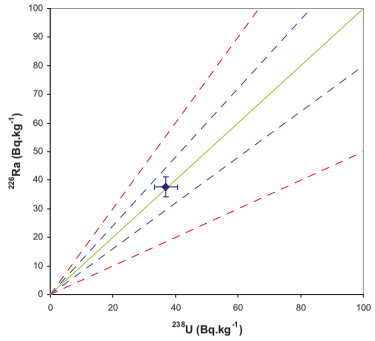

Fig. 7 Age Range

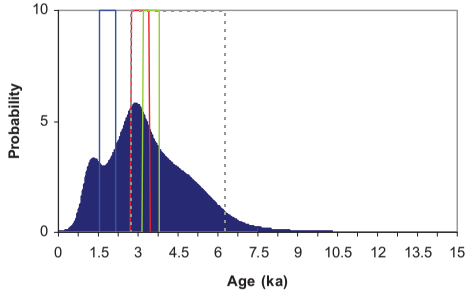

Fig. 1 Signal Calibration

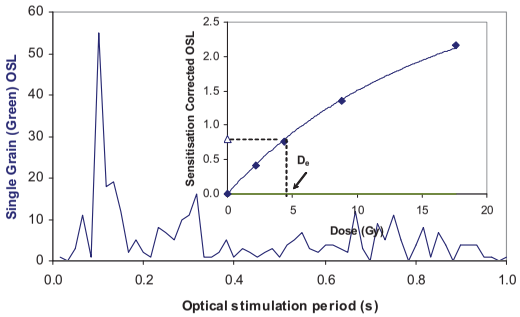

Fig. 1 Signal Calibration Single quartz sand grain natural (green) OSL signal. Inset, the natural green OSL signal (open triangle) of each aliquot is calibrated against known laboratory doses to yield equivalent dose (D_e) values.

Fig. 2 Irradiation-Preheat Cycling

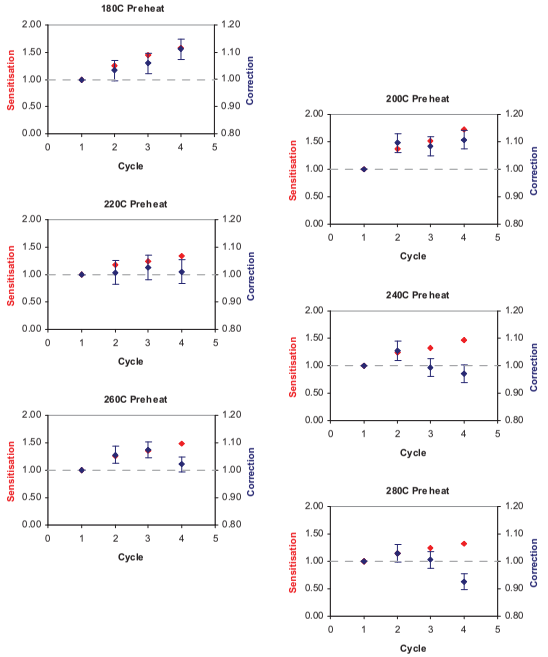

Fig. 2 Irradiation-Preheat Cycling The acquisition of D_e values is necessarily predicated upon thermal treatment of aliquots succeeding environmental and laboratory irradiation. Repeated irradiation and thermal treatment results in aliquot sensitisation, rendering calibration of the natural signal inaccurate. This sensitisation can be monitored and corrected for. The accuracy of correction can be preheat dependent; irradiation-preheat cycling quantifies this dependence for laboratory-induced signals, examining the reproducibility of corrected OSL resultant of repeat laboratory doses. This element was based on multi-grain aliquots.

Fig. 3 D_e Preheat Dependence

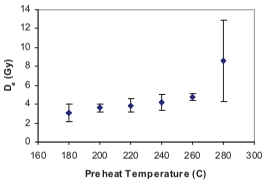

Fig. 3 D_e Preheat Dependence Quantifies the combined effects of thermal transfer and sensitisation on the natural signal. Insignificant adjustment in D_e may reflect limited influence of these effects. This element was based on multi-grain aliquots.

Fig. 4 Dose Recovery

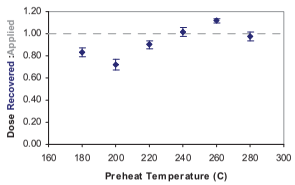

Fig. 4 Dose Recovery Attempts to replicate the above diagnostic, yet provide improved resolution of thermal effects through removal of variability induced by heterogeneous dose absorption in the environment and using a precise lab dose to simulate natural dose. This element was performed on multi-grain aliquots. Based on this and preceding data an appropriate thermal treatment is selected to refine the final D_e value.

Fig. 5 Inter-grain D_e distribution

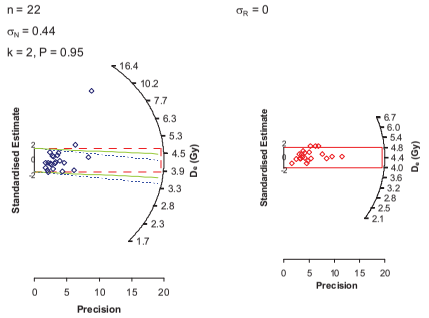

Fig. 5 Inter-grain D_e distribution Provides a measure of inter-grain dispersion in D_e values derived from **natural** and **laboratory** irradiation. Discordant data (those points lying beyond **±2 standardised ln D_e**) reflects heterogeneous dose absorption and/or inaccuracies in calibration. Three estimates of post-burial D_e values are illustrated based on the Minimum, Finite Mixture and Central Age Models. n is the number of grains fulfilling acceptability citeria; σ_N is the fractional overdispersion of D_e values about the Central De value; σ_R is the fractional overdispersion of D_e values about a known regenerative-dose value; k indicates the component number and P the proportion of grains within that component generated by the Finite Mixture Model.

Fig. 6 U Activity

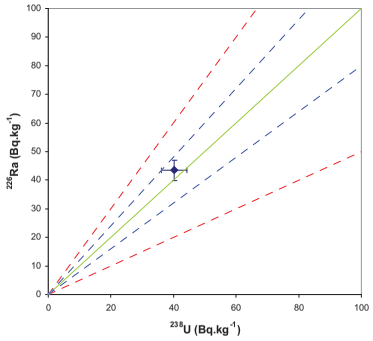

Fig. 7 U Activity Statistical concordance (equilibrium) in the activities of the daughter radioisotope ^{226}Ra with its parent ^{238}U may signify the temporal stability of D_r emissions from these chains. Significant differences (disequilibrium; >50%) in activity indicate addition or removal of isotopes creating a time-dependent shift in D_r values and increased uncertainty in the accuracy of age estimates. 20% disequilibrium marker also shown.

Fig. 7 Age Range

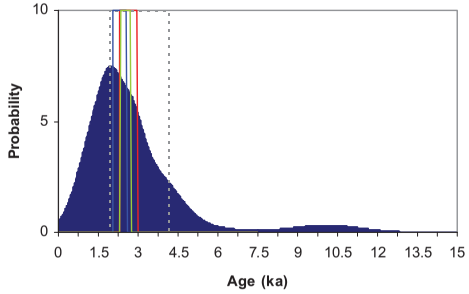

Fig. 8 Age Range An estimate of sediment burial period based on mean D_r values and D_e values derived from Minimum, Finite Mixture and Central Age Models, along with associated analytical uncertainties. The probability distribution indicates the inter-grain variability in age. The maximum influence of temporal variations in D_r forced by minima-maxima variation in moisture content and overburden thickness, here coupled with Finite Mixture D_e values, may prove instructive where there is uncertainty in these parameters, however the combined extremes represented should not be construed as preferred age estimates.

Sample: GL06008

Fig. 1 Signal Calibration

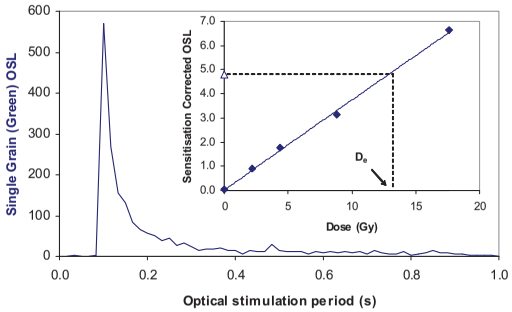

Fig. 1 Signal Calibration Single quartz sand grain natural (green) OSL signal. Inset, the natural green OSL signal (open triangle) of each aliquot is calibrated against known laboratory doses to yield equivalent dose (D_e) values.

Fig. 2 Irradiation-Preheat Cycling

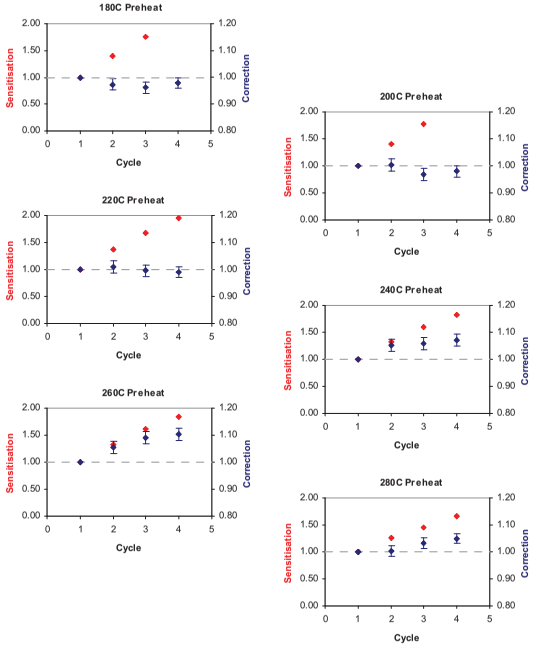

Fig. 2 Irradiation-Preheat Cycling The acquisition of D_e values is necessarily predicated upon thermal treatment of aliquots succeeding environmental and laboratory irradiation. Repeated irradiation and thermal treatment results in aliquot sensitisation, rendering calibration of the natural signal inaccurate. This sensitisation can be monitored and corrected for. The accuracy of correction can be preheat dependent; irradiation-preheat cycling quantifies this dependence for laboratory-induced signals, examining the reproducibility of corrected OSL resultant of repeat laboratory doses. This element was based on multi-grain aliquots.

Fig. 3 D_e Preheat Dependence

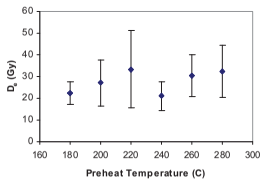

Fig. 3 D_e Preheat Dependence Quantifies the combined effects of thermal transfer and sensitisation on the natural signal. Insignificant adjustment in D_e may reflect limited influence of these effects. This element was based on multi-grain aliquots.

Fig. 4 Dose Recovery

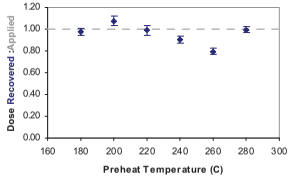

Fig. 4 Dose Recovery Attempts to replicate the above diagnostic, yet provide improved resolution of thermal effects through removal of variability induced by heterogeneous dose absorption in the environment and using a precise lab dose to simulate natural dose. This element was performed on multi-grain aliquots. Based on this and preceding data an appropriate thermal treatment is selected to refine the final D_e value.

Fig. 5 Inter-grain D_e distribution

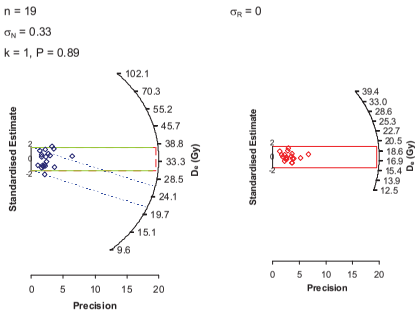

Fig. 5 Inter-grain D_e distribution Provides a measure of inter-grain dispersion in D_e values derived from **natural** and **laboratory** irradiation. Discordant data (those points lying beyond **±2 standardised ln D_e**) reflects heterogeneous dose absorption and/or inaccuracies in calibration. Three estimates of post-burial D_e values are illustrated based on the Minimum, Finite Mixture and Central Age Models. n is the number of grains fulfilling acceptability citeria; σ_N is the fractional overdispersion of D_e values about the Central De value; σ_R is the fractional overdispersion of D_e values about a known regenerative-dose value; k indicates the component number and P the proportion of grains within that component generated by the Finite Mixture Model.

Fig. 6 U Activity

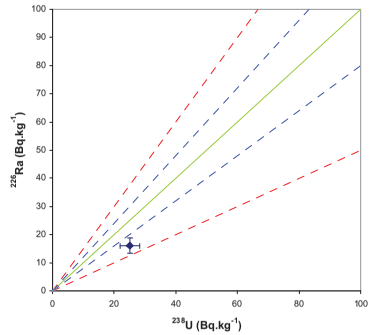

Fig. 7 U Activity Statistical concordance (equilibrium) in the activities of the daughter radioisotope ^{226}Ra with its parent ^{238}U may signify the temporal stability of D_r emissions from these chains. Significant differences (disequilibrium; >50%) in activity indicate addition or removal of isotopes creating a time-dependent shift in D_r values and increased uncertainty in the accuracy of age estimates. 20% disequilibrium marker also shown.

Fig. 7 Age Range

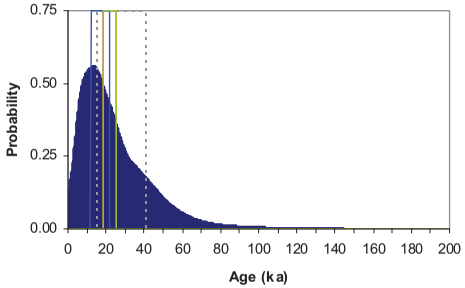

Fig. 8 Age Range An estimate of sediment burial period based on mean D_r values and D_e values derived from Minimum, Finite Mixture and Central Age Models, along with associated analytical uncertainties. The probability distribution indicates the inter-grain variability in age. The maximum influence of temporal variations in D_r forced by minima-maxima variation in moisture content and overburden thickness, here coupled with Finite Mixture D_e values, may prove instructive where there is uncertainty in these parameters, however the combined extremes represented should not be construed as preferred age estimates.

Sample: GL06009

Fig. 1 Signal Calibration

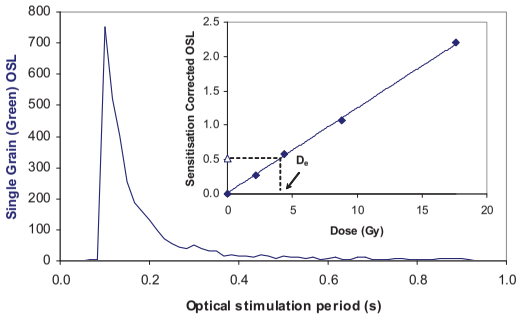

Fig. 1 Signal Calibration Single quartz sand grain natural (green) OSL signal. Inset, the natural green OSL signal (open triangle) of each aliquot is calibrated against known laboratory doses to yield equivalent dose (D_e) values.

Fig. 2 Irradiation-Preheat Cycling The acquisition of D_e values is necessarily predicated upon thermal treatment of aliquots succeeding environmental and laboratory irradiation. Repeated irradiation and thermal treatment results in aliquot sensitisation, rendering calibration of the natural signal inaccurate. This sensitisation can be monitored and corrected for. The accuracy of correction can be preheat dependent; irradiation-preheat cycling quantifies this dependence for laboratory-induced signals, examining the reproducibility of corrected OSL resultant of repeat laboratory doses. This element was based on multi-grain aliquots.

Fig. 3 D_e Preheat Dependence Quantifies the combined effects of thermal transfer and sensitisation on the natural signal. Insignificant adjustment in D_e may reflect limited influence of these effects. This element was based on multi-grain aliquots.

Fig. 4 Dose Recovery Attempts to replicate the above diagnostic, yet provide improved resolution of thermal effects through removal of variability induced by heterogeneous dose absorption in the environment and using a precise lab dose to simulate natural dose. This element was performed on multi-grain aliquots. Based on this and preceding data an appropriate thermal treatment is selected to refine the final D_e value.

Fig. 5 Inter-grain D_e distribution Provides a measure of inter-grain dispersion in D_e values derived from **natural** and **laboratory** irradiation. Discordant data (those points lying beyond **±2 standardised ln D_e**) reflects heterogeneous dose absorption and/or inaccuracies in calibration. Three estimates of post-burial D_e values are illustrated based on the Minimum, Finite Mixture and Central Age Models. n is the number of grains fulfilling acceptability citeria; σ_N is the fractional overdispersion of D_e values about the Central De value; σ_R is the fractional overdispersion of D_e values about a known regenerative-dose value; k indicates the component number and P the proportion of grains within that component generated by the Finite Mixture Model.

Fig. 7 U Activity Statistical concordance (equilibrium) in the activities of the daughter radioisotope ^{226}Ra with its parent ^{238}U may signify the temporal stability of D_r emissions from these chains. Significant differences (disequilibrium; >50%) in activity indicate addition or removal of isotopes creating a time-dependent shift in D_r values and increased uncertainty in the accuracy of age estimates. 20% disequilibrium marker also shown.

Fig. 8 Age Range An estimate of sediment burial period based on mean D_r values and D_e values derived from Minimum, Finite Mixture and Central Age Models, along with associated analytical uncertainties. The probability distribution indicates the inter-grain variability in age. The maximum influence of temporal variations in D_r forced by minima-maxima variation in moisture content and overburden thickness, here coupled with Finite Mixture D_e values, may prove instructive where there is uncertainty in these parameters, however the combined extremes represented should not be construed as preferred age estimates.

Fig. 2 Irradiation-Preheat Cycling

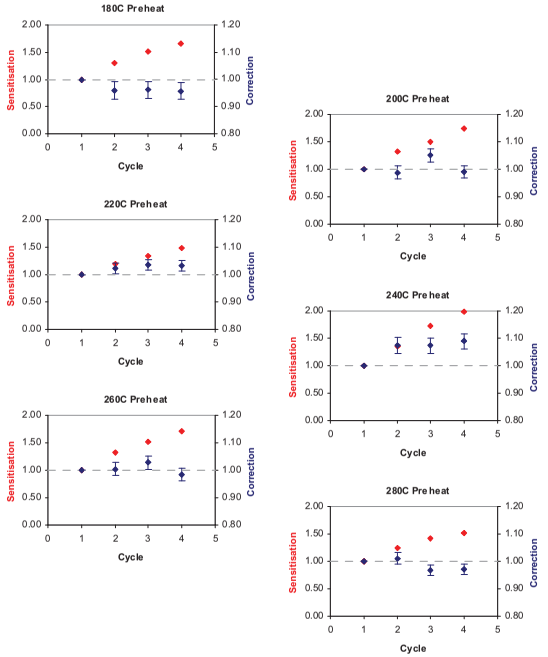

Fig. 3 D_e Preheat Dependence

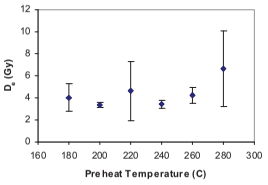

Fig. 4 Dose Recovery

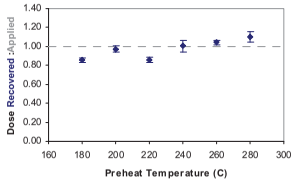

Sample: GL06014

Fig. 5 Inter-grain D_e distribution

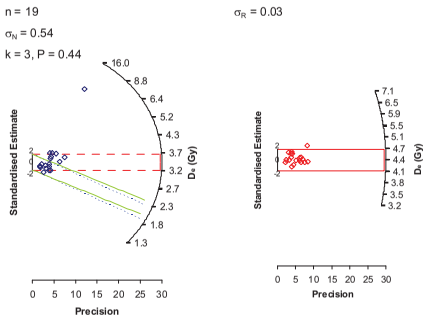

Fig. 6 U Activity

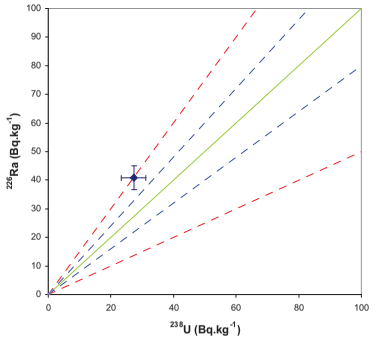

Fig. 7 Age Range

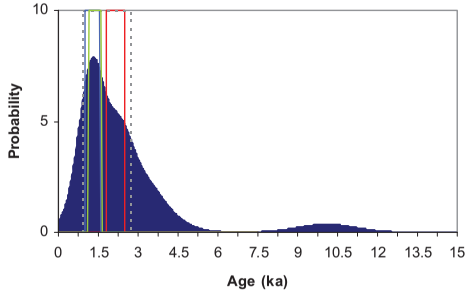

Fig. 1 Signal Calibration

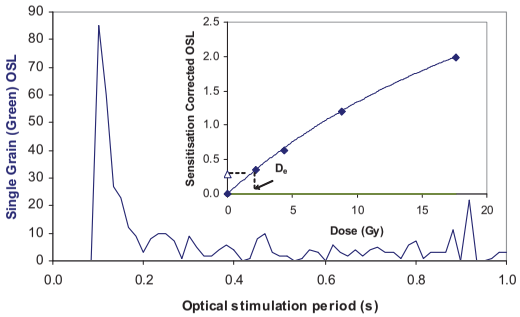

Fig. 1 Signal Calibration Single quartz sand grain natural (green) OSL signal. Inset, the natural green OSL signal (open triangle) of each aliquot is calibrated against known laboratory doses to yield equivalent dose (D_e) values.

Fig. 2 Irradiation-Preheat Cycling The acquisition of D_e values is necessarily predicated upon thermal treatment of aliquots succeeding environmental and laboratory irradiation. Repeated irradiation and thermal treatment results in aliquot sensitisation, rendering calibration of the natural signal inaccurate. This sensitisation can be monitored and corrected for. The accuracy of correction can be preheat dependent; irradiation-preheat cycling quantifies this dependence for laboratory-induced signals, examining the reproducibility of corrected OSL resultant of repeat laboratory doses. This element was based on multi-grain aliquots.

Fig. 3 D_e Preheat Dependence Quantifies the combined effects of thermal transfer and sensitisation on the natural signal. Insignificant adjustment in D_e may reflect limited influence of these effects. This element was based on multi-grain aliquots.

Fig. 4 Dose Recovery Attempts to replicate the above diagnostic, yet provide improved resolution of thermal effects through removal of variability induced by heterogeneous dose absorption in the environment and using a precise lab dose to simulate natural dose. This element was performed on multi-grain aliquots. Based on this and preceding data an appropriate thermal treatment is selected to refine the final D_e value.

Fig. 5 Inter-grain D_e distribution Provides a measure of inter-grain dispersion in D_e values derived from **natural** and **laboratory** irradiation. Discordant data (those points lying beyond **±2 standardised ln D_e**) reflects heterogeneous dose absorption and/or inaccuracies in calibration. Three estimates of post-burial D_e values are illustrated based on the Minimum, Finite Mixture and Central Age Models. n is the number of grains fulfilling acceptability citeria; σ_N is the fractional overdispersion of D_e values about the Central De value; σ_R is the fractional overdispersion of D_e values about a known regenerative-dose value; k indicates the component number and P the proportion of grains within that component generated by the Finite Mixture Model.

Fig. 7 U Activity Statistical concordance (equilibrium) in the activities of the daughter radioisotope ^{226}Ra with its parent ^{238}U may signify the temporal stability of D_r emissions from these chains. Significant differences (disequilibrium; >50%) in activity indicate addition or removal of isotopes creating a time-dependent shift in D_r values and increased uncertainty in the accuracy of age estimates. 20% disequilibrium marker also shown.

Fig. 8 Age Range An estimate of sediment burial period based on mean D_r values and D_e values derived from Minimum, Finite Mixture and Central Age Models, along with associated analytical uncertainties. The probability distribution indicates the inter-grain variability in age. The maximum influence of temporal variations in D_r forced by minima-maxima variation in moisture content and overburden thickness, here coupled with Finite Mixture D_e values, may prove instructive where there is uncertainty in these parameters, however the combined extremes represented should not be construed as preferred age estimates.

Fig. 2 Irradiation-Preheat Cycling

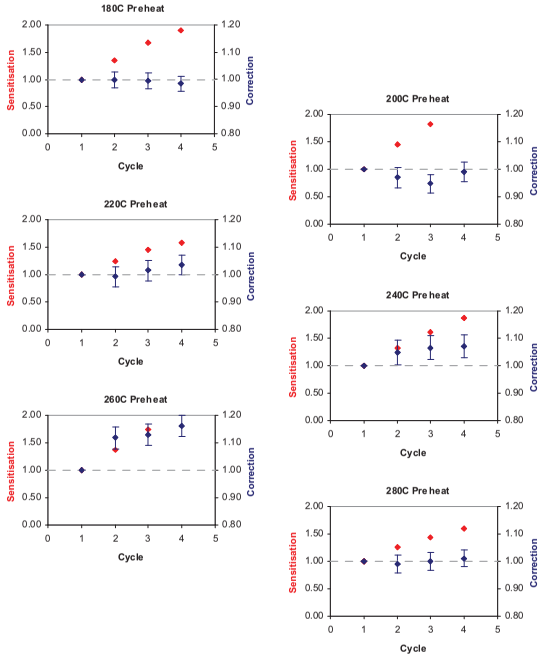

Fig. 3 D_e Preheat Dependence

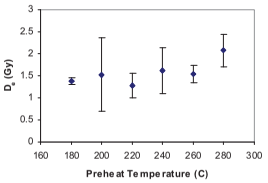

Fig. 4 Dose Recovery

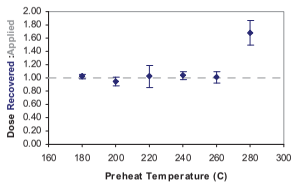

Sample: GL06015

Fig. 5 Inter-grain D_e distribution

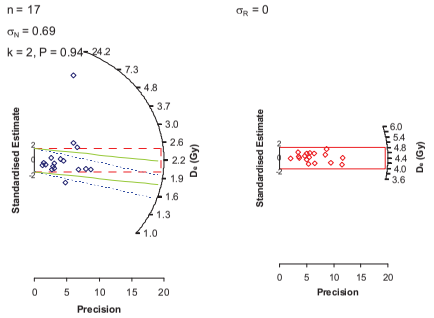

Fig. 6 U Activity

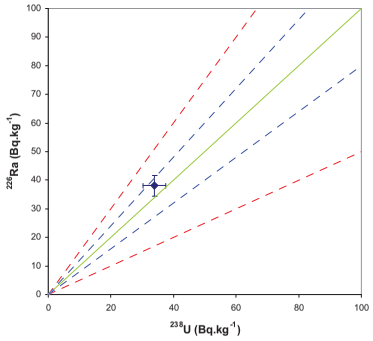

Fig. 7 Age Range

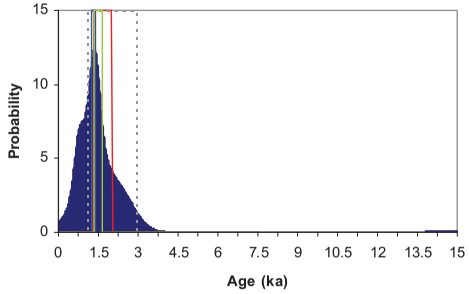

Fig. 1 Signal Calibration

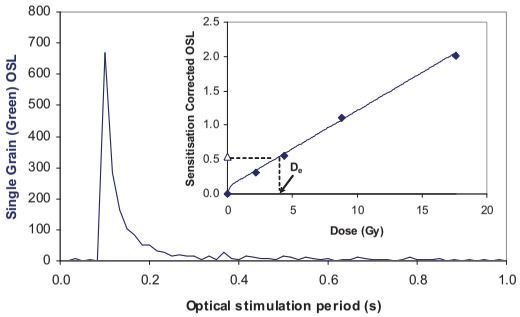

Fig. 1 Signal Calibration Single quartz sand grain natural (green) OSL signal. Inset, the natural green OSL signal (open triangle) of each aliquot is calibrated against known laboratory doses to yield equivalent dose (D_e) values.

Fig. 2 Irradiation-Preheat Cycling The acquisition of D_e values is necessarily predicated upon thermal treatment of aliquots succeeding environmental and laboratory irradiation. Repeated irradiation and thermal treatment results in aliquot sensitisation, rendering calibration of the natural signal inaccurate. This sensitisation can be monitored and corrected for. The accuracy of correction can be preheat dependent; irradiation-preheat cycling quantifies this dependence for laboratory-induced signals, examining the reproducibility of corrected OSL resultant of repeat laboratory doses. This element was based on multi-grain aliquots.

Fig. 3 D_e Preheat Dependence Quantifies the combined effects of thermal transfer and sensitisation on the natural signal. Insignificant adjustment in D_e may reflect limited influence of these effects. This element was based on multi-grain aliquots.

Fig. 4 Dose Recovery Attempts to replicate the above diagnostic, yet provide improved resolution of thermal effects through removal of variability induced by heterogeneous dose absorption in the environment and using a precise lab dose to simulate natural dose. This element was performed on multi-grain aliquots. Based on this and preceding data an appropriate thermal treatment is selected to refine the final D_e value.

Fig. 5 Inter-grain D_e distribution Provides a measure of inter-grain dispersion in D_e values derived from **natural** and **laboratory** irradiation. Discordant data (those points lying beyond **±2 standardised ln D_e**) reflects heterogeneous dose absorption and/or inaccuracies in calibration. Three estimates of post-burial D_e values are illustrated based on the Minimum, Finite Mixture and Central Age Models. n is the number of grains fulfilling acceptability citeria; σ_N is the fractional overdispersion of D_e values about the Central De value; σ_R is the fractional overdispersion of D_e values about a known regenerative-dose value; k indicates the component number and P the proportion of grains within that component generated by the Finite Mixture Model.

Fig. 7 U Activity Statistical concordance (equilibrium) in the activities of the daughter radioisotope ^{226}Ra with its parent ^{238}U may signify the temporal stability of D_r emissions from these chains. Significant differences (disequilibrium; >50%) in activity indicate addition or removal of isotopes creating a time-dependent shift in D_r values and increased uncertainty in the accuracy of age estimates. 20% disequilibrium marker also shown.

Fig. 8 Age Range An estimate of sediment burial period based on mean D_r values and D_e values derived from Minimum, Finite Mixture and Central Age Models, along with associated analytical uncertainties. The probability distribution indicates the inter-grain variability in age. The maximum influence of temporal variations in D_r forced by minima-maxima variation in moisture content and overburden thickness, here coupled with Finite Mixture D_e values, may prove instructive where there is uncertainty in these parameters, however the combined extremes represented should not be construed as preferred age estimates.

Fig. 2 Irradiation-Preheat Cycling

Insufficient Sample Mass

Fig. 3 D_e Preheat Dependence

Insufficient Sample Mass

Fig. 4 Dose Recovery

Insufficient Sample Mass

Sample: GL06016

Fig. 5 Inter-grain D_e distribution

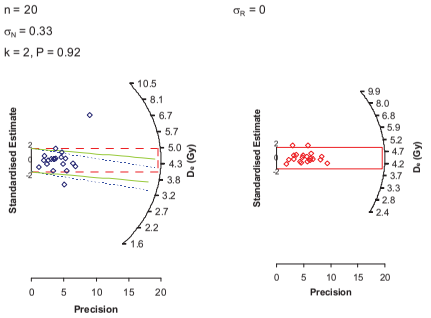

Fig. 6 U Activity

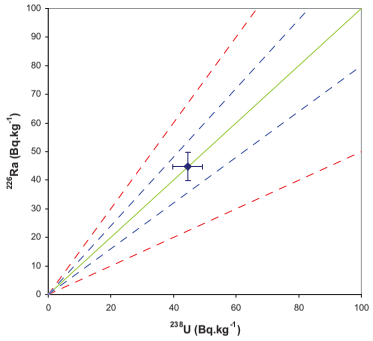

Fig. 7 Age Range

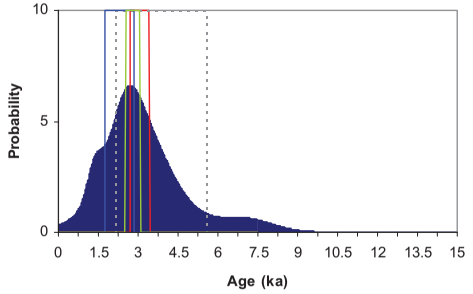

Fig. 1 Signal Calibration

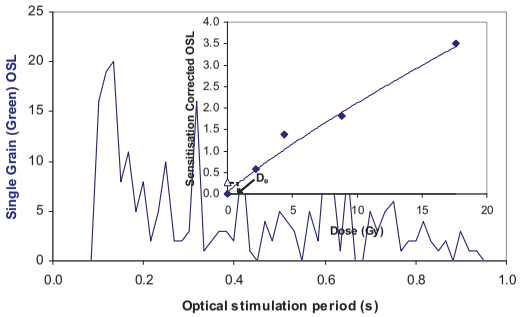

Fig. 1 Signal Calibration Single quartz sand grain natural (green) OSL signal. Inset, the natural green OSL signal (open triangle) of each aliquot is calibrated against known laboratory doses to yield equivalent dose (D_e) values.

Fig. 2 Irradiation-Preheat Cycling The acquisition of D_e values is necessarily predicated upon thermal treatment of aliquots succeeding environmental and laboratory irradiation. Repeated irradiation and thermal treatment results in aliquot sensitisation, rendering calibration of the natural signal inaccurate. This sensitisation can be monitored and corrected for. The accuracy of correction can be preheat dependent; irradiation-preheat cycling quantifies this dependence for laboratory-induced signals, examining the reproducibility of corrected OSL resultant of repeat laboratory doses. This element was based on multi-grain aliquots.

Fig. 3 D_e Preheat Dependence Quantifies the combined effects of thermal transfer and sensitisation on the natural signal. Insignificant adjustment in D_e may reflect limited influence of these effects. This element was based on multi-grain aliquots.

Fig. 4 Dose Recovery Attempts to replicate the above diagnostic, yet provide improved resolution of thermal effects through removal of variability induced by heterogeneous dose absorption in the environment and using a precise lab dose to simulate natural dose. This element was performed on multi-grain aliquots. Based on this and preceding data an appropriate thermal treatment is selected to refine the final D_e value.

Fig. 5 Inter-grain D_e distribution Provides a measure of inter-grain dispersion in D_e values derived from **natural** and **laboratory** irradiation. Discordant data (those points lying beyond **±2 standardised ln D_e**) reflects heterogeneous dose absorption and/or inaccuracies in calibration. Three estimates of post-burial D_e values are illustrated based on the Minimum, Finite Mixture and Central Age Models. n is the number of grains fulfilling acceptability citeria; σ_N is the fractional overdispersion of D_e values about the Central De value; σ_R is the fractional overdispersion of D_e values about a known regenerative-dose value; k indicates the component number and P the proportion of grains within that component generated by the Finite Mixture Model.

Fig. 7 U Activity Statistical concordance (equilibrium) in the activities of the daughter radioisotope ^{226}Ra with its parent ^{238}U may signify the temporal stability of D_r emissions from these chains. Significant differences (disequilibrium; >50%) in activity indicate addition or removal of isotopes creating a time-dependent shift in D_r values and increased uncertainty in the accuracy of age estimates. 20% disequilibrium marker also shown.

Fig. 8 Age Range An estimate of sediment burial period based on mean D_r values and D_e values derived from Minimum, Finite Mixture and Central Age Models, along with associated analytical uncertainties. The probability distribution indicates the inter-grain variability in age. The maximum influence of temporal variations in D_r forced by minima-maxima variation in moisture content and overburden thickness, here coupled with Finite Mixture D_e values, may prove instructive where there is uncertainty in these parameters, however the combined extremes represented should not be construed as preferred age estimates.

Fig. 2 Irradiation-Preheat Cycling

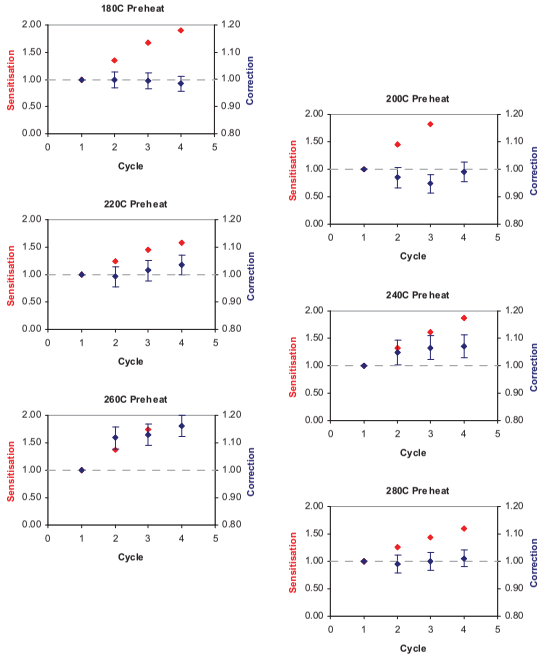

Fig. 3 D_e Preheat Dependence

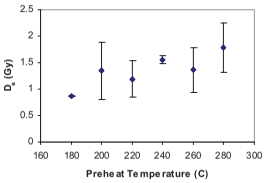

Fig. 4 Dose Recovery

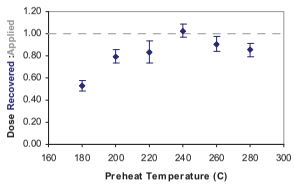

Sample: GL06017

Fig. 5 Inter-grain D_e distribution

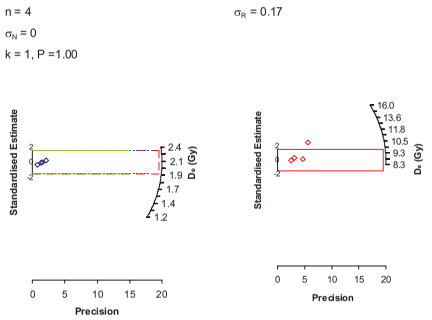

Fig. 6 U Activity

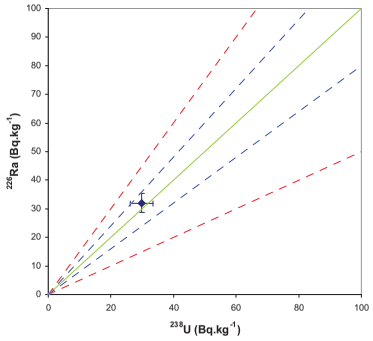

Fig. 7 Age Range

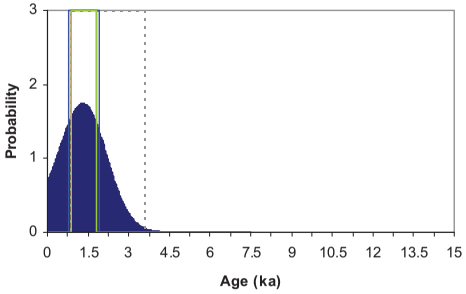

Fig. 1 Signal Calibration

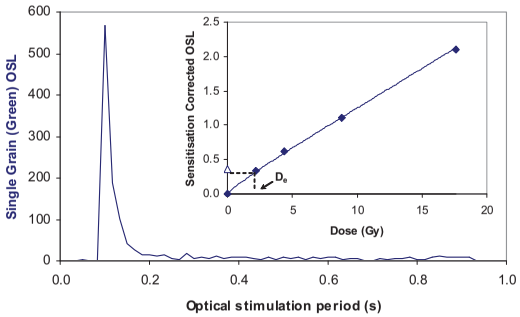

Fig. 1 Signal Calibration Single quartz sand grain natural (green) OSL signal. Inset, the natural green OSL signal (open triangle) of each aliquot is calibrated against known laboratory doses to yield equivalent dose (D_e) values.

Fig. 2 Irradiation-Preheat Cycling The acquisition of D_e values is necessarily predicated upon thermal treatment of aliquots succeeding environmental and laboratory irradiation. Repeated irradiation and thermal treatment results in aliquot sensitisation, rendering calibration of the natural signal inaccurate. This sensitisation can be monitored and corrected for. The accuracy of correction can be preheat dependent; irradiation-preheat cycling quantifies this dependence for laboratory-induced signals, examining the reproducibility of corrected OSL resultant of repeat laboratory doses. This element was based on multi-grain aliquots.

Fig. 3 D_e Preheat Dependence Quantifies the combined effects of thermal transfer and sensitisation on the natural signal. Insignificant adjustment in D_e may reflect limited influence of these effects. This element was based on multi-grain aliquots.

Fig. 4 Dose Recovery Attempts to replicate the above diagnostic, yet provide improved resolution of thermal effects through removal of variability induced by heterogeneous dose absorption in the environment and using a precise lab dose to simulate natural dose. This element was performed on multi-grain aliquots. Based on this and preceding data an appropriate thermal treatment is selected to refine the final D_e value.

Fig. 5 Inter-grain D_e distribution Provides a measure of inter-grain dispersion in D_e values derived from **natural** and **laboratory** irradiation. Discordant data (those points lying beyond **±2 standardised ln D_e**) reflects heterogeneous dose absorption and/or inaccuracies in calibration. Three estimates of post-burial D_e values are illustrated based on the Minimum, Finite Mixture and Central Age Models. n is the number of grains fulfilling acceptability citeria; σ_N is the fractional overdispersion of D_e values about the Central De value; σ_R is the fractional overdispersion of D_e values about a known regenerative-dose value; k indicates the component number and P the proportion of grains within that component generated by the Finite Mixture Model.

Fig. 7 U Activity Statistical concordance (equilibrium) in the activities of the daughter radioisotope ^{226}Ra with its parent ^{238}U may signify the temporal stability of D_r emissions from these chains. Significant differences (disequilibrium; >50%) in activity indicate addition or removal of isotopes creating a time-dependent shift in D_r values and increased uncertainty in the accuracy of age estimates. 20% disequilibrium marker also shown.

Fig. 8 Age Range An estimate of sediment burial period based on mean D_r values and D_e values derived from Minimum, Finite Mixture and Central Age Models, along with associated analytical uncertainties. The probability distribution indicates the inter-grain variability in age. The maximum influence of temporal variations in D_r forced by minima-maxima variation in moisture content and overburden thickness, here coupled with Finite Mixture D_e values, may prove instructive where there is uncertainty in these parameters, however the combined extremes represented should not be construed as preferred age estimates.

Fig. 2 Irradiation-Preheat Cycling

Insufficient Sample Mass

Fig. 5 Inter-grain D_e distribution

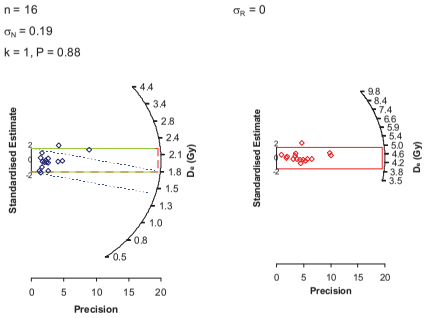

Fig. 6 U Activity

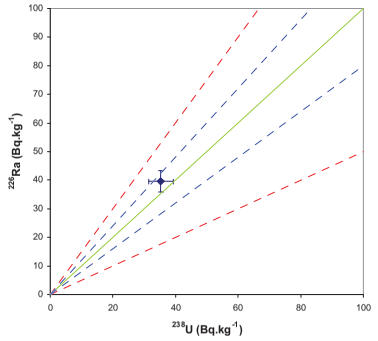

Fig. 3 D_e Preheat Dependence

Insufficient Sample Mass

Fig. 4 Dose Recovery

Insufficient Sample Mass

Fig. 7 Age Range

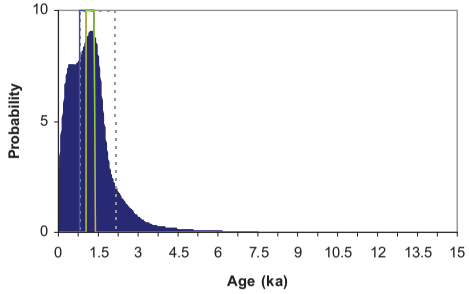

Sample: GL06018

Fig. 1 Signal Calibration

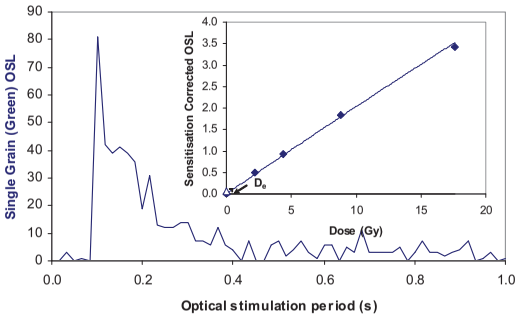

Fig. 1 Signal Calibration Single quartz sand grain natural (green) OSL signal. Inset, the natural green OSL signal (open triangle) of each aliquot is calibrated against known laboratory doses to yield equivalent dose (D_e) values.

Fig. 2 Irradiation-Preheat Cycling The acquisition of D_e values is necessarily predicated upon thermal treatment of aliquots succeeding environmental and laboratory irradiation. Repeated irradiation and thermal treatment results in aliquot sensitisation, rendering calibration of the natural signal inaccurate. This sensitisation can be monitored and corrected for. The accuracy of correction can be preheat dependent; irradiation-preheat cycling quantifies this dependence for laboratory-induced signals, examining the reproducibility of corrected OSL resultant of repeat laboratory doses. This element was based on multi-grain aliquots.

Fig. 3 D_e Preheat Dependence Quantifies the combined effects of thermal transfer and sensitisation on the natural signal. Insignificant adjustment in D_e may reflect limited influence of these effects. This element was based on multi-grain aliquots.

Fig. 4 Dose Recovery Attempts to replicate the above diagnostic, yet provide improved resolution of thermal effects through removal of variability induced by heterogeneous dose absorption in the environment and using a precise lab dose to simulate natural dose. This element was performed on multi-grain aliquots. Based on this and preceding data an appropriate thermal treatment is selected to refine the final D_e value.

Fig. 5 Inter-grain D_e distribution Provides a measure of inter-grain dispersion in D_e values derived from **natural** and **laboratory** irradiation. Discordant data (those points lying beyond **±2 standardised ln D_e**) reflects heterogeneous dose absorption and/or inaccuracies in calibration. Three estimates of post-burial D_e values are illustrated based on the Minimum, Finite Mixture and Central Age Models. n is the number of grains fulfilling acceptability citeria; σ_N is the fractional overdispersion of D_e values about the Central De value; σ_R is the fractional overdispersion of D_e values about a known regenerative-dose value; k indicates the component number and P the proportion of grains within that component generated by the Finite Mixture Model.

Fig. 7 U Activity Statistical concordance (equilibrium) in the activities of the daughter radioisotope ^{226}Ra with its parent ^{238}U may signify the temporal stability of D_r emissions from these chains. Significant differences (disequilibrium; >50%) in activity indicate addition or removal of isotopes creating a time-dependent shift in D_r values and increased uncertainty in the accuracy of age estimates. 20% disequilibrium marker also shown.

Fig. 8 Age Range An estimate of sediment burial period based on mean D_r values and D_e values derived from Minimum, Finite Mixture and Central Age Models, along with associated analytical uncertainties. The probability distribution indicates the inter-grain variability in age. The maximum influence of temporal variations in D_r forced by minima-maxima variation in moisture content and overburden thickness, here coupled with Finite Mixture D_e values, may prove instructive where there is uncertainty in these parameters, however the combined extremes represented should not be construed as preferred age estimates.

Fig. 2 Irradiation-Preheat Cycling

Insufficient Sample Mass

Fig. 3 D_e Preheat Dependence

Insufficient Sample Mass

Fig. 4 Dose Recovery

Insufficient Sample Mass

Sample: GL06019

Fig. 5 Inter-grain D_e distribution

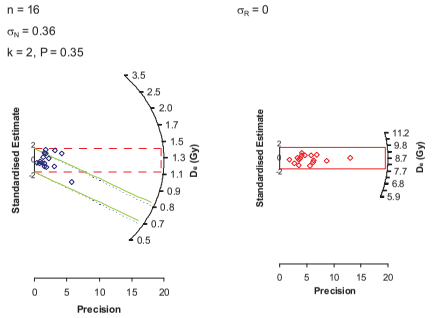

Fig. 6 U Activity

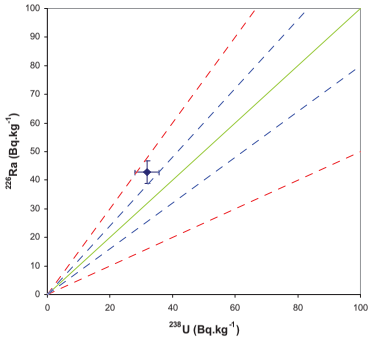

Fig. 7 Age Range

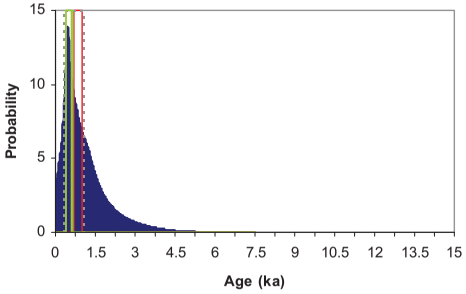

Fig. 1 Signal Calibration

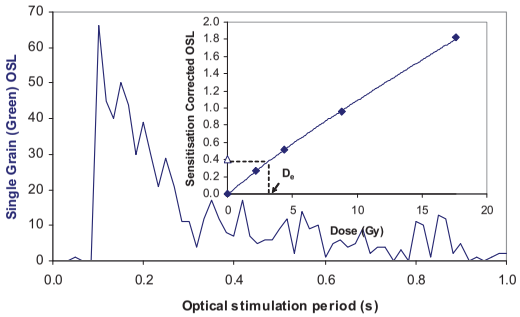

Fig. 1 Signal Calibration Single quartz sand grain natural (green) OSL signal. Inset, the natural green OSL signal (open triangle) of each aliquot is calibrated against known laboratory doses to yield equivalent dose (D_e) values.

Fig. 2 Irradiation-Preheat Cycling The acquisition of D_e values is necessarily predicated upon thermal treatment of aliquots succeeding environmental and laboratory irradiation. Repeated irradiation and thermal treatment results in aliquot sensitisation, rendering calibration of the natural signal inaccurate. This sensitisation can be monitored and corrected for. The accuracy of correction can be preheat dependent; irradiation-preheat cycling quantifies this dependence for laboratory-induced signals, examining the reproducibility of corrected OSL resultant of repeat laboratory doses. This element was based on multi-grain aliquots.

Fig. 3 D_e Preheat Dependence Quantifies the combined effects of thermal transfer and sensitisation on the natural signal. Insignificant adjustment in D_e may reflect limited influence of these effects. This element was based on multi-grain aliquots.

Fig. 4 Dose Recovery Attempts to replicate the above diagnostic, yet provide improved resolution of thermal effects through removal of variability induced by heterogeneous dose absorption in the environment and using a precise lab dose to simulate natural dose. This element was performed on multi-grain aliquots. Based on this and preceding data an appropriate thermal treatment is selected to refine the final D_e value.

Fig. 5 Inter-grain D_e distribution Provides a measure of inter-grain dispersion in D_e values derived from **natural** and **laboratory** irradiation. Discordant data (those points lying beyond **±2 standardised ln D_e**) reflects heterogeneous dose absorption and/or inaccuracies in calibration. Three estimates of post-burial D_e values are illustrated based on the Minimum, Finite Mixture and Central Age Models. n is the number of grains fulfilling acceptability citeria; σ_N is the fractional overdispersion of D_e values about the Central De value; σ_R is the fractional overdispersion of D_e values about a known regenerative-dose value; k indicates the component number and P the proportion of grains within that component generated by the Finite Mixture Model.

Fig. 7 U Activity Statistical concordance (equilibrium) in the activities of the daughter radioisotope ^{226}Ra with its parent ^{238}U may signify the temporal stability of D_r emissions from these chains. Significant differences (disequilibrium; >50%) in activity indicate addition or removal of isotopes creating a time-dependent shift in D_r values and increased uncertainty in the accuracy of age estimates. 20% disequilibrium marker also shown.

Fig. 8 Age Range An estimate of sediment burial period based on mean D_r values and D_e values derived from Minimum, Finite Mixture and Central Age Models, along with associated analytical uncertainties. The probability distribution indicates the inter-grain variability in age. The maximum influence of temporal variations in D_r forced by minima-maxima variation in moisture content and overburden thickness, here coupled with Finite Mixture D_e values, may prove instructive where there is uncertainty in these parameters, however the combined extremes represented should not be construed as preferred age estimates.

Fig. 2 Irradiation-Preheat Cycling

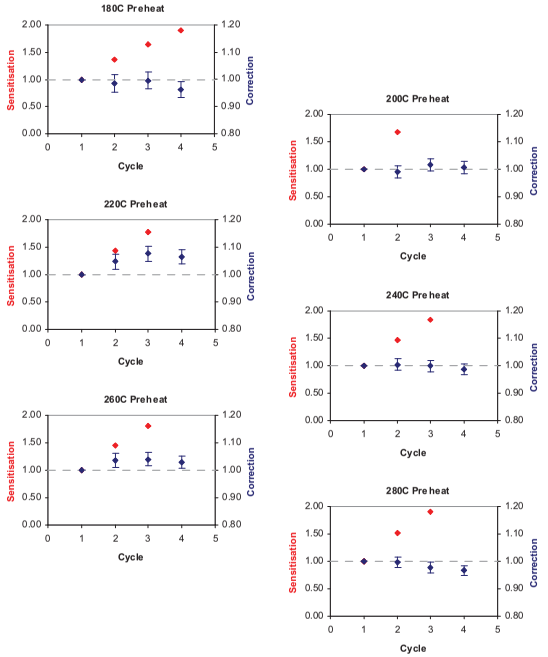

Fig. 3 D_e Preheat Dependence

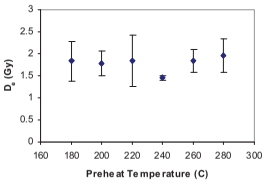

Fig. 4 Dose Recovery

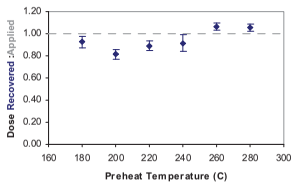

Sample: GL06020

Fig. 5 Inter-grain D_e distribution

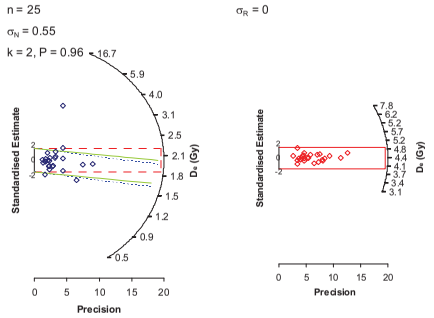

Fig. 6 U Activity

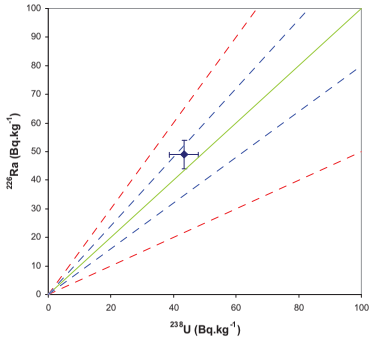

Fig. 7 Age Range

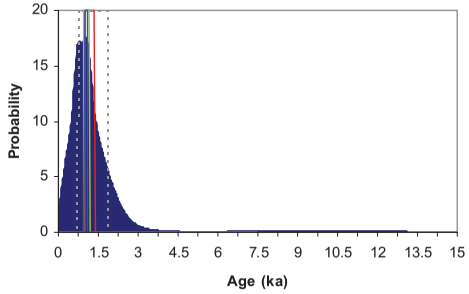

Fig. 1 Signal Calibration

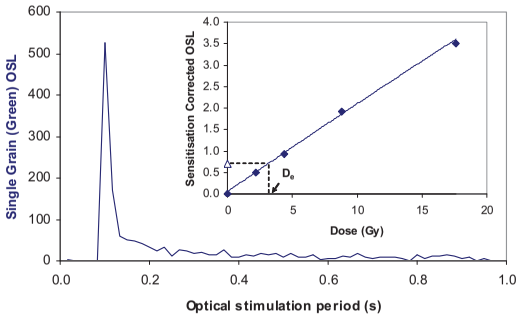

Fig. 1 Signal Calibration Single quartz sand grain natural (green) OSL signal. Inset, the natural green OSL signal (open triangle) of each aliquot is calibrated against known laboratory doses to yield equivalent dose (D_e) values.

Fig. 2 Irradiation-Preheat Cycling The acquisition of D_e values is necessarily predicated upon thermal treatment of aliquots succeeding environmental and laboratory irradiation. Repeated irradiation and thermal treatment results in aliquot sensitisation, rendering calibration of the natural signal inaccurate. This sensitisation can be monitored and corrected for. The accuracy of correction can be preheat dependent; irradiation-preheat cycling quantifies this dependence for laboratory-induced signals, examining the reproducibility of corrected OSL resultant of repeat laboratory doses. This element was based on multi-grain aliquots.

Fig. 3 D_e Preheat Dependence Quantifies the combined effects of thermal transfer and sensitisation on the natural signal. Insignificant adjustment in D_e may reflect limited influence of these effects. This element was based on multi-grain aliquots.

Fig. 4 Dose Recovery Attempts to replicate the above diagnostic, yet provide improved resolution of thermal effects through removal of variability induced by heterogeneous dose absorption in the environment and using a precise lab dose to simulate natural dose. This element was performed on multi-grain aliquots. Based on this and preceding data an appropriate thermal treatment is selected to refine the final D_e value.

Fig. 5 Inter-grain D_e distribution Provides a measure of inter-grain dispersion in D_e values derived from **natural** and **laboratory** irradiation. Discordant data (those points lying beyond **±2 standardised ln D_e**) reflects heterogeneous dose absorption and/or inaccuracies in calibration. Three estimates of post-burial D_e values are illustrated based on the Minimum, Finite Mixture and Central Age Models. n is the number of grains fulfilling acceptability citeria; σ_N is the fractional overdispersion of D_e values about the Central De value; σ_R is the fractional overdispersion of D_e values about a known regenerative-dose value; k indicates the component number and P the proportion of grains within that component generated by the Finite Mixture Model.

Fig. 7 U Activity Statistical concordance (equilibrium) in the activities of the daughter radioisotope ^{226}Ra with its parent ^{238}U may signify the temporal stability of D_r emissions from these chains. Significant differences (disequilibrium; >50%) in activity indicate addition or removal of isotopes creating a time-dependent shift in D_r values and increased uncertainty in the accuracy of age estimates. 20% disequilibrium marker also shown.

Fig. 8 Age Range An estimate of sediment burial period based on mean D_r values and D_e values derived from Minimum, Finite Mixture and Central Age Models, along with associated analytical uncertainties. The probability distribution indicates the inter-grain variability in age. The maximum influence of temporal variations in D_r forced by minima-maxima variation in moisture content and overburden thickness, here coupled with Finite Mixture D_e values, may prove instructive where there is uncertainty in these parameters, however the combined extremes represented should not be construed as preferred age estimates.

Fig. 2 Irradiation-Preheat Cycling

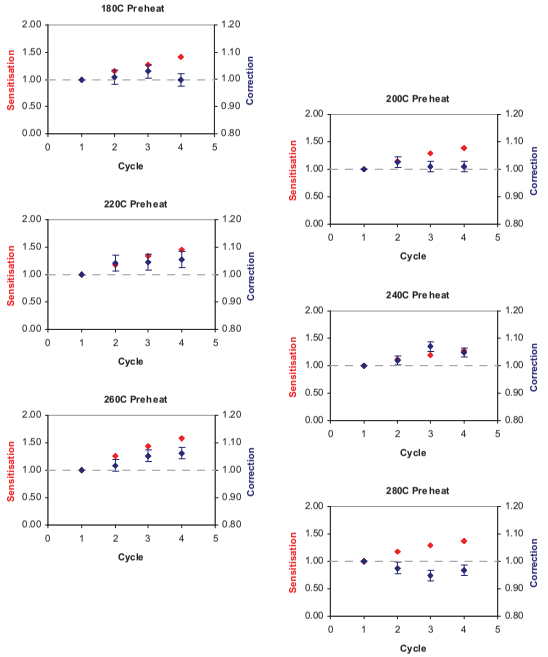

Fig. 3 D_e Preheat Dependence

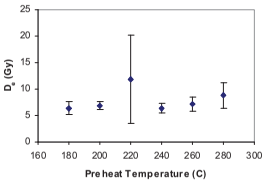

Fig. 4 Dose Recovery

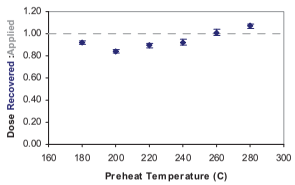

Sample: GL06021

Fig. 5 Inter-grain D_e distribution

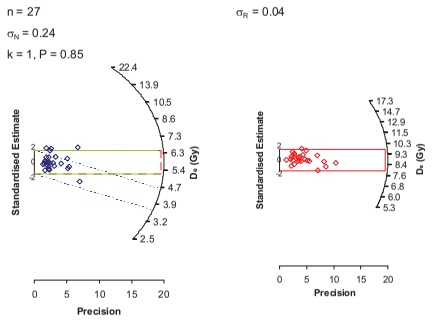

Fig. 6 U Activity

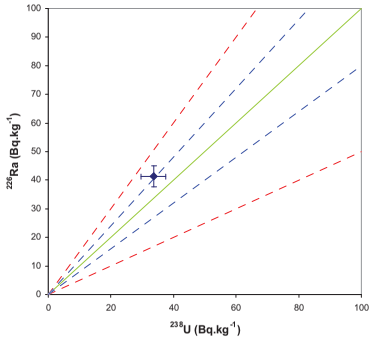

Fig. 7 Age Range

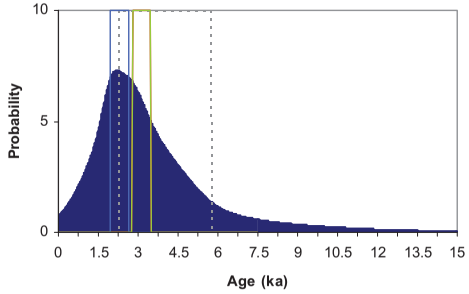

Fig. 1 Signal Calibration

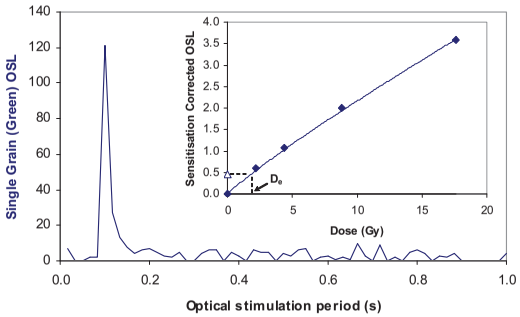

Fig. 1 Signal Calibration Single quartz sand grain natural (green) OSL signal. Inset, the natural green OSL signal (open triangle) of each aliquot is calibrated against known laboratory doses to yield equivalent dose (D_e) values.

Fig. 2 Irradiation-Preheat Cycling The acquisition of D_e values is necessarily predicated upon thermal treatment of aliquots succeeding environmental and laboratory irradiation. Repeated irradiation and thermal treatment results in aliquot sensitisation, rendering calibration of the natural signal inaccurate. This sensitisation can be monitored and corrected for. The accuracy of correction can be preheat dependent; irradiation-preheat cycling quantifies this dependence for laboratory-induced signals, examining the reproducibility of corrected OSL resultant of repeat laboratory doses. This element was based on multi-grain aliquots.

Fig. 3 D_e Preheat Dependence Quantifies the combined effects of thermal transfer and sensitisation on the natural signal. Insignificant adjustment in D_e may reflect limited influence of these effects. This element was based on multi-grain aliquots.

Fig. 4 Dose Recovery Attempts to replicate the above diagnostic, yet provide improved resolution of thermal effects through removal of variability induced by heterogeneous dose absorption in the environment and using a precise lab dose to simulate natural dose. This element was performed on multi-grain aliquots. Based on this and preceding data an appropriate thermal treatment is selected to refine the final D_e value.

Fig. 5 Inter-grain D_e distribution Provides a measure of inter-grain dispersion in D_e values derived from **natural** and **laboratory** irradiation. Discordant data (those points lying beyond **±2 standardised ln D_e**) reflects heterogeneous dose absorption and/or inaccuracies in calibration. Three estimates of post-burial D_e values are illustrated based on the Minimum, Finite Mixture and Central Age Models. n is the number of grains fulfilling acceptability citeria; σ_N is the fractional overdispersion of D_e values about the Central De value; σ_R is the fractional overdispersion of D_e values about a known regenerative-dose value; k indicates the component number and P the proportion of grains within that component generated by the Finite Mixture Model.

Fig. 7 U Activity Statistical concordance (equilibrium) in the activities of the daughter radioisotope ^{226}Ra with its parent ^{238}U may signify the temporal stability of D_r emissions from these chains. Significant differences (disequilibrium; >50%) in activity indicate addition or removal of isotopes creating a time-dependent shift in D_r values and increased uncertainty in the accuracy of age estimates. 20% disequilibrium marker also shown.

Fig. 8 Age Range An estimate of sediment burial period based on mean D_r values and D_e values derived from Minimum, Finite Mixture and Central Age Models, along with associated analytical uncertainties. The probability distribution indicates the inter-grain variability in age. The maximum influence of temporal variations in D_r forced by minima-maxima variation in moisture content and overburden thickness, here coupled with Finite Mixture D_e values, may prove instructive where there is uncertainty in these parameters, however the combined extremes represented should not be construed as preferred age estimates.

Fig. 2 Irradiation-Preheat Cycling

Insufficient Sample Mass

Fig. 3 D_e Preheat Dependence

Insufficient Sample Mass

Fig. 4 Dose Recovery

Insufficient Sample Mass

Sample: GL06022

Fig. 5 Inter-grain D_e distribution

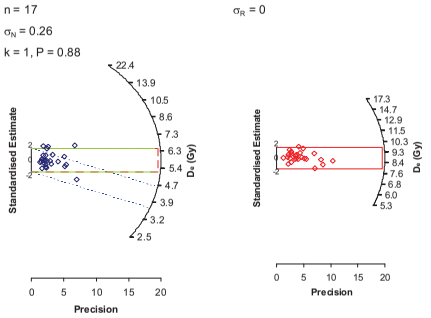

Fig. 6 U Activity

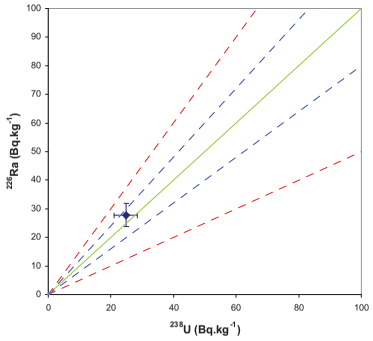

Fig. 7 Age Range

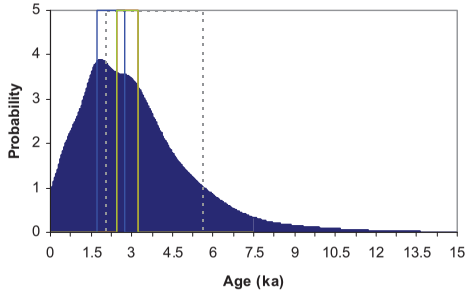

Fig. 1 Signal Calibration

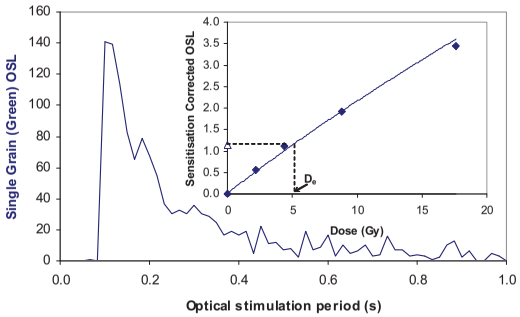

Fig. 1 Signal Calibration Single quartz sand grain natural (green) OSL signal. Inset, the natural green OSL signal (open triangle) of each aliquot is calibrated against known laboratory doses to yield equivalent dose (D_e) values.

Fig. 2 Irradiation-Preheat Cycling The acquisition of D_e values is necessarily predicated upon thermal treatment of aliquots succeeding environmental and laboratory irradiation. Repeated irradiation and thermal treatment results in aliquot sensitisation, rendering calibration of the natural signal inaccurate. This sensitisation can be monitored and corrected for. The accuracy of correction can be preheat dependent; irradiation-preheat cycling quantifies this dependence for laboratory-induced signals, examining the reproducibility of corrected OSL resultant of repeat laboratory doses. This element was based on multi-grain aliquots.

Fig. 3 D_e Preheat Dependence Quantifies the combined effects of thermal transfer and sensitisation on the natural signal. Insignificant adjustment in D_e may reflect limited influence of these effects. This element was based on multi-grain aliquots.

Fig. 4 Dose Recovery Attempts to replicate the above diagnostic, yet provide improved resolution of thermal effects through removal of variability induced by heterogeneous dose absorption in the environment and using a precise lab dose to simulate natural dose. This element was performed on multi-grain aliquots. Based on this and preceding data an appropriate thermal treatment is selected to refine the final D_e value.

Fig. 5 Inter-grain D_e distribution Provides a measure of inter-grain dispersion in D_e values derived from **natural** and **laboratory** irradiation. Discordant data (those points lying beyond **±2 standardised ln D_e**) reflects heterogeneous dose absorption and/or inaccuracies in calibration. Three estimates of post-burial D_e values are illustrated based on the Minimum, Finite Mixture and Central Age Models. n is the number of grains fulfilling acceptability citeria; σ_N is the fractional overdispersion of D_e values about the Central De value; σ_R is the fractional overdispersion of D_e values about a known regenerative-dose value; k indicates the component number and P the proportion of grains within that component generated by the Finite Mixture Model.

Fig. 7 U Activity Statistical concordance (equilibrium) in the activities of the daughter radioisotope ^{226}Ra with its parent ^{238}U may signify the temporal stability of D_r emissions from these chains. Significant differences (disequilibrium; >50%) in activity indicate addition or removal of isotopes creating a time-dependent shift in D_r values and increased uncertainty in the accuracy of age estimates. 20% disequilibrium marker also shown.

Fig. 8 Age Range An estimate of sediment burial period based on mean D_r values and D_e values derived from Minimum, Finite Mixture and Central Age Models, along with associated analytical uncertainties. The probability distribution indicates the inter-grain variability in age. The maximum influence of temporal variations in D_r forced by minima-maxima variation in moisture content and overburden thickness, here coupled with Finite Mixture D_e values, may prove instructive where there is uncertainty in these parameters, however the combined extremes represented should not be construed as preferred age estimates.

Fig. 2 Irradiation-Preheat Cycling

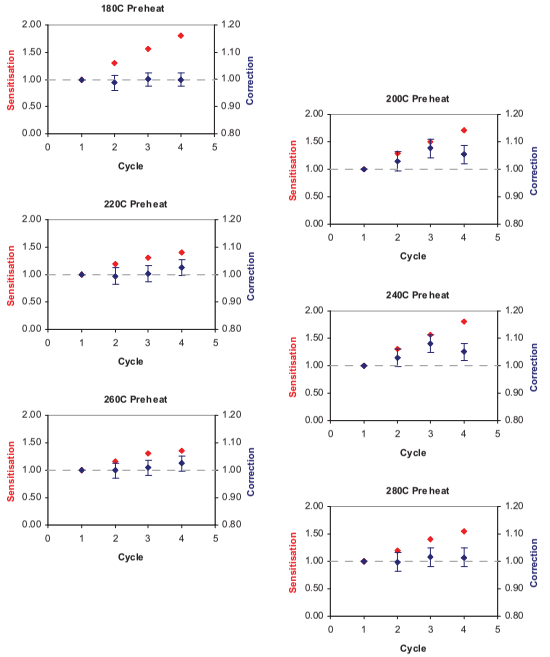

Fig. 3 D_e Preheat Dependence

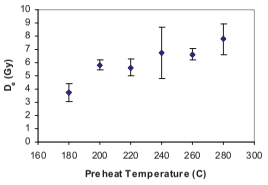

Fig. 4 Dose Recovery

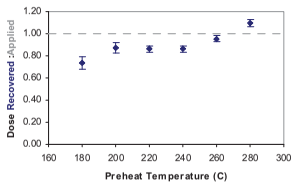

Sample: GL06023

Fig. 5 Inter-grain D_e distribution

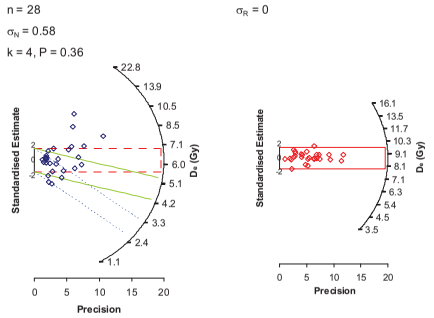

Fig. 6 U Activity

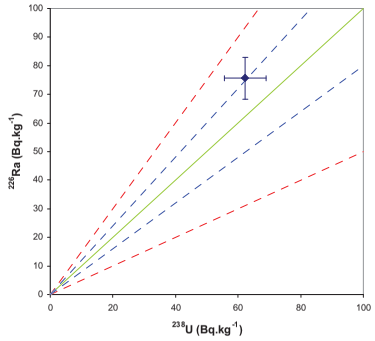

Fig. 7 Age Range

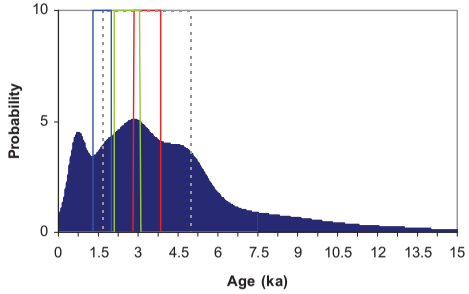

Fig. 1 Signal Calibration

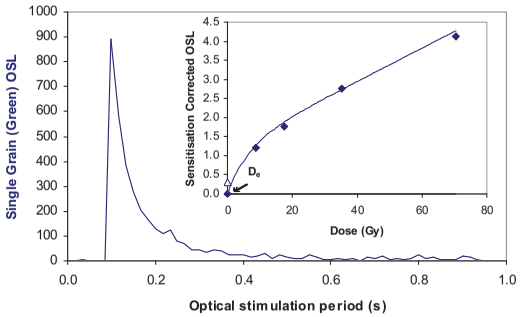

Fig. 1 Signal Calibration Single quartz sand grain natural (green) OSL signal. Inset, the natural green OSL signal (open triangle) of each aliquot is calibrated against known laboratory doses to yield equivalent dose (D_e) values.

Fig. 2 Irradiation-Preheat Cycling The acquisition of D_e values is necessarily predicated upon thermal treatment of aliquots succeeding environmental and laboratory irradiation. Repeated irradiation and thermal treatment results in aliquot sensitisation, rendering calibration of the natural signal inaccurate. This sensitisation can be monitored and corrected for. The accuracy of correction can be preheat dependent; irradiation-preheat cycling quantifies this dependence for laboratory-induced signals, examining the reproducibility of corrected OSL resultant of repeat laboratory doses. This element was based on multi-grain aliquots.

Fig. 3 D_e Preheat Dependence Quantifies the combined effects of thermal transfer and sensitisation on the natural signal. Insignificant adjustment in D_e may reflect limited influence of these effects. This element was based on multi-grain aliquots.

Fig. 4 Dose Recovery Attempts to replicate the above diagnostic, yet provide improved resolution of thermal effects through removal of variability induced by heterogeneous dose absorption in the environment and using a precise lab dose to simulate natural dose. This element was performed on multi-grain aliquots. Based on this and preceding data an appropriate thermal treatment is selected to refine the final D_e value.

Fig. 5 Inter-grain D_e distribution Provides a measure of inter-grain dispersion in D_e values derived from **natural** and **laboratory** irradiation. Discordant data (those points lying beyond **±2 standardised ln D_e**) reflects heterogeneous dose absorption and/or inaccuracies in calibration. Three estimates of post-burial D_e values are illustrated based on the Minimum, Finite Mixture and Central Age Models. n is the number of grains fulfilling acceptability citeria; σ_N is the fractional overdispersion of D_e values about the Central De value; σ_R is the fractional overdispersion of D_e values about a known regenerative-dose value; k indicates the component number and P the proportion of grains within that component generated by the Finite Mixture Model.

Fig. 7 U Activity Statistical concordance (equilibrium) in the activities of the daughter radioisotope ^{226}Ra with its parent ^{238}U may signify the temporal stability of D_r emissions from these chains. Significant differences (disequilibrium; >50%) in activity indicate addition or removal of isotopes creating a time-dependent shift in D_r values and increased uncertainty in the accuracy of age estimates. 20% disequilibrium marker also shown.

Fig. 8 Age Range An estimate of sediment burial period based on mean D_r values and D_e values derived from Minimum, Finite Mixture and Central Age Models, along with associated analytical uncertainties. The probability distribution indicates the inter-grain variability in age. The maximum influence of temporal variations in D_r forced by minima-maxima variation in moisture content and overburden thickness, here coupled with Finite Mixture D_e values, may prove instructive where there is uncertainty in these parameters, however the combined extremes represented should not be construed as preferred age estimates.

Fig. 2 Irradiation-Preheat Cycling

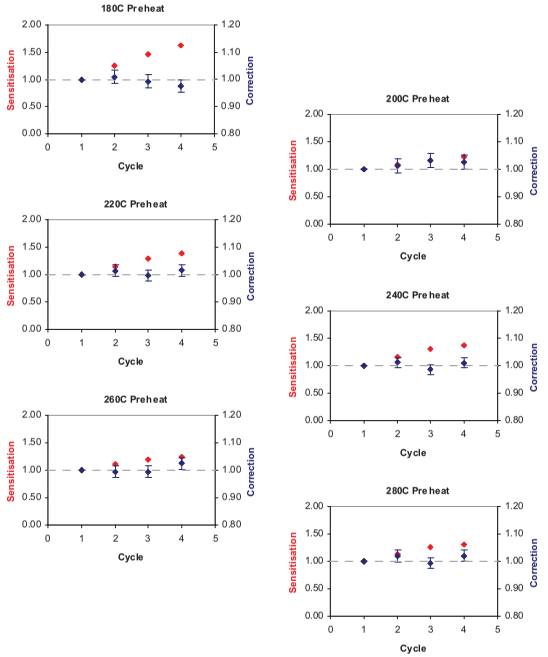

Fig. 3 D_e Preheat Dependence

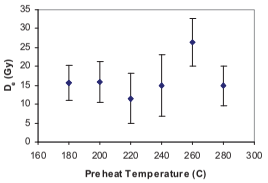

Fig. 4 Dose Recovery

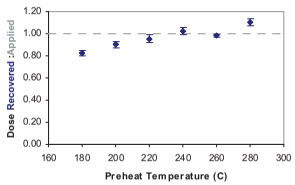

Sample: GL06024

Fig. 5 Inter-grain D_e distribution

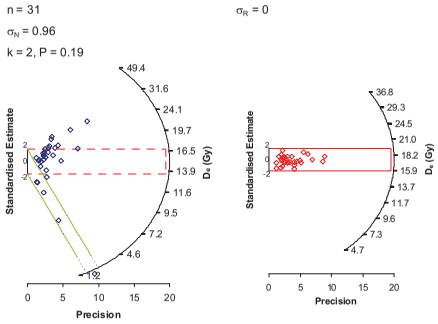

Fig. 6 U Activity

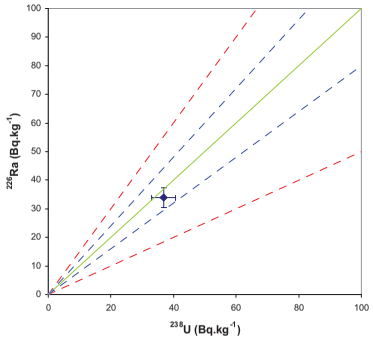

Fig. 7 Age Range

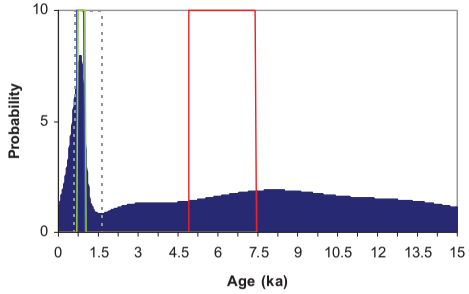

Fig. 1 Signal Calibration

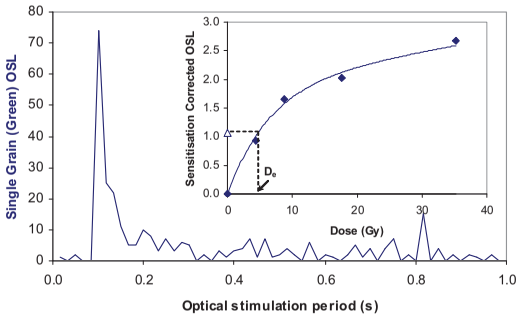

Fig. 2 Irradiation-Preheat Cycling

Insufficient Sample Mass

Fig. 5 Inter-grain D_e distribution

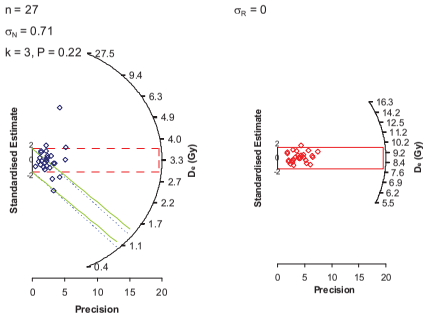

Fig. 1 Signal Calibration Single quartz sand grain natural (green) OSL signal. Inset, the natural green OSL signal (open triangle) of each aliquot is calibrated against known laboratory doses to yield equivalent dose (D_e) values.

Fig. 2 Irradiation-Preheat Cycling The acquisition of D_e values is necessarily predicated upon thermal treatment of aliquots succeeding environmental and laboratory irradiation. Repeated irradiation and thermal treatment results in aliquot sensitisation, rendering calibration of the natural signal inaccurate. This sensitisation can be monitored and corrected for. The accuracy of correction can be preheat dependent; irradiation-preheat cycling quantifies this dependence for laboratory-induced signals, examining the reproducibility of corrected OSL resultant of repeat laboratory doses. This element was based on multi-grain aliquots.

Fig. 3 D_e Preheat Dependence Quantifies the combined effects of thermal transfer and sensitisation on the natural signal. Insignificant adjustment in D_e may reflect limited influence of these effects. This element was based on multi-grain aliquots.

Fig. 4 Dose Recovery Attempts to replicate the above diagnostic, yet provide improved resolution of thermal effects through removal of variability induced by heterogeneous dose absorption in the environment and using a precise lab dose to simulate natural dose. This element was performed on multi-grain aliquots. Based on this and preceding data an appropriate thermal treatment is selected to refine the final D_e value.

Fig. 5 Inter-grain D_e distribution Provides a measure of inter-grain dispersion in D_e values derived from **natural** and **laboratory** irradiation. Discordant data (those points lying beyond **±2 standardised ln D_e**) reflects heterogeneous dose absorption and/or inaccuracies in calibration. Three estimates of post-burial D_e values are illustrated based on the Minimum, Finite Mixture and Central Age Models. n is the number of grains fulfilling acceptability citeria; σ_N is the fractional overdispersion of D_e values about the Central De value; σ_R is the fractional overdispersion of D_e values about a known regenerative-dose value; k indicates the component number and P the proportion of grains within that component generated by the Finite Mixture Model.

Fig. 7 U Activity Statistical concordance (equilibrium) in the activities of the daughter radioisotope ^{226}Ra with its parent ^{238}U may signify the temporal stability of D_r emissions from these chains. Significant differences (disequilibrium; >50%) in activity indicate addition or removal of isotopes creating a time-dependent shift in D_r values and increased uncertainty in the accuracy of age estimates. 20% disequilibrium marker also shown.

Fig. 8 Age Range An estimate of sediment burial period based on mean D_r values and D_e values derived from Minimum, Finite Mixture and Central Age Models, along with associated analytical uncertainties. The probability distribution indicates the inter-grain variability in age. The maximum influence of temporal variations in D_r forced by minima-maxima variation in moisture content and overburden thickness, here coupled with Finite Mixture D_e values, may prove instructive where there is uncertainty in these parameters, however the combined extremes represented should not be construed as preferred age estimates.

Fig. 6 U Activity

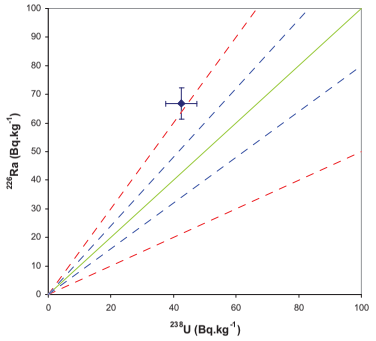

Fig. 3 D_e Preheat Dependence

Insufficient Sample Mass

Fig. 4 Dose Recovery

Insufficient Sample Mass

Fig. 7 Age Range

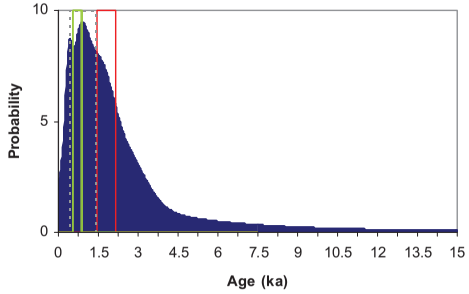

Sample: GL06025

Fig. 1 Signal Calibration

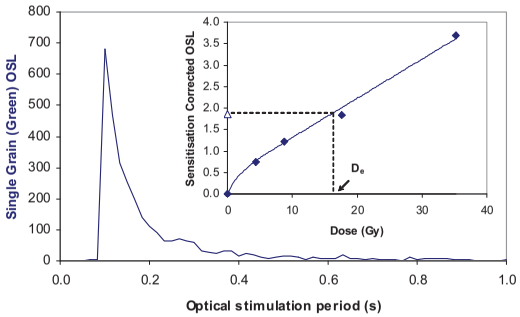

Fig. 1 Signal Calibration Single quartz sand grain natural (green) OSL signal. Inset, the natural green OSL signal (open triangle) of each aliquot is calibrated against known laboratory doses to yield equivalent dose (D_e) values.

Fig. 2 Irradiation-Preheat Cycling The acquisition of D_e values is necessarily predicated upon thermal treatment of aliquots succeeding environmental and laboratory irradiation. Repeated irradiation and thermal treatment results in aliquot sensitisation, rendering calibration of the natural signal inaccurate. This sensitisation can be monitored and corrected for. The accuracy of correction can be preheat dependent; irradiation-preheat cycling quantifies this dependence for laboratory-induced signals, examining the reproducibility of corrected OSL resultant of repeat laboratory doses. This element was based on multi-grain aliquots.

Fig. 3 D_e Preheat Dependence Quantifies the combined effects of thermal transfer and sensitisation on the natural signal. Insignificant adjustment in D_e may reflect limited influence of these effects. This element was based on multi-grain aliquots.

Fig. 4 Dose Recovery Attempts to replicate the above diagnostic, yet provide improved resolution of thermal effects through removal of variability induced by heterogeneous dose absorption in the environment and using a precise lab dose to simulate natural dose. This element was performed on multi-grain aliquots. Based on this and preceding data an appropriate thermal treatment is selected to refine the final D_e value.

Fig. 5 Inter-grain D_e distribution Provides a measure of inter-grain dispersion in D_e values derived from **natural** and **laboratory** irradiation. Discordant data (those points lying beyond **±2 standardised ln D_e**) reflects heterogeneous dose absorption and/or inaccuracies in calibration. Three estimates of post-burial D_e values are illustrated based on the Minimum, Finite Mixture and Central Age Models. n is the number of grains fulfilling acceptability citeria; σ_N is the fractional overdispersion of D_e values about the Central De value; σ_R is the fractional overdispersion of D_e values about a known regenerative-dose value; k indicates the component number and P the proportion of grains within that component generated by the Finite Mixture Model.

Fig. 7 U Activity Statistical concordance (equilibrium) in the activities of the daughter radioisotope ^{226}Ra with its parent ^{238}U may signify the temporal stability of D_r emissions from these chains. Significant differences (disequilibrium; >50%) in activity indicate addition or removal of isotopes creating a time-dependent shift in D_r values and increased uncertainty in the accuracy of age estimates. 20% disequilibrium marker also shown.

Fig. 8 Age Range An estimate of sediment burial period based on mean D_r values and D_e values derived from Minimum, Finite Mixture and Central Age Models, along with associated analytical uncertainties. The probability distribution indicates the inter-grain variability in age. The maximum influence of temporal variations in D_r forced by minima-maxima variation in moisture content and overburden thickness, here coupled with Finite Mixture D_e values, may prove instructive where there is uncertainty in these parameters, however the combined extremes represented should not be construed as preferred age estimates.

Fig. 2 Irradiation-Preheat Cycling

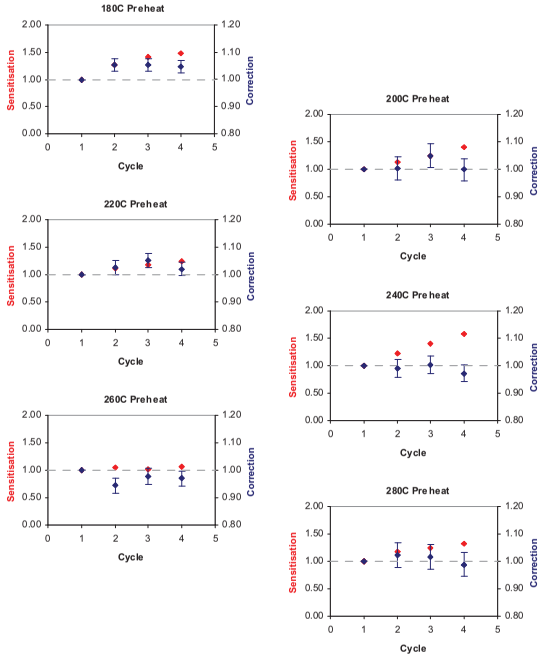

Fig. 3 D_e Preheat Dependence

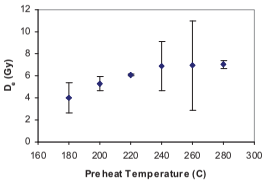

Fig. 4 Dose Recovery

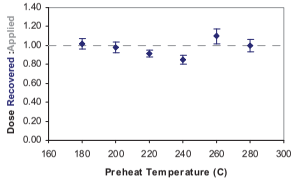

Sample: GL06026

Fig. 5 Inter-grain D_e distribution

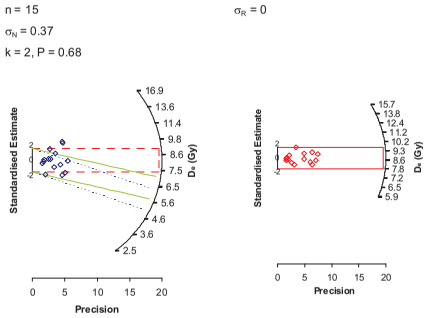

Fig. 6 U Activity

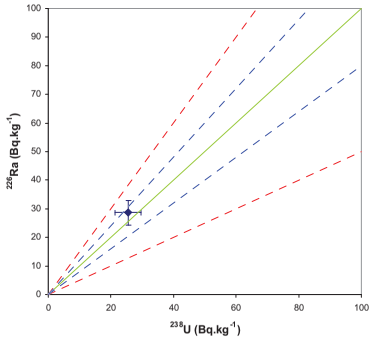

Fig. 7 Age Range

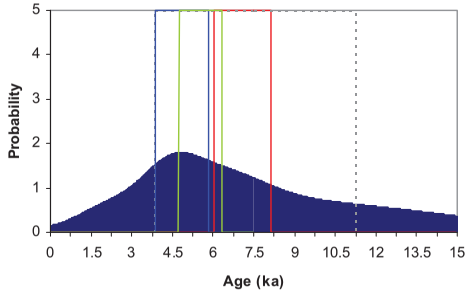

Fig. 1 Signal Calibration

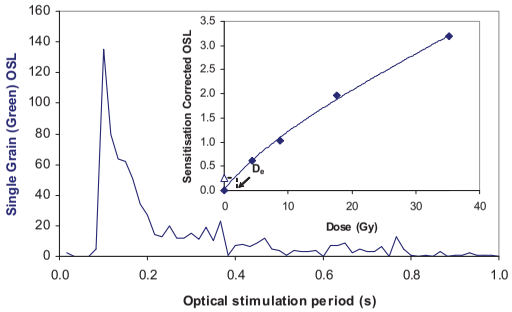

Fig. 1 Signal Calibration Single quartz sand grain natural (green) OSL signal. Inset, the natural green OSL signal (open triangle) of each aliquot is calibrated against known laboratory doses to yield equivalent dose (D_e) values.

Fig. 2 Irradiation-Preheat Cycling The acquisition of D_e values is necessarily predicated upon thermal treatment of aliquots succeeding environmental and laboratory irradiation. Repeated irradiation and thermal treatment results in aliquot sensitisation, rendering calibration of the natural signal inaccurate. This sensitisation can be monitored and corrected for. The accuracy of correction can be preheat dependent; irradiation-preheat cycling quantifies this dependence for laboratory-induced signals, examining the reproducibility of corrected OSL resultant of repeat laboratory doses. This element was based on multi-grain aliquots.

Fig. 3 D_e Preheat Dependence Quantifies the combined effects of thermal transfer and sensitisation on the natural signal. Insignificant adjustment in D_e may reflect limited influence of these effects. This element was based on multi-grain aliquots.

Fig. 4 Dose Recovery Attempts to replicate the above diagnostic, yet provide improved resolution of thermal effects through removal of variability induced by heterogeneous dose absorption in the environment and using a precise lab dose to simulate natural dose. This element was performed on multi-grain aliquots. Based on this and preceding data an appropriate thermal treatment is selected to refine the final D_e value.

Fig. 5 Inter-grain D_e distribution Provides a measure of inter-grain dispersion in D_e values derived from **natural** and **laboratory** irradiation. Discordant data (those points lying beyond **±2 standardised ln D_e**) reflects heterogeneous dose absorption and/or inaccuracies in calibration. Three estimates of post-burial D_e values are illustrated based on the Minimum, Finite Mixture and Central Age Models. n is the number of grains fulfilling acceptability citeria; σ_N is the fractional overdispersion of D_e values about the Central De value; σ_R is the fractional overdispersion of D_e values about a known regenerative-dose value; k indicates the component number and P the proportion of grains within that component generated by the Finite Mixture Model.

Fig. 7 U Activity Statistical concordance (equilibrium) in the activities of the daughter radioisotope ^{226}Ra with its parent ^{238}U may signify the temporal stability of D_r emissions from these chains. Significant differences (disequilibrium; >50%) in activity indicate addition or removal of isotopes creating a time-dependent shift in D_r values and increased uncertainty in the accuracy of age estimates. 20% disequilibrium marker also shown.

Fig. 8 Age Range An estimate of sediment burial period based on mean D_r values and D_e values derived from Minimum, Finite Mixture and Central Age Models, along with associated analytical uncertainties. The probability distribution indicates the inter-grain variability in age. The maximum influence of temporal variations in D_r forced by minima-maxima variation in moisture content and overburden thickness, here coupled with Finite Mixture D_e values, may prove instructive where there is uncertainty in these parameters, however the combined extremes represented should not be construed as preferred age estimates.

Fig. 2 Irradiation-Preheat Cycling

Insufficient Sample Mass

Fig. 3 D_e Preheat Dependence

Insufficient Sample Mass

Fig. 4 Dose Recovery

Insufficient Sample Mass

Sample: GL06028

Fig. 5 Inter-grain D_e distribution

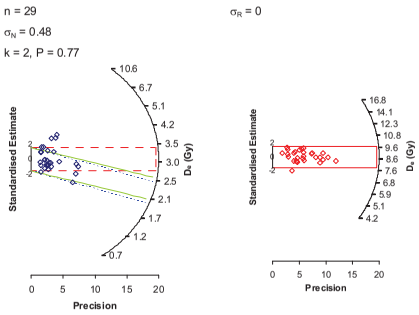

Fig. 6 U Activity

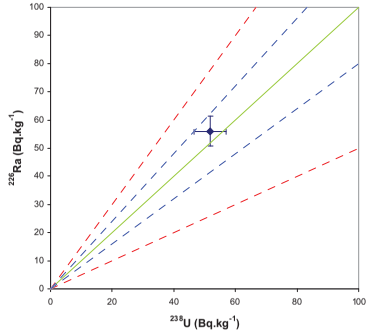

Fig. 7 Age Range

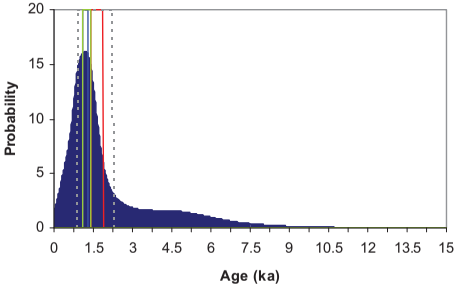

Fig. 1 Signal Calibration

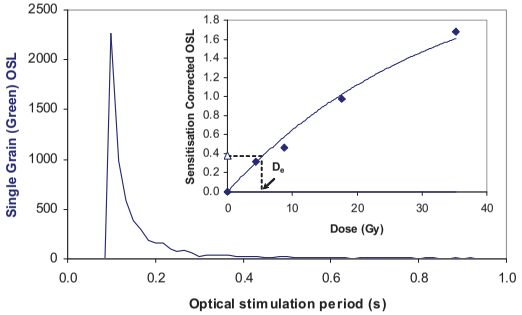

Fig. 1 Signal Calibration Single quartz sand grain natural (green) OSL signal. Inset, the natural green OSL signal (open triangle) of each aliquot is calibrated against known laboratory doses to yield equivalent dose (D_e) values.

Fig. 2 Irradiation-Preheat Cycling The acquisition of D_e values is necessarily predicated upon thermal treatment of aliquots succeeding environmental and laboratory irradiation. Repeated irradiation and thermal treatment results in aliquot sensitisation, rendering calibration of the natural signal inaccurate. This sensitisation can be monitored and corrected for. The accuracy of correction can be preheat dependent; irradiation-preheat cycling quantifies this dependence for laboratory-induced signals, examining the reproducibility of corrected OSL resultant of repeat laboratory doses. This element was based on multi-grain aliquots.

Fig. 3 D_e Preheat Dependence Quantifies the combined effects of thermal transfer and sensitisation on the natural signal. Insignificant adjustment in D_e may reflect limited influence of these effects. This element was based on multi-grain aliquots.

Fig. 4 Dose Recovery Attempts to replicate the above diagnostic, yet provide improved resolution of thermal effects through removal of variability induced by heterogeneous dose absorption in the environment and using a precise lab dose to simulate natural dose. This element was performed on multi-grain aliquots. Based on this and preceding data an appropriate thermal treatment is selected to refine the final D_e value.

Fig. 5 Inter-grain D_e distribution Provides a measure of inter-grain dispersion in D_e values derived from **natural** and **laboratory** irradiation. Discordant data (those points lying beyond **±2 standardised ln D_e**) reflects heterogeneous dose absorption and/or inaccuracies in calibration. Three estimates of post-burial D_e values are illustrated based on the Minimum, Finite Mixture and Central Age Models. n is the number of grains fulfilling acceptability citeria; σ_N is the fractional overdispersion of D_e values about the Central De value; σ_R is the fractional overdispersion of D_e values about a known regenerative-dose value; k indicates the component number and P the proportion of grains within that component generated by the Finite Mixture Model.

Fig. 7 U Activity Statistical concordance (equilibrium) in the activities of the daughter radioisotope ^{226}Ra with its parent ^{238}U may signify the temporal stability of D_r emissions from these chains. Significant differences (disequilibrium; >50%) in activity indicate addition or removal of isotopes creating a time-dependent shift in D_r values and increased uncertainty in the accuracy of age estimates. 20% disequilibrium marker also shown.

Fig. 8 Age Range An estimate of sediment burial period based on mean D_r values and D_e values derived from Minimum, Finite Mixture and Central Age Models, along with associated analytical uncertainties. The probability distribution indicates the inter-grain variability in age. The maximum influence of temporal variations in D_r forced by minima-maxima variation in moisture content and overburden thickness, here coupled with Finite Mixture D_e values, may prove instructive where there is uncertainty in these parameters, however the combined extremes represented should not be construed as preferred age estimates.

Fig. 2 Irradiation-Preheat Cycling

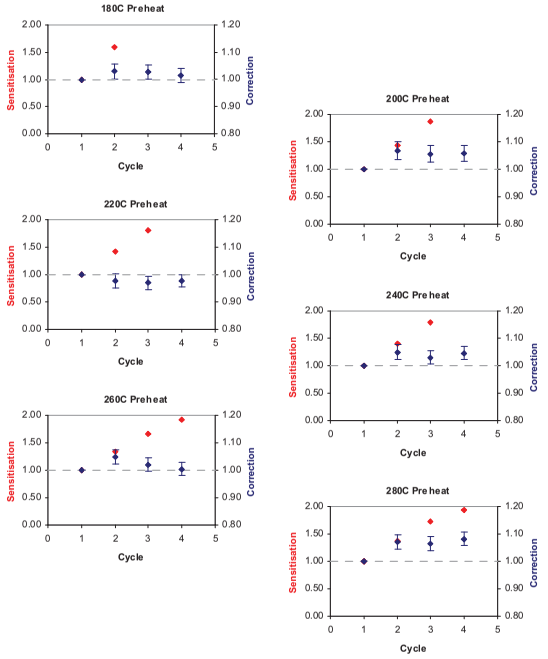

Fig. 3 D_e Preheat Dependence

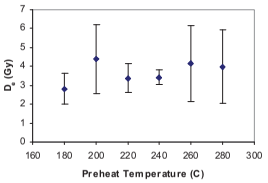

Fig. 4 Dose Recovery

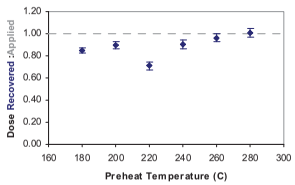

Sample: GL06030

Fig. 5 Inter-grain D_e distribution

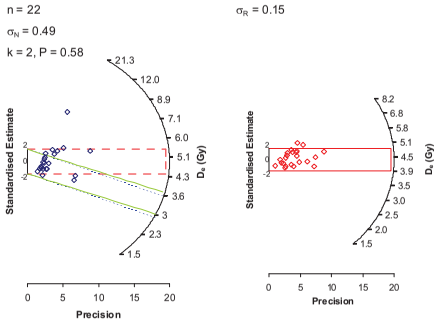

Fig. 6 U Activity

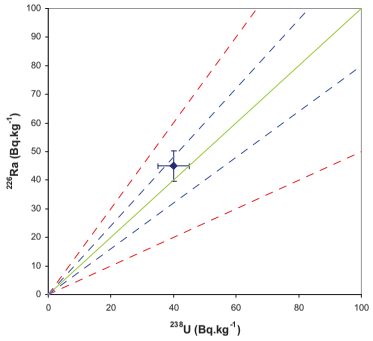

Fig. 7 Age Range

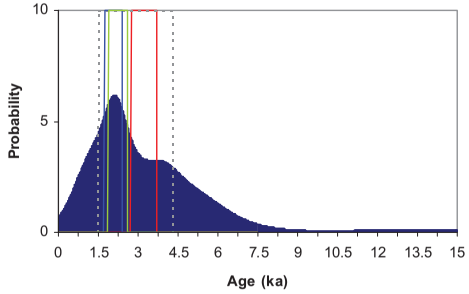

Fig. 1 Signal Calibration

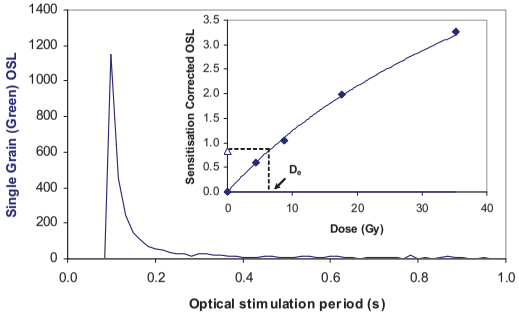

Fig. 1 Signal Calibration Single quartz sand grain natural (green) OSL signal. Inset, the natural green OSL signal (open triangle) of each aliquot is calibrated against known laboratory doses to yield equivalent dose (D_e) values.

Fig. 2 Irradiation-Preheat Cycling The acquisition of D_e values is necessarily predicated upon thermal treatment of aliquots succeeding environmental and laboratory irradiation. Repeated irradiation and thermal treatment results in aliquot sensitisation, rendering calibration of the natural signal inaccurate. This sensitisation can be monitored and corrected for. The accuracy of correction can be preheat dependent; irradiation-preheat cycling quantifies this dependence for laboratory-induced signals, examining the reproducibility of corrected OSL resultant of repeat laboratory doses. This element was based on multi-grain aliquots.

Fig. 3 D_e Preheat Dependence Quantifies the combined effects of thermal transfer and sensitisation on the natural signal. Insignificant adjustment in D_e may reflect limited influence of these effects. This element was based on multi-grain aliquots.

Fig. 4 Dose Recovery Attempts to replicate the above diagnostic, yet provide improved resolution of thermal effects through removal of variability induced by heterogeneous dose absorption in the environment and using a precise lab dose to simulate natural dose. This element was performed on multi-grain aliquots. Based on this and preceding data an appropriate thermal treatment is selected to refine the final D_e value.

Fig. 5 Inter-grain D_e distribution Provides a measure of inter-grain dispersion in D_e values derived from **natural** and **laboratory** irradiation. Discordant data (those points lying beyond **±2 standardised ln D_e**) reflects heterogeneous dose absorption and/or inaccuracies in calibration. Three estimates of post-burial D_e values are illustrated based on the Minimum, Finite Mixture and Central Age Models. n is the number of grains fulfilling acceptability citeria; σ_N is the fractional overdispersion of D_e values about the Central De value; σ_R is the fractional overdispersion of D_e values about a known regenerative-dose value; k indicates the component number and P the proportion of grains within that component generated by the Finite Mixture Model.

Fig. 7 U Activity Statistical concordance (equilibrium) in the activities of the daughter radioisotope ^{226}Ra with its parent ^{238}U may signify the temporal stability of D_r emissions from these chains. Significant differences (disequilibrium; >50%) in activity indicate addition or removal of isotopes creating a time-dependent shift in D_r values and increased uncertainty in the accuracy of age estimates. 20% disequilibrium marker also shown.

Fig. 8 Age Range An estimate of sediment burial period based on mean D_r values and D_e values derived from Minimum, Finite Mixture and Central Age Models, along with associated analytical uncertainties. The probability distribution indicates the inter-grain variability in age. The maximum influence of temporal variations in D_r forced by minima-maxima variation in moisture content and overburden thickness, here coupled with Finite Mixture D_e values, may prove instructive where there is uncertainty in these parameters, however the combined extremes represented should not be construed as preferred age estimates.

Fig. 2 Irradiation-Preheat Cycling

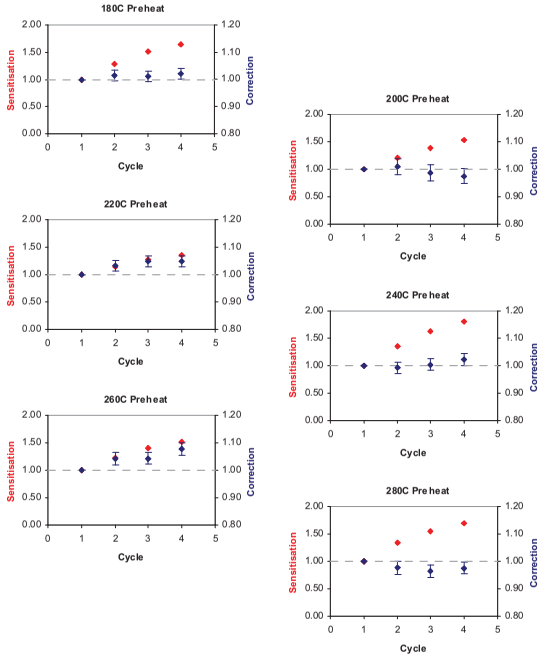

Fig. 3 D_e Preheat Dependence

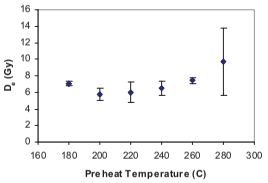

Fig. 4 Dose Recovery

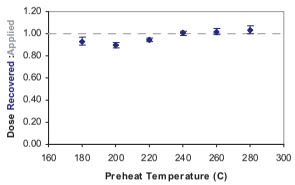

Sample: GL06031

Fig. 5 Inter-grain D_e distribution

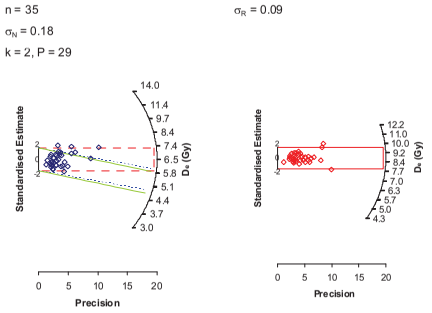

Fig. 6 U Activity

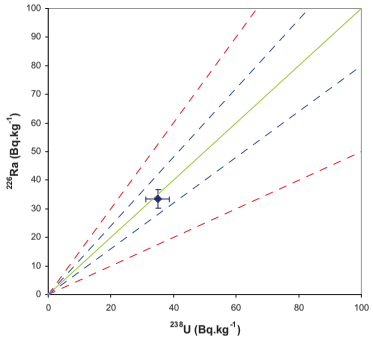

Fig. 7 Age Range

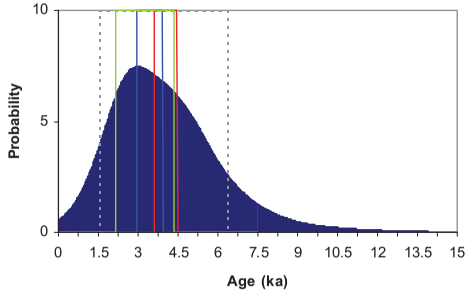

References

Adamiec, G. and Aitken, M.J. (1998) Dose-rate conversion factors: new data. *Ancient TL*, 16, 37-50.

Agersnap-Larsen, N., Bulur, E., Bøtter-Jensen, L. and McKeever, S.W.S. (2000) Use of the LM-OSL technique for the detection of partial bleaching in quartz. *Radiation Measurements*, 32, 419-425.

Aitken, M.J. (1985) Thermoluminescence dating. Academic Press, London.

Aitken, M. J. (1998) An introduction to optical dating: the dating of Quaternary sediments by the use of photon-stimulated luminescence. Oxford University Press.

Bailey, R.M. (2004) Paper I—simulation of dose absorption in quartz over geological timescales and its implications for the precision and accuracy of optical dating. *Radiation Measurements*, 38, 299-310.

Bailey, R.M., Singarayer, J.S. , Ward, S. and Stokes, S. (2003) Identification of partial resetting using D_e as a function of illumination time. *Radiation Measurements*, 37, 511-518.

Banerjee, D., Murray, A.S., Bøtter-Jensen, L. and Lang, A. (2001) Equivalent dose estimation using a single aliquot of polymineral fine grains. *Radiation Measurements*, 33, 73-94.

Bateman, M.D., Frederick, C.D., Jaiswal, M.K., Singhvi, A.K. (2003) Investigations into the potential effects of pedoturbation on luminescence dating. *Quaternary Science Reviews*, 22, 1169-1176.

Berger, G.W. (2003). Luminescence chronology of late Pleistocene loess-paleosol and tephra sequences near Fairbanks, Alaska. *Quaternary Research*, 60, 70-83.

Bøtter-Jensen, L., Mejdahl, V. and Murray, A.S. (1999) New light on OSL. *Quaternary Science Reviews*, 18, 303-310.

Bøtter-Jensen, L., McKeever, S.W.S. and Wintle, A.G. (2003) Optically Stimulated Luminescence Dosimetry. Elsevier, Amsterdam.

Duller, G.A.T. (2003) Distinguishing quartz and feldspar in single grain luminescence measurements. *Radiation Measurements*, 37, 161-165.

Duller, G.A.T., Bøtter-Jensen, L., Kohsiek, P. and Murray, A.S. (1999) A high sensitivity optically stimulated luminescence scanning system for measurement of single sand-sized grains. *Radiation Protection Dosimetry*, 84, 325-330.

Galbraith, R, F. (1990) The radial plot: graphical assessment of spread in ages. *Nuclear Tracks and Radiation Measurements*, 17, 207-214.

Galbraith, R.F. and Green, P.F. (1990) Estimating the component ages in a finite mixture. *Nuclear Tracks and Radiation Measurements*, 17, 197-206.

Galbraith, R.F. and Laslett, G. (1993) Statistical models for mixed fission track ages. *Radiation Measurements*, 21, 459-470.

Galbraith, R. F., Roberts, R. G., Laslett, G. M., Yoshida, H. and Olley, J. M. (1999) Optical dating of single and multiple grains of quartz from Jinmium rock shelter (northern Australia): Part I, Experimental design and statistical models. *Archaeometry*, 41, 339-364.

Green, J. R. and Margerison, D. (1978) Statistical treatment of experimental data. Elsevier Scientific Publications. New York.

Hubble, J. H. (1982) Photon mass attenuation and energy-absorption coefficients from 1keV to 20MeV. *International Journal of Applied Radioisotopes*, 33, 1269-1290.

Huntley, D.J., Godfrey-Smith, D.I. and Thewalt, M.L.W. (1985) Optical dating of sediments. *Nature*, 313, 105-107.

Ixaru, L., Vandenberghe, G. and Hazewinkel, M. (2004) Exponential Fitting. Kluwer.

Jacobs, Z., Duller, G.A.T. and Wintle A.G. (2006) Interpretation of single grain D_e distributions and calculation of D_e. *Radiation Measurements*, 41, 264-277.

Markey, B.G., Bøtter-Jensen, L., and Duller, G.A.T. (1997) A new flexible system for measuring thermally and optically stimulated luminescence. *Radiation Measurements*, 27, 83-89.

Mejdahl, V. (1979) Thermoluminescence dating: beta-dose attenuation in quartz grains. *Archaeometry*, 21, 61-72.

Murray, A.S. and Olley, J.M. (2002) Precision and accuracy in the Optically Stimulated Luminescence dating of sedimentary quartz: a status review. *Geochronometria*, 21, 1-16.

Murray, A.S. and Wintle, A.G. (2000) Luminescence dating of quartz using an improved single-aliquot regenerative-dose protocol. *Radiation Measurements*, 32, 57-73.

Murray, A.S. and Wintle, A.G. (2003) The single aliquot regenerative dose protocol: potential for improvements in reliability. *Radiation Measurements*, 37, 377-381.

Murray, A.S., Olley, J.M. and Caitcheon, G.G. (1995) Measurement of equivalent doses in quartz from contemporary water-lain sediments using optically stimulated luminescence. *Quaternary Science Reviews*, 14, 365-371.

Olley, J.M., Murray, A.S. and Roberts, R.G. (1996) The effects of disequilibria in the Uranium and Thorium decay chains on burial dose rates in fluvial sediments. *Quaternary Science Reviews*, 15, 751-760.

Olley, J.M., Caitcheon, G.G. and Murray, A.S. (1998) The distribution of apparent dose as determined by optically stimulated luminescence in small aliquots of fluvial quartz: implications for dating young sediments. *Quaternary Science Reviews*, 17, 1033-1040.

Olley, J.M., Caitcheon, G.G. and Roberts R.G. (1999) The origin of dose distributions in fluvial sediments, and the prospect of dating single grains from fluvial deposits using -optically stimulated luminescence. *Radiation Measurements,* 30**,** 207-217.

Olley, J.M., Pietsch, T. and Roberts, R.G. (2004) Optical dating of Holocene sediments from a variety of geomorphic settings using single grains of quartz. *Geomorphology*, 60, 337-358.

Prescott, J.R. and Hutton, J.T. (1994) Cosmic ray contributions to dose rates for luminescence and ESR dating: large depths and long-term time variations. *Radiation Measurements*, 23, 497-500.

Roberts, R.G., Galbraith, R.F., Yoshida, H., Laslett, G.M., Olley, J.M. (2000) Distinguishing dose populations in sediment mixtures: a test of single-grain optical dating procedures using mixtures of laboratory dosed quartz. *Radiation Measurements*, 32, 459-465.

Rodnight, H., Duller, G.A.T, Wintle, A.G. and Tooth, S. (2006) Assessing the reproducibility and accuracy of optical dating of fluvial deposits. *Quaternary Geochronology*, 1, 109-120.

Singhvi, A.K., Bluszcz, A.., Bateman, M.D., Someshwar Rao, M. (2001). Luminescence dating of loess-palaeosol sequences and coversands: methodological aspects and palaeoclimatic implications. *Earth Science Reviews*, 54, 193-211.

Smith, B.W., Rhodes, E.J., Stokes, S., Spooner, N.A. (1990) The optical dating of sediments using quartz. *Radiation Protection Dosimetry*, 34, 75-78.

Spooner, N.A. (1993) The validity of optical dating based on feldspar. Unpublished D.Phil. thesis, Oxford University.

Templer, R.H. (1985) The removal of anomalous fading in zircons. *Nuclear Tracks and Radiation Measurements*, 10, 531-537.

Toms, P.S., Hosfield, R.T., Chambers, J.C., Green, C.P. and Marshall, P. (2005) Optical dating of the Broom Palaeolithic sites, Devon and Dorset. English Heritage Centre for Archaeology dating report 16/2005.

Truscott, A.J., Duller, G.A.T, Botter-Jensen, L., Murray A.S. and Wintle, A.G. (2000) Reproducibility of optically stimulated luminescence measurements from single grains of Al_2O_3:C and annealed quartz. *Radiation Measurements*, 32, 447-451.

Wallinga, J. (2002) Optically stimulated luminescence dating of fluvial deposits: a review. *Boreas*, 31, 303-322.

Wintle, A.G. (1973) Anomalous fading of thermoluminescence in mineral samples. *Nature*, 245, 143-144.

Zimmerman, D. W. (1971) Thermoluminescent dating using fine grains from pottery. *Archaeometry*, 13, 29-52.

Predictive Modelling at a River Confluence: Radiocarbon dating

By W D Hamilton, P D Marshall, T Brown, C Carey, C Bronk Ramsey, and J van der Plicht

A total of 37 samples were submitted for radiocarbon dating by Accelerator Mass Spectrometry (AMS), producing a total of 39 results, to the Oxford Radiocarbon Accelerator Unit (ORAU) and the Centre for Isotope Study, the University of Groningen, The Netherlands. These consisted of two waterlogged twigs, 19 Monocotyledon samples, and 15 sediment samples.

The samples submitted to ORAU were prepared according to methods given in Hedges *et al* (1989) and measured as described in Bronk Ramsey *et al* (2004). Those submitted to Groningen were processed and measured as described by Aerts-Bijma *et al* (1997; 2001) and van der Plicht *et al* (2000).

Both laboratories maintain continual programmes of quality assurance procedures, in addition to participation in international inter-comparisons (Scott 2003). These tests indicate no laboratory offsets and demonstrate the validity of the measurements quoted.

The results, given in Table 1, are conventional radiocarbon ages (Stuiver and Polach 1977), and are quoted in accordance with the international standard known as the Trondheim convention (Stuiver and Kra 1986).

The calibrations of these results, relating the radiocarbon measurements directly to calendar dates, have been calculated using the calibration curve of Reimer *et al* (2004) and the computer program OxCal (v3.10) (Bronk Ramsey 1995; 1998; 2001). The calibrated date ranges for these samples are given in Table 1 and have been calculated using the maximum intercept method (Stuiver and Reimer 1986). They are quoted in the form recommended by Mook (1986), with the end points rounded outwards to 10 years. The graphical distributions of the calibrated dates, given in outline in Figures 1–4, are derived from the probability method (Stuiver and Reimer 1993).

Objectives

The overall aim of the scientific dating programme was to provide a chronological framework with which to interpret the palaeoenvironmental analyses and relate this to the known archaeological record for the area

Sampling

The dating of environmental cores and monoliths can present various problems, most of which can be investigated through a rigorous programme of radiocarbon dating and sample selection.

Macrofossils
Although macrofossils are now often preferred as samples from environmental cores, as they can be identified as short-lived material, care must be taken when they come from aqueous environments (*eg* fluvial, alluvial, estuarine, etc). In these instances there is some possibility that the macrofossils were in-washed. While in-washing is more likely to bring in material that is of an older, rather than younger, date, wet-dry cycles and invasive reeds, such as *Phragmites,* present the possibility of younger material being brought down through the

sediment column. Because of these potential problems, the radiocarbon programme employed is one with consistency as its foremost aim.

Consistency can be demonstrated in two ways. The first is through good overall agreement between the radiocarbon measurements and the core sequence. The second is through the replication of results from a specific level in the core. The replication of results is why it is preferred to have two macrofossils submitted from any given level, it is also part of the reasoning behind dating multiple fractions of peats, soils, and sediment, which are dealt with in the next section. If the resultant measurements are statistically consistent (*ie* $T'<3.8$, $\nu=1$) then it is probable that the two dates correctly date that level. When the two dates are not statistically consistent, the data need to be re-evaluated.

Sediment

The second type of material submitted for radiocarbon dating consisted of sediment. The dating of sediment and the reliability of the resultant dates from various fractions (eg humins, humic acids, etc) has been a topic of contention in the literature (see Blaauw *et al* 2004; Kilian *et al* 1995; 2000; and Shore *et al* 1995). The two most commonly dated fractions from these samples are the humins (ie alkali and acid insoluble organic detritus) and the humic acids (ie alkali soluble and acid insoluble matter). A third fraction that is sometime dated consists of the fulvic acids (ie the acid soluble fraction). Finally, if there is not enough available material to date the separate fractions then the bulk sediment can be dated (ie humin and humic fractions combined).

As the humin fraction is composed of the actual organic detritus, the resultant date from measuring this fraction is subject to many of the same processes that affect the dating of macrofossils in the same type of environment. Firstly, organic material that forms all or part of the humin fraction could be in-washed, which would result in a date that is too old. Contamination of this material by geological age carbon (eg coal, hard-water error) would have the same effect. The humin fraction can also be too young, if for example the environment is prone to wet-dry episodes or bioturbation, allowing intrusive material to work its way down the sediment column. Therefore, the humin fraction is not necessarily homogenous, and so it might be best to avoid dating this fraction by AMS as the smallest contamination would greatly affect the resultant measurement. Humins may better be dated through conventional radiocarbon dating techniques, as it is unlikely that a sufficient volume of such contamination would be present to bias such results significantly.

The second fraction that is often dated is the humic acids, which are the *in situ* products of plant decay. Although they are produced *in situ* and imply a stability to the ground surface, it has been shown that they can be mobile in groundwater, both vertically and horizontally (Shore *et al* 1995), but that their mobility is probably limited. Therefore, humic acids cannot be relied upon to always correctly date the level from which they were collected either. However, unlike the humin fraction, humic acids are homogenous, as they are alkali soluble, and therefore can be more reliably dated through AMS.

Fulvic acids are acid soluble and therefore can be suspended in a homogenous solution. Shore *et al* (1995) have shown that fulvic acids are nearly always the youngest fraction within a sediment profile. However, they also show that in a few cases they are by far the oldest of the three dated fractions at a level. They go on to suggest that this is likely due to the fact that fulvic acids are soluble in water and therefore are highly mobile, moving up and down with the water table and laterally within the subterranean drainage patterns.

In some cases, when there is not enough material for dating of separate fractions, the humic acid and humin fractions can be bulked together to provide an average date for all the organic material in that level. As stated earlier however, it is preferable to have the dates on the two fractions as this provides the data necessary for using replication as a measure of consistency.

When the dates on two fractions are obtained, if they are statistically consistent, a weighted average can be taken before calibration as described in Ward and Wilson (1978). In most cases this creates a date that is more reliable. However, if the two results are not in agreement then the data need to be re-evaluated, in an attempt to determine which sample more reliably relates to the date of the level under consideration.

Results and Discussion

Three of the four series of dates have produced one or more results that calibrate to the modern period (post AD 1950). In total, five measurements have all of their calibrated date range in this period and one overlaps into this period upon calibration, but this is most likely due to the rounding of the resulting date. All of the five 'modern' samples are waterlogged macrofossils or wood, and while in some cases these samples may accurately date the level from which they were retrieved, in some cases they are likely to be the result of sampling contamination from the gouge corer. These dates are discussed in further detail in the relevant series sections below.

TFG
Four samples were submitted from locations along core TFG. The four radiocarbon measurements are consistent with their relative order in the sequence (Fig 1).

T1
Eighteen samples were submitted across nine cores from palaeochannels that form series T1. The results are presented in the proposed ordering of the palaochannels, from earliest to most recent, based upon early chrono-stratigraphic work (Fig 2).

Two samples were dated from core C14, a proposed late Devensian/early Holocene sequence. The two results are consistent with their relative stratigraphic order, however, they suggest that the sequence spans the Bronze Age to Anglo-Saxon periods.

Six samples were submitted from five levels along core C7, a proposed early Holocene sequence with excellent preservation for palaeoenvironmental analysis. The result on monocotyledon fragments from the base of the sequence (OxA-15889) calibrates to the modern period and is likely to be the result of contamination through the use of the gouge corer. The two results from C7 1.51m (OxA-16159/60) on the humin fraction and humic acid, respectively, of sediment are not statistically consistent (T'=811.7; v=1; T'(5%)=3.8; Ward and Wilson 1978). Furthermore, both of these dates are significantly older than the resulting date on Monocotyledon fragments from almost a half metre below (GrA-31951). Also, it should be pointed out that the bulk sediment date from C7 0.95m is also older than GrA-31951. The lack of consistency within and between the two sample types (sediment and macrofossil) means this core must remain 'undated' with the radiocarbon measurements providing no means to tie the changes in land-use evident in the pollen record to the existing archaeological record from the area.

Three samples of Monocotyledon were dated from a sequence in core C12. The results are not in agreement with their relative stratigraphic order. This is again likely the result of sampling contamination given the result from C12 0.5m (GrA-31987) is modern in date.

Three results were produced on sediment from three levels in core C10. While the lower two results (GrA-31998 and OxA-15931) are consistent with their relative stratigraphic order, the uppermost result is over 3500 years older (OxA-15972). This discrepancy is likely the result of reworked organic material being inwashed and breaking down *in situ*.

A single sample was submitted from core C2 1.24m, and the result (OxA-15887) dates the infilling of this palaeochannel to the late-5th–8th centuries cal AD.

A single sample was submitted from core C6 1.61m, and the result (GrA-31949) is a modern date, suggesting that this level has been contaminated.

A single sample was submitted from core C3 1.6m, and the result (GrA-31774) dates the infilling of this palaeochannel to the 7th century cal AD.

A single sample was submitted from core C4 0.98m, and the result (OxA-15971) dates the infilling of this palaeochannel to the late-9th–early-6th centuries cal BC.

A single sample was submitted from core C8 1.3m, and the result (GrA-31986) dates the infilling of this palaeochannel to the late-1st–early-4th centuries cal AD.

WQF
A total of 12 radiocarbon results were obtained from four monoliths from exposed sections of the quarry at Sawley. While CH5 was clearly the earliest monolith, monoliths CH1–3 were unrelatable to one another based on stratigraphy (Fig 3).

Three samples were submitted from two levels of monolith CH5. The two measurements on samples from 0.0m depth in the monolith are not statistically consistent (T'=55.3; v=1; T'(5%)=3.8; Ward and Wilson 1978). The earliest result (GrA-32001) came from bulk sediment while the later result (OxA-15893) was from Monocotyledon fragments. The later result provides a better estimate for this depth.

Two samples were submitted from CH3 0.5m and the two measurements are not statistically consistent (T'=461.6; v=1; T'(5%)=3.8; Ward and Wilson). The earlier result (OxA-15932) is on the humic acid fraction of sediment, while the later result (GrA-31941) is on Monocotyledon fragments. The later result provides a better estimate for this depth.

Three samples of Monocotyledon fragments were submitted from CH2. Although one sample (OxA-15892) has produced a modern result, all three measurements are in agreement with their stratigraphic order and so based upon the radiocarbon measurements and the relative order there is no reason to question this result.

Finally, four measurements were made on material from three levels in monolith CH1. The lower two results, from Monocotyledon fragments (OxA-15891 and GrA-31953) are in agreement with their relative stratigraphy. However, the two results from CH1 0.24m are either earlier or apparently coeval with the results from the lowest level (OxA-15891). These two results from 0.24m (OxA-16128/9) were made on the humin fraction and humic acid, respectively, of a sediment sample. These results are not statistically consistent (T'=166.0; v=1; T'(5%)=3.8; Ward and Wilson 1978).

Because of the many discrepancies within these results, it is imperative that all results are used with the utmost caution, and that thesediment dates from series WQF provide at best a *terminus post quem* (*tpq*) for deposition and the macros at worst a *terminus ante quem* (*taq*) for any given level.

MF
A total of four radiocarbon measurements were made on material from the two MF-series cores, with their calibrated probability distributions shown in Figure 4.

There was only one measurement from MFC1 (OxA-15894, 368 ±28BP), which provides a date of cal AD 1440–1640 (95% confidence) for 1.53m down the core.

The three measurements from MFC2 are not in the expected chronological order based upon their stratigraphy. These three measurements come from two sample locations (1.0 and 1.69m), with the two measurements from 1.0m differing by over 4500 years. If we accept that the modern result of Monocotyledon fragments (GrA-31989) is intrusive we are left with two results on the humic acid fraction of sediment samples that are not in agreement with their stratigraphic order. Based upon the information at hand, it is impossible to determine which, if either, of the two results accurately dates its level.

Conclusion

The discrepancy between the humic acid and humin fraction results in the results from this project can be attributed to reworking of sediment that contains old carbon in many cases. Additionally with cores WQF CH3 and CH5 we have also dated horizons by sediment and macrofossil where the macrofossil results were more recent than the sediment. Similar outcomes have been noticed before, which have produced the following possible and non-exclusive explanations/hypotheses (Hamilton *et al* forthcoming):

1) the humin fractions are contaminated/contain reworked mineral carbon

2) the humic acids reflect a small, but significant, component from older mineral older carbon, or contain humic acid from the breakdown of older plant material

3) the macrofossil material is intrusive

Because of the overall lack of consistency amongst these results it is difficult to say with any confidence that a level of a core/monolith has an accurate date. While the discrepancy amongst the sediment dates might lead us to the conclusion that the dates on macrofossil material is a more accurate representation of the true age at any given level, the fact that five out the 21 macrofossil results (24%) are modern means we cannot place much faith in those results as 'reliable' either.

The sediment dates from the Trent/Soar project provide at best a *terminus post quem* (*tpq*) for deposition and the macros at worst a *terminus ante quem* (*taq*).

Table 1: Radiocarbon results from the Trent/Soar project

Laboratory ID	Sample ID and depth	Material	$\delta^{13}C$ (‰)	Radiocarbon Age (BP)	Calibrated Date (95% confidence)
TFG					
GrA-31771	C14 2.5m	unidentified twig	-29.9	3300 ±40	1690–1490 cal BC
OxA-15886	C14 3m	Monocotyledon fragments	-27.9	3410 ±60	1890–1530 cal BC
GrA-31456	C14 3.5m	Monocotyledon fragments	-29.9	3880 ±35	2470–2200 cal BC
GrA-31948	C14 3.8m	bulk sediment	-29.1	4725 ±40	3640–3370 cal BC
T1					
GrA-31986	C8 1.3m	Monocotyledon fragments	-28.6	1820 ±30	cal AD 90–320
OxA-15971	C4 0.98m	sediment, humic acid	-26.9	2561 ±30	810–590 cal BC
GrA-31774	C3 1.6m	Monocotyledon fragments	-28.7	1370 ±35	cal AD 610–690
GrA-31949	C6 1.61m	unidentified twig	-28.7	110.11 ±0.44%mod	cal AD 1996–1999
OxA-15887	C2 1.24m	Monocotyledon fragments	-25.9	1430 ±80	cal AD 430–770
OxA-15972	C10 1m	sediment, humic acid	-27.6	7300 ±40	6240–6060 cal BC
GrA-31998	C10 1.45m	bulk sediment	-26.6	3920 ±35	2550–2290 cal BC
OxA-15931	C10 1.8m	sediment, humic acid	-28.2	4334 ±30	3030–2890 cal BC
GrA-31987	C12 0.5m	Monocotyledon fragments	-29.4	109.31 ±0.39%mod	cal AD 1997–2001
OxA-15890	C12 1.93m	Monocotyledon fragments	-27.5	1174 ±35	cal AD 730–970
GrA-31988	C12 2.14m	Monocotyledon fragments	-29.5	1030 ±40	cal AD 890–1120
OxA-15888	C7 0.5m	Monocotyledon fragments	-27.4	129 ±31	cal AD 1660–1960
GrA-31950	C7 0.95m	bulk sediment	-29.5	1020 ±35	cal AD 970–1120
OxA-16159	C7 1.51m	sediment, humin fraction	-30.4	2638 ±31	840–780 cal BC
OxA-16160	C7 1.51m	sediment, humic acid	-28.6	1406 ±30	cal AD 590–670
GrA-31951	C7 2m	Monocotyledon fragments	-28.4	590 ±35	cal AD 1290–1420
OxA-15889	C7 2.25m	Monocotyledon fragments	-28.2	121.8 ±0.9%mod	cal AD 1958–1986
OxA-15973	C14 0.45m	sediment, humic acid	-28.6	1309 ±28	cal AD 650–780
GrA-31492	C14 0.9m	bulk sediment	-27.6	3005 ±35	1390–1120 cal BC
WQF					
OxA-16128	CH1 0.24m	sediment, humin fraction	-29.1	3517 ±30	1940–1740 cal BC
OxA-16129	CH1 0.24m	sediment, humic acid	-29.3	2989 ±28	1380–1120 cal BC
GrA-31953	CH1 0.5m	Monocotyledon fragments	-28.1	2580 ±35	810–600 cal BC
OxA-15891	CH1 0.68m	Monocotyledon fragments	-28.8	2730 ±160	1370–410 cal BC
OxA-15892	CH2 M1 0.5m	Monocotyledon fragments	-26.1	104.0 ±0.3%mod	modern
GrA-31940	CH2 M2 0.5m	Monocotyledon fragments	-27.2	2500 ±35	790–410 cal BC
GrA-31999	CH2 M3 0.5m	Monocotyledon fragments	-30.8	2820 ±35	1060–890 cal BC

OxA-15932	CH3 0.5m (a)	sediment, humic acid	-28.2	4078 ±30	2860–2490 cal BC
GrA-31941	CH3 0.5m (b)	Monocotyledon fragments	-29.1	3075 ±35	1430–1260 cal BC
OxA-15893	CH5 0m (a)	Monocotyledon fragments	-27.5	11505 ±55	11510–11290 cal BC
GrA-32001	CH5 0m (b)	bulk sediment	-29.4	12060 ±50	12100–11830 cal BC
GrA-31943	CH5 0.36m	bulk sediment	-28.2	13870 ±60	14980–14180 cal BC
MFC					
OxA-15894	1 1.53m	not identified on form?!?!	-28.2	368 ±28	cal AD 1440–1640
OxA-15974	2 1m (a)	sediment, humic acid	-26.6	4168 ±31	2890–2620 cal BC
GrA-31989	2 1m (b)	Monocotyledon fragments	-29.6	109.0 ±0.78%mod	1996–present
OxA-16161	2 1.69m	sediment, humic acid	-27.7	2609 ±32	800–510 cal BC

Figure 1: Calibrated radiocarbon dates from core TFG. The probability distributions have been calculated following Stuiver and Reimer (1993)

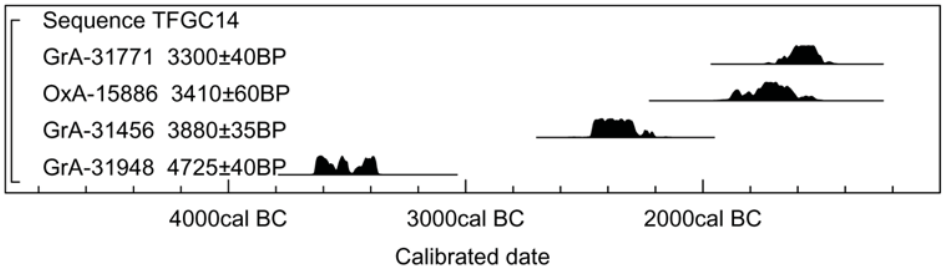

Figure 2: Calibrated radiocarbon dates from cores in the T1 series. The dates have been ordered by the proposed date order for the basal sample. The probability distributions have been calculated following Stuiver and Reimer (1993)

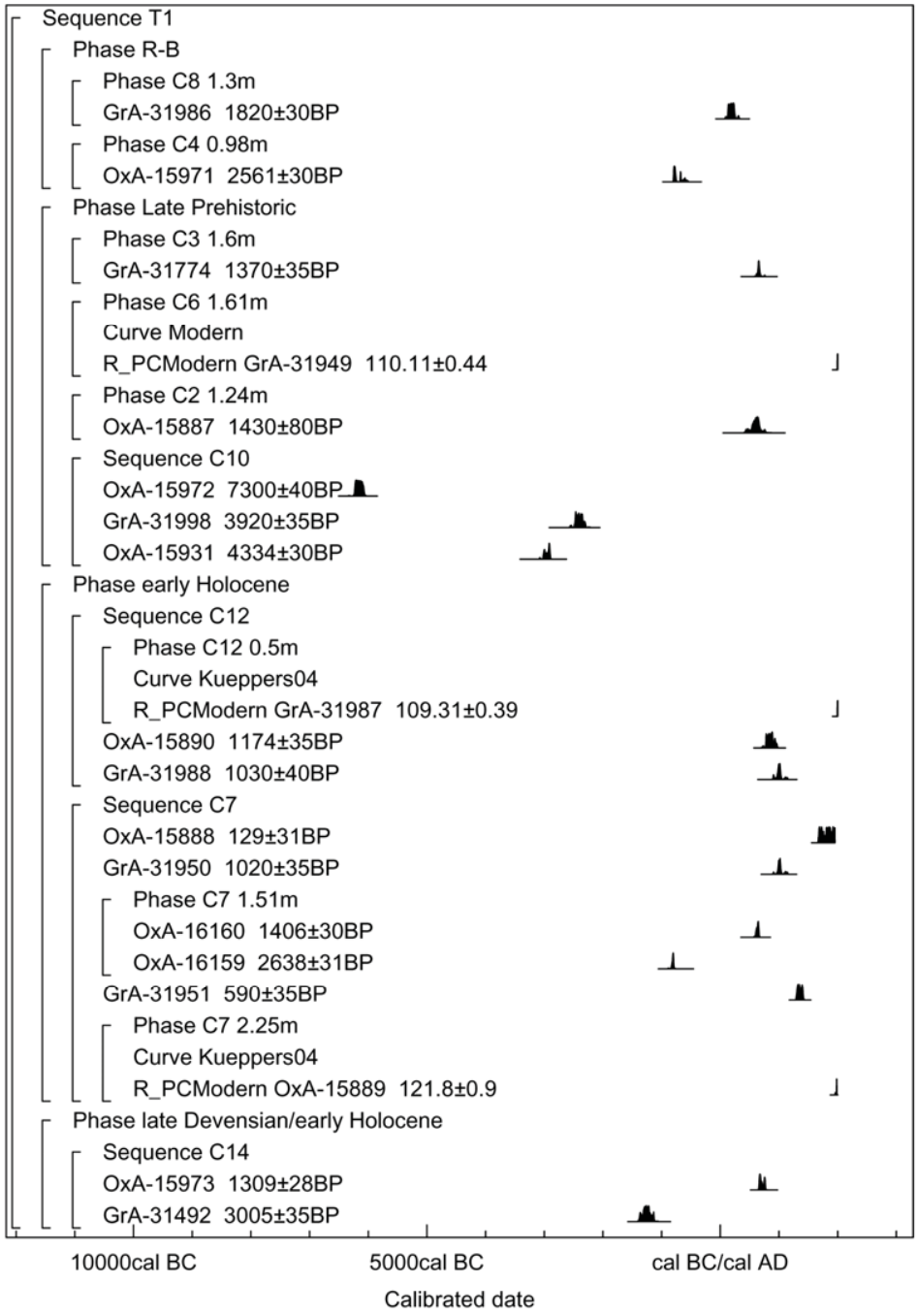

Figure 3: Calibrated radiocarbon dates from monoliths in the WQF series. The probability distributions have been calculated following Stuiver and Reimer (1993)

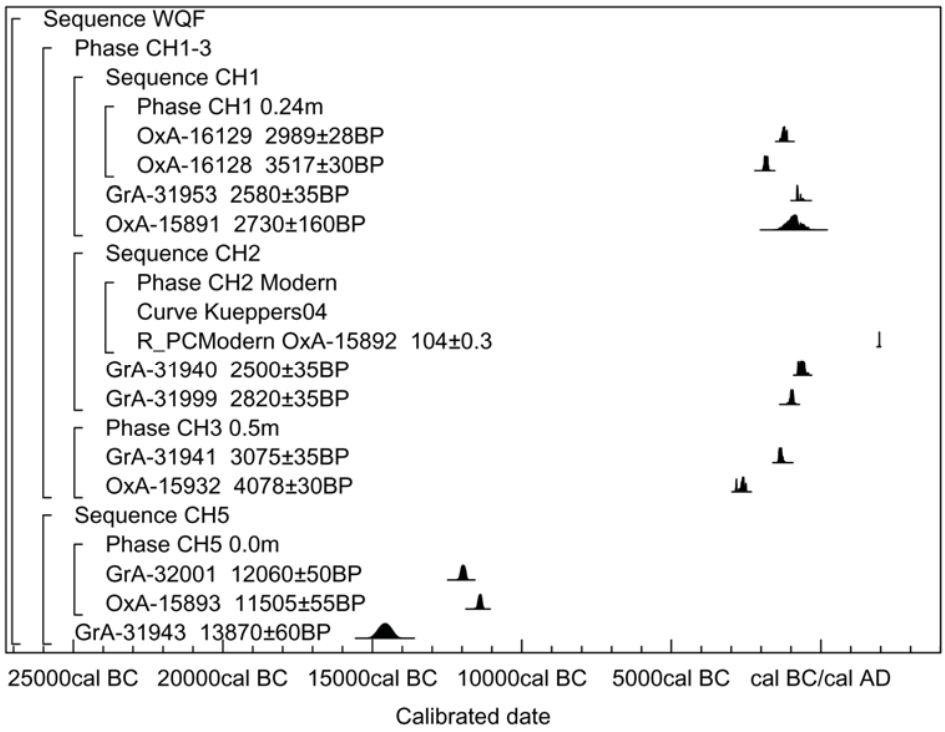

Figure 4: Calibrated radiocarbon dates from cores in the MFC series. The probability distributions have been calculated following Stuiver and Reimer (1993)

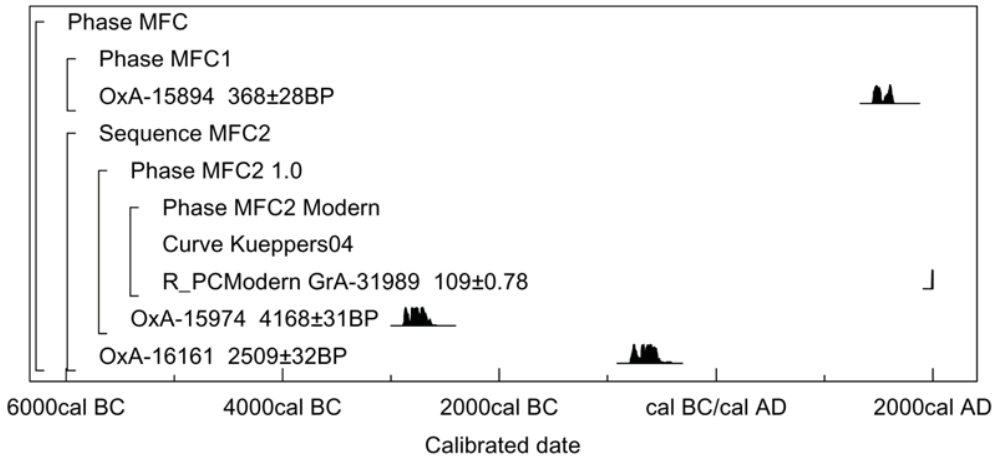

Works Cited

Aerts-Bijma, A T, Meijer, H A J, and van der Plicht, J, 1997 AMS sample handling in Groningen, *Nuclear Instruments and Methods in Physics Research B*, **123**, 221–5

Aerts-Bijma, A T, van der Plicht, J, and Meijer, H A J, 2001 Automatic AMS sample combustion and CO_2 collection, *Radiocarbon*, **43(2A)**, 293–8

Blaauw, M, van der Plicht, J, and val Geel, B, 2004 Radiocarbon dating of bulk peat samples from raised bogs: non-existence of a previously reported 'reservoir effect'?, *Quaternary Sci Rev*, **23**, 1537–42

Bronk Ramsey, C, 1995 Radiocarbon calibration and analysis of stratigraphy, *Radiocarbon*, **36**, 425–30

Bronk Ramsey, C, 1998 Probability and dating, *Radiocarbon*, **40**, 461–74

Bronk Ramsey, C, 2001 Development of the radiocarbon calibration program, *Radiocarbon*, **43**, 355–63

Bronk Ramsey, C, Higham, T, and Leach, P, 2004 Towards high precision AMS: progress and limitations, *Radiocarbon*, **46(1)**, 17–24

Hamilton, W D, Marshall, P D, Brown, T, Allen, P, Meadows, I, and Cook G, forthcoming Radiocarbon dating, in *The Nene Valley Project*

Hedges, R E M, Bronk, C R, and Housley, R A, 1989 The Oxford Accelerator Mass Spectrometry facility: technical developments in routine dating, *Archaeometry*, **31**, 99–113

Kilian, M R, van der Plicht, J, and van Geel, B, 1995 Dating raised bogs: new aspects of AMS ^{14}C wiggle matching, a reservoir effect and climatic change, *Quaternary Sci Rev*, **14**, 959–66

Kilian, M R, van der Plicht, J, and van Geel, B, 2000 ^{14}C wiggle matching of raised bog deposits and models of peat accumulation, *Quaternary Sci Rev*, **19**, 1011–33

Mook, W G, 1986 Business meeting: Recommendations/Resolutions adopted by the Twelfth International Radiocarbon Conference, *Radiocarbon*, **28**, 799

van der Plicht, J, Wijma, S, Aerts, A T, Pertuisot, M H, and Meijer, H A J, 2000
Status report: the Groningen AMS facility, *Nuclear Instruments and Methods in Physics Research B*, **172**, 58–65

Reimer, P J, Baillie, M G L, Bard, E, Bayliss, A, Beck, J W, Bertrand, C J H, Blackwell, P G, Buck, C E, Burr, G S, Cutler, K B, Damon, P E, Edwards, R L, Fairbanks, R G, Friedrich, M, Guilderson, T P, Hogg, A G, Hughen, K A, Kromer, B, McCormac, G, Manning, S, Bronk Ramsey, C, Reimer, R W, Remmele, S, Southon, J R, Stuiver, M, Talamo, S, Taylor, F W, van der Plicht, J, and Weyhenmeyer, C E, 2004 IntCal04 Terrestrial radiocarbon age calibration, 0–26 Cal Kyr BP, *Radiocarbon*, **46**, 1029–58

Scott, E M (ed), 2003 The Third International Radiocarbon Intercomparison (TIRI) and the Fourth International Radiocarbon Intercomparison (FIRI) 1990–2002: results, analysis, and conclusions, *Radiocarbon*, **45**, 135–408

Shore, J S, Bartley, D D, and Harkness, D D, 1995 Problems encountered with the ^{14}C dating of peat, *Quaternary Sci Rev*, **14**, 373–83

Stuiver, M, and Kra, R S, 1986 Editorial comment, *Radiocarbon*, **28(2B)**, ii

Stuiver, M, and Polach, H A, 1977 Reporting of ^{14}C data, *Radiocarbon*, **19**, 355–63

Stuiver, M, and Reimer, P J, 1986 A computer program for radiocarbon age calculation, *Radiocarbon*, **28**, 1022–30

Stuiver, M, and Reimer, P J, 1993 Extended ^{14}C data base and revised CALIB 3.0 ^{14}C age calibration program, *Radiocarbon*, **35**, 215–30

Ward, G K, & Wilson, S R, 1978 Procedures for comparing and combining radiocarbon age determinations: a critique, *Archaeometry*, **20**, 19–31

Dendrochronology

Robert Howard

Figure x: Bar diagram of the samples in site chronology LOKQSQ01

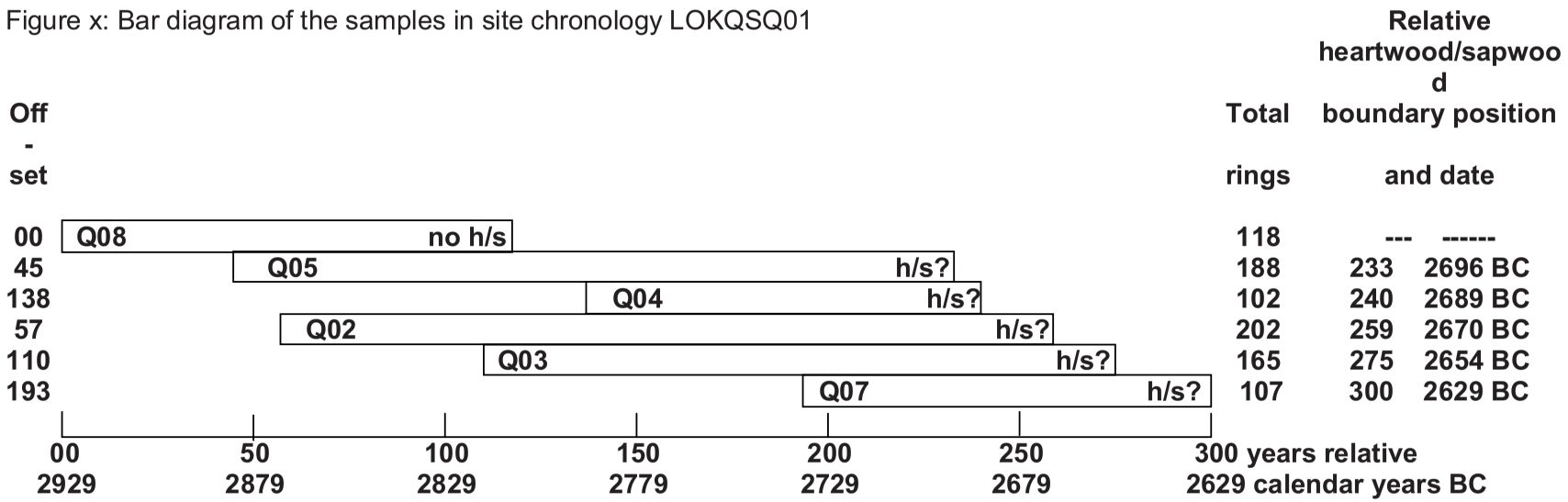

h/s? = the last ring on the sample is probably at or approaching the heartwood/sapwood boundary

Table 1: Details of samples from Lockington Quarry on the river Trent in Leicestershire

Sample number	Sample location	Total rings	*Sapwood rings	First measured ring date	Last heartwood ring date	Last measured ring date
LOK-Q01	Quarry oak	84	h/s?	------	------	------
LOK-Q02	Quarry oak	202	h/s?	2871 BC	2670 BC	2670 BC
LOK-Q03	Quarry oak	165	h/s?	2818 BC	2654 BC	2654 BC
LOK-Q04	Quarry oak	102	h/s?	2790 BC	2689 BC	2689 BC
LOK-Q05	Quarry oak	188	h/s?	2883 BC	2696 BC	2696 BC
LOK-Q06	Quarry oak	105	h/s?	2623 BC	2519 BC	2519 BC
LOK-Q07	Quarry oak	107	h/s?	2735 BC	2629 BC	2629 BC
LOK-Q08	Quarry oak	118	no h/s	2928 BC	------	2811 BC

*h/s? = the last ring on the sample is at or approaching the heartwood/sapwood boundary

Table 2: Results of the cross-matching of site chronology LOKQSQ01 and relevant reference chronologies when first ring date is 2928 BC and last ring date is 2629 BC

Reference chronology	Span of chronology	*t*-value	
England National	4989 - 1681 BC	12.5	(Hillam pers comm)
Shardlow Quarry, Derbys	2942 - 2610 BC	10.9	(Tyers 2000)
East Anglia: regional	3196 - 1681 BC	9.5	(Brown pers comm)
Langford quarry, Notts	2979 - 2125 BC	7.9	(Hillam unpubl)
Colwick Hall 1	3054 - 2697 BC	6.7	(Brown pers comm)
Stourport on Seven, Worcs	2869 - 2698 BC	6.5	(Hillam pers comm)

Table 3: Results of the cross-matching of sample LOK-Q06 and relevant reference chronologies when first ring date is 2623 BC and last ring date is 22519 BC

Reference chronology	Span of chronology	*t*-value	
Wootton Quarry, Isle of Wight	3463 - 2557 BC	6.0	(Hillam 1994)
England National	4989 - 1681 BC	5.8	(Hillam pers comm)
East Anglia: regional	3196 - 1681 BC	5.0	(Brown pers comm)
Langford quarry, Notts	2979 - 2125 BC	5.4	(Hillam unpubl)

Hillam J 1994, The dating of oak timbers from the Wootton Quarry Survey, Isle of Wight, Anc Mon Lab Rep 10/1994
Tyers, I, 2000, Tree-ring analysis of prehistoric archaeological timbers from Shardlow Gravel Pit, Derbyshire, Anc Mon Lab Rep, **32/2000**